Final Report

Advanced Personal Gas Detectors for Mining Applications

CDC (NIOSH) Grant 2R44OH009026-02A1
SBIR Phase II

SUBMITTED BY

SYNKERA TECHNOLOGIES, INC.
2605 Trade Centre Ave, Suite C
Longmont, CO 80503

Tel: (720) 494-8401 •Fax: (720) 494-8402

November 29, 2011

Table of Contents

List of Abbreviations

AAO – anodic aluminum oxide

Al_2O_3 – aluminum oxide

°C – degress centigrade

Ce – cerium

FE – finite element

I – current

K - Kelvin

LTT – long term test

M – molar

m – meter

mm – millimeter

mV – millivolte

PCB – printed circuit board

Pd – palladium

PRS – product requirment specification

Pt – platinum

V – voltage

Wt% - weight percent

Zr – zirconium

Abstract

Synkera demonstrated ultra-low power combustible gas microsensors, based on our nano/microfabrication platform technology that integrates nanostructured sensing elements into a robust monolithic ceramic device. This sensor is aimed at enabling widespread protection of workers (miners, plant workers, first responders) because of it applicability in portable detection and the low cost, scaleable manufacturing routes used that will make it such protection affordable to a greater cross-section of potential users.

A systematic development of the combustible gas microsensor technology was performed to meet the application requirements and advance the microsensor to a readiness level that enables integration with prototype instrumentation. The Phase II established a viable route to new combustible gas microsensors using AAO as the base material. The new sensors are highly sensitive, selective, and are robust and reliable. Through this development routes to commercialization and scale-up have been identified. One such route is the possible inclusion of this sensor under an effort funded by the Department of Homeland Security for the development of a multi-gas instrument for use by fire fighters.

Title: Advanced Personal Detectors for Mining Applications
PI: Clayton J. Kostelecky
Company: Synkera Technologies, Inc.
Address: 2605 Trade Centre Ave., Suite C
Longmont, CO 80503

Section 1

Highlights/Significant Findings

A focus on the Specific Aims throughout the development effort lead to the following significant findings.

- Reliable sensor performance, and good sensitivity to methane was achieved for the microsensors at 70 mW per element. This was greater than the targeted 50 mW per element.
- Based on work during Phase II and other related sensor efforts, the targeted sensor cost of $15 for sensors in quantities of 10,000 per year is feasible. From work on other instrumentation efforts at Synkera, a cost of $50 for a low cost single gas detector in those quantities is possible, but will depend on the required (and desired) features for the device.
- A complete instrument was not produced during Phase II, as more effort in the development of the sensor itself was undertaken. However, operating circuitry was developed for the microsensors.
- Based on the current power consumption, ~140 mW total for both elements (active + reference), it is unlikely that the target of 1-week between charges is possible with the current sensor.

Translation of Findings

The sigificant findings from the Phase II effort have highlighted areas of further improvement to fully achieve the initial goals of the development.

- To reduce power consumption to the targeted 50 mW per element further refinement of the sensor geometry and sensing material deposition will be explored. Power management schemes, such as duty cycling or operating the reference element at a lower temperature than the active element, could reduce the total power further.
- To ensure that cost targets can be met we will continue to work with potential customers on required and desired features of the device. Costs will can also be reduced as Synkera's overall product line expands and additional process scaling is implemented.
- For incorporation of the new, novel combustible gas microsensor into instrumentation, in the near term, Synkera will continue to work with partners that already provide such devices. In the longer term we intend to establish our own instrumentation around this (and other) gas sensors.
- In addition to refining sensor geometry and sensing material deposition methods, power management schemes, such as duty cycling or operating the reference element at a lower temperature than the active element, could reduce the total power further. This could enable the ability to achieve the original target of 1-week between instrument charging. However, based on discussions with customers and end-users this may not be critical, as this type of instrument is typically charged at the end of every shift.

Outcomes/Relevance/Impact

While all the Specific Aims were not met in Phase II, substantial progress was made on this new, novel combustible gas microsensor. Even though further improvements are desirable, the Phase II effort produced sensors that are relevant for use in personal detectors, to protect workers from explosion in mines and in other hazardous locations such as industrial plants and accident scenes.

A significant outcome of the Phase II is the fact that the combustible gas microsensor that was developed is being considered for use by an instrument manufacturer partner in a multigas instrument aimed to provide reliable, low-cost protection to first responders.

Section 2

A. PROJECT OVERVIEW

In spite of continuous improvements in safety, mining remains one of the most dangerous occupations in America. The risk of explosions in underground mines is high and for workers caught in the vicinity of an explosion, the consequences are frequently catastrophic. The greatest concern is the build-up of hazardous gases (such as combustible gases and carbon monoxide) and reduction of oxygen levels. Although mining operators are now required to provide handheld multi-gas detectors to each group of underground miners, it is recognized that fatalities related to gas explosions and fire would likely be prevented or reduced if all personnel were equipped with reliable personal gas detectors.

However, the size, cost and power consumption of current portable instruments has been a barrier to such deployment. Many end users have suggested that they would be eager to outfit all employees (not just the groups or those working alone) with personal protection devices if they were more affordable (currently from $350 for combustible gases to over $575 for multi-gas units). Also, due to their high power consumption, these sensors require relatively large batteries (often with daily recharging), further complicating the logistics, increasing operational costs and presenting additional burden to the miner.

Synkera aimed to addresses these issues by developing and commercializing a new generation of inexpensive, reliable and portable combustible gas detectors for personal use – the credit card sized Smart Gas Card – that eliminate current size, cost, performance and lifetime barriers in broad use of such safety tools. To achieve this goal, a new groundbreaking sensor technology is needed to support size, power, performance, and reliability requirements of Smart Gas Cards.

In Phase I of this project Synkera demonstrated the feasibility of ultra-low power combustible gas microsensors, based on our nano/microfabrication platform technology that integrates nanostructured sensing elements into a robust monolithic ceramic device. Phase II aimed to perform systematic development of the combustible gas microsensor technology to meet the application requirements and advance it to a readiness level that enables functional Smart Combustible Gas Card™ prototypes. In support of these goals, specific aims of the Phase II project included:

- Use of sensor simulation model, improve the sensor design to increase catalytic volume
- Completion of the microsensor development by optimizing catalyst and support
- Definition and realization targeted sensor performance and initiate development of application-specific prototypes
- Validation of sensor performance both at Synkera and at the facilities of our OEM partners
- Identification of approaches to scale microsensor fabrication that ensure reproducibility and reliability
- Development of low power electronics and fabrication of prototypes of Smart Combustible Gas Card™ for internal and external evaluation
- Establish partnerships for commercialization of combustible gas microsensors and related Smart Gas Card.

B. PHASE II WORK

B.1. SENSOR REQUIREMENTS

In order to define the required specifications for the combustible gas sensor we created a Product Requirement Specification (PRS). Information for the PRS was gathered through conversations

with customers, review of existing combustible gas sensors, and Synkera personnel's experience in the field. The PRS is attached as *Appendix A*.

B.2. SUBSTRATE DEVELOPMENT

The overall aim in the development of the sensor substrate was to achieve a robust, low-power design that could be reproducibly manufactured with a high yield using Synkera's Anodic Aluminum Oxide (AAO) technology. This section describes the fabrication, evaluation, optimization, and modeling efforts related to the substrate.

i) Fabrication

The processing route used to fabricate high-resolution AAO dies via bulk micromachining includes the following steps: (1) anodize the aluminum (Al) foil to required thickness and pore morphology; (2) pattern the surface of AAO with the photoresist to define sensors; (3) etch the exposed AAO to micromachine sensor dies; and (4) separate blank sensor dies from Al by selective etch. The AAO morphology is tuned in two steps: the "primary porosity" is defined during anodization and the "secondary porosity" is formed during annealing at elevated temperatures.

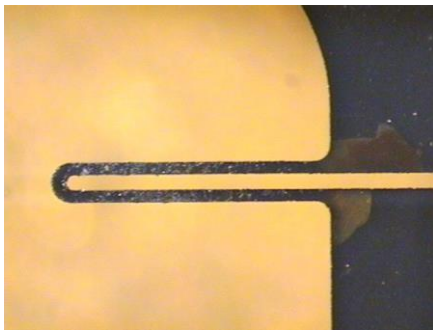

Figure 1: Close up of sensor element with Pt heater. Top to bottom of "finger" is 150 µm.

Following the fabrication of the AAO dies microheaters are deposited to create a functional sensor substrate. Platinum (Pt) is use as a thin film microheater in these sensors, due to its excellent thermal stability. The Pt is plasma sputtered onto the sensor substrates through a shadow masks in a two step process. The shadow masks define where the material is deposited, allow the creation of low high resistance traces on the active sensing area (which causes it to heat when voltage is applied), and lower resistance contacts. The sputtering conditions used facilitate formation of the fine-grained dense films that are preferable for increased stability.

Following heater deposition the sensor substrates are mounted onto TO-39 headers using conductive epoxy (Figure 2). Once packaged catalyst can be applied, the sensor can be capped, the performance evaluated and sensors shipped.

Figure 2: Packaged sensor element (uncapped).

ii) Surface Area Optimization

As-fabricated AAO is amorphous with Al:O:H stoichiometry dependent upon the conditions of electrochemical synthesis. Annealing using varied temperatures and durations is used to convert amorphous AAO into a crystalline state (□-, □-, or □-alumina or the mixed states around the phase transitions) with certain grain size, surface area, and surface chemistry. Through this transformation "secondary porosity" is formed along the intrinsic pores of the AAO. This leads to a very high surface area, which leads to high catalytic volume and in turns improves sensitivity.

To determine optimum processing conditions to create high surface area sensor dies a comprehensive study was performed on the effect of annealing and catalyst deposition on specific surface area of the nanoporous AAO used in sensor fabrication. It was found that the optimal temperature to yield maximized surface area was 825°C, which leads to a surface area of >100 m^2/g, (Figure 3). Catalyst deposition following annealing was shown to have a minimal impact on specific surface area (~91 m^2/g), confirming that secondary porosity could be used in catalyst performance optimization.

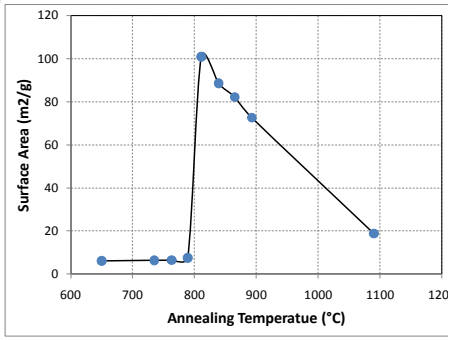

Figure 3: Surface area as a function of annealing temperature.

iii) Power/Temperature Characterization

Sensor substrates that were produced with different sized microheaters and from AAO of varying thickness were packaged characterized to compare their thermal behavior. Because Pt is a thermistor material (that is the resistivity changes predictably with temperature) the microheaters themselves were used as part of the calibration. The basic procedure was: 1) place microheater in a furnace and record heater resistance as the furnace temperature was increased; 2) at room temperature ramp a voltage (V) across the microheater and record the current (i); 3) calculate power (V/i) and power (V*i); 4) correlate the data and calculations from the two experiments to determine Temperature vs. Power curves.

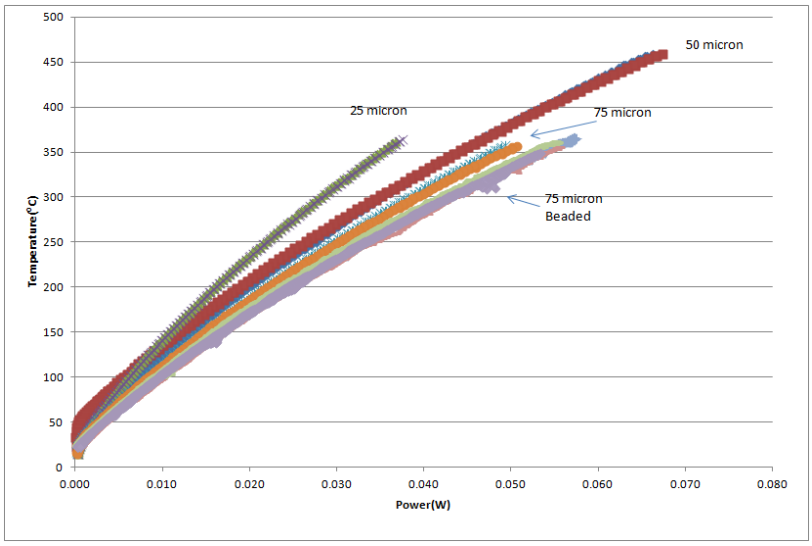

Figure 4: Temperature vs. Power curves for varying microheater thicknesses.

By this procedure it was determined that small changes in microheater dimensions had a minimal effect on power consumption, but that substrate thickness (25, 50, or 75 µm) did have a relatively large effect. Figure 4 presents data for the chosen microheater design with the three thicknesses.

iv) Heater Stability Testing

To verify that the Pt microheaters were stable over time as the sensors were operated several packaged sensor elements were continuously powered at the anticipated operating power/temperature and measurements of the microheater resistance were made occasionally. Through this testing it was verified that the Pt heaters are stable, after an initial "burn-in" period, when operated continuously at high temperatures (400-600°C for this application). **Error! Reference source not found.** presents long-term heater testing data.

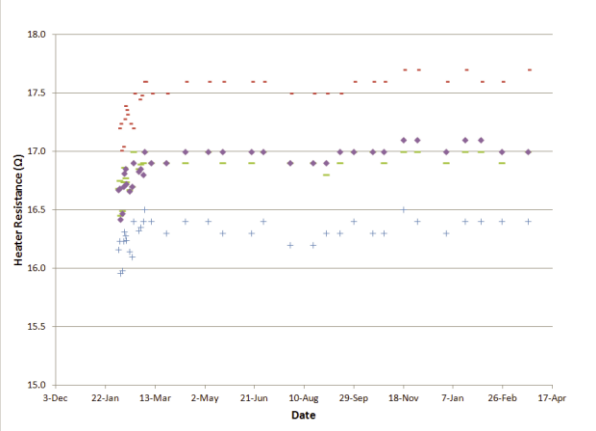

Figure 5: Microheater stability testing.

v) Physical Testing

The packaged sensor substrates that were produced with different sized microheaters and of varying thickness were also put through drop and vibration testing to determine the physical robustness of the AAO.

Vibration testing was performed based on two standards that apply to these sensors (MSHA and ISA/CSA). As Synkera does not have in-house facility to perform vibration testing this work was outsourced to a local testing house (Percept Technology Labs, Boulder, CO), after sensors were mounted by Synkera as they likely would be as part of an instrument. None of the 24 sensors tested, indifferent to microheater geometry, show any effect (cracks, change in heater resistance) following the vibration testing.

Drop testing was performed in-house using the same substrate/sensor lots. Sensors were capped for this testing (as they would be in an instrument). The sensors were then dropped on to a concrete from 1, 3, and 6 feet. In this testing it was seen that AAO thickness played a big role, with 75% of the 25 µm and 50% of the 50 µm elements breaking, while none of the 75 µm elements broke. Based on this the 75 µm was chosen to move forward with for commercial development.

vi) Modeling

Under a subcontract with Prof. Martin Dunn's research group at The University of Colorado at Boulder a high-fidelity model to allow the parametric study of variables to facilitate optimal sensor design. The goal of the model was to permit the efficient study of a wide parameter space to facilitate design decisions.

Through this effort a reasonably good thermal model of the gas sensor was developed with the help of the experiments and finite element analyses. The finite element model was used to extract the thermal properties of AAO and predict the thermal behavior of different designs. The flexible nature of the finite element model should allow for a future detailed parametric study of the geometry so as to optimize the power consumption of the device and be able to predict the thermal behavior of a new design. Also, a future study on the effect of forced convection on the device operation will be very important, since heat loss in such conditions is accelerated and will affect the functioning of the sensor. The final report on this effort is attached as *Appendix B*.

B.3. SENSOR DEVELOPMENT – INTRINSIC AAO

Due to the inherent porous structure of AAO, particularly after heat treatment (as described above), it was expected that the AAO could provide sufficient catalytic surface area without the traditional application of a ceramic bead. To try to achieve this the development was initially focused on using the AAO as the catalyst support, and the exploration of varying the catalytic precursors. The objectives of the development work with the intrinsic AAO were:

- Test the effectiveness of the AAO itself as a catalyst support
- Determine whether the high surface area AAO improves sensor response
- Determine the optimal catalyst precursor

i) Fabrication

The sensor substrates were annealed to either 750°C or to 825°C. At 750°C, the AAO does not change phase, keeping the surface area similar to that of “as prepared” AAO. The heat treatment in this case was only used to condition the Pt heaters. At 825°C, the phase change of the AAO has occurred, such that additional secondary porosity is available.

For each sensor element, a coat of the catalyst precursor was applied using a paintbrush. To maintain uniformity as best as possible, the same person applied the solution, and the solution was applied in such a manner that it formed a uniform coating on the sensor element. Due to the small size of the sensor element, this was a good method to maintain consistency.

Two coats of the solution were applied to the sensor element. Then the catalyst was calcined by running a CV on the element. Two sizes of elements were used, 150 and 50 µm. For the 150 µm sensors the calcining profile was: 0-2.2V-0, at 0.035V/s, for the 50 µm sensors it is: 0-1.5V-0 at 0.023V/s. The difference in profiles is due to the fact that the smaller (50 µm) sensors have less mass and thus required a lower input to heat to an equivalent temperature to the larger elements. A test protocol was then run, in which the sensor was placed into a sealed chamber and exposed to air, then methane, and CV sweeps were taken in each. A CV sweep is an electrochemical method where the voltage is swept and the current is monitored. Performing such measurements on catalytic gas sensors provides information regarding the magnitude of response and where the power plateau occurs. The maximum voltage for testing CVs was 0.1 V below that of the calcining profile. This process was repeated until an optimum catalyst loading was achieved.

Multiple catalyst precursors were explored. In each case the palladium salt loading was approximately 6 wt%. The solutions were:

- Palladium nitrate in 1M nitric acid (baseline solution)
- Palladium nitrate in methanol
- Palladium nitrate with citric acid in methanol
- Palladium acetate in methanol

- Palladium nitrate with citric acid in water

ii) Testing

The original palladium nitrate in 1M nitric acid was the best performing catalyst precursor based on the CV sweeps. The solution had the highest sensor response at a given power. Additionally, it was easiest to apply to the AAO elements, and had the longest shelf life, thus was determined to be most desirable of all the solutions for eventual manufacturing. As is seen in Figure 6, the Pd nitrate in nitric acid sensors had a response of nearly twice that of the next best solution. No longevity experiments were conducted on these sensors to determine if the catalyst precursor effects the lifetime of the sensors.

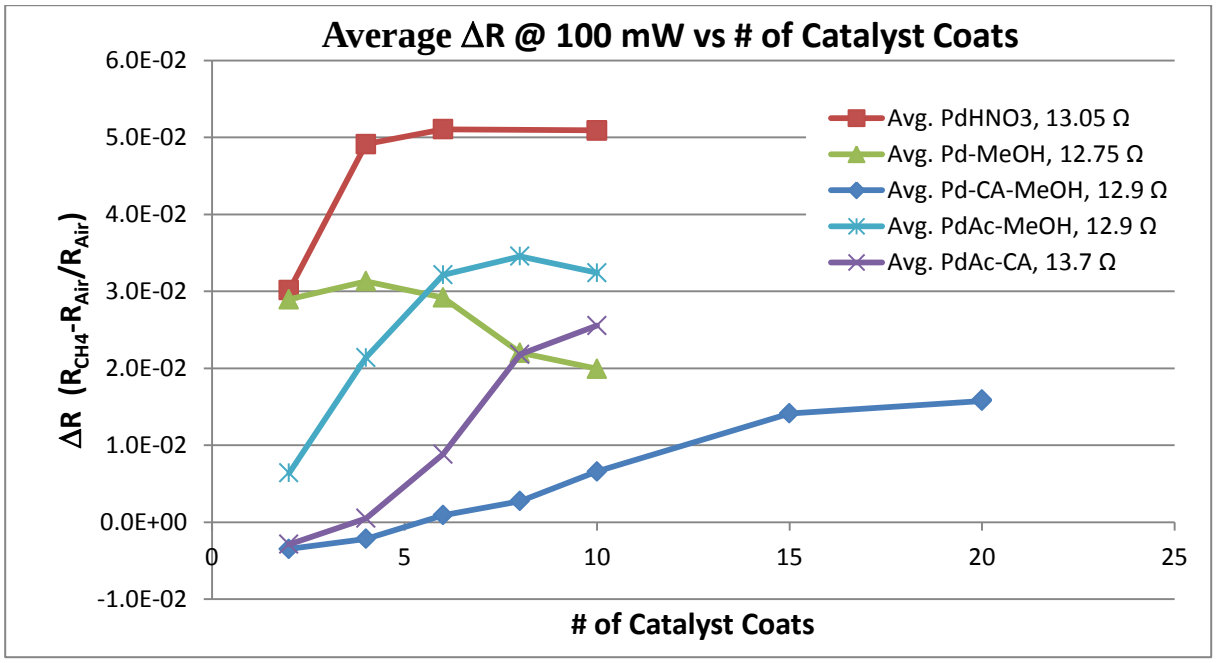

Figure 5: Average delta R response for set of sensor elements made from each type of catalyst precursor versus the number of coats of catalyst applied.

When the effect of annealing temperature was tested (same catalyst precursor used), the results were surprising. The lower surface area AAO (750°C annealed) actually provided a much higher response than the higher surface area AAO. We speculate that this is because the secondary pores that are created during high temperature annealing, which lead to the very high AAO surface area, are too small, and not accessible for reaction. Also, the catalyst particles are likely to be larger than the secondary pores, and with the addition of more catalyst solution, the overall active catalyst surface is diminished. The response of identically prepared sensors, with differing surface area can be seen in Figure 7.

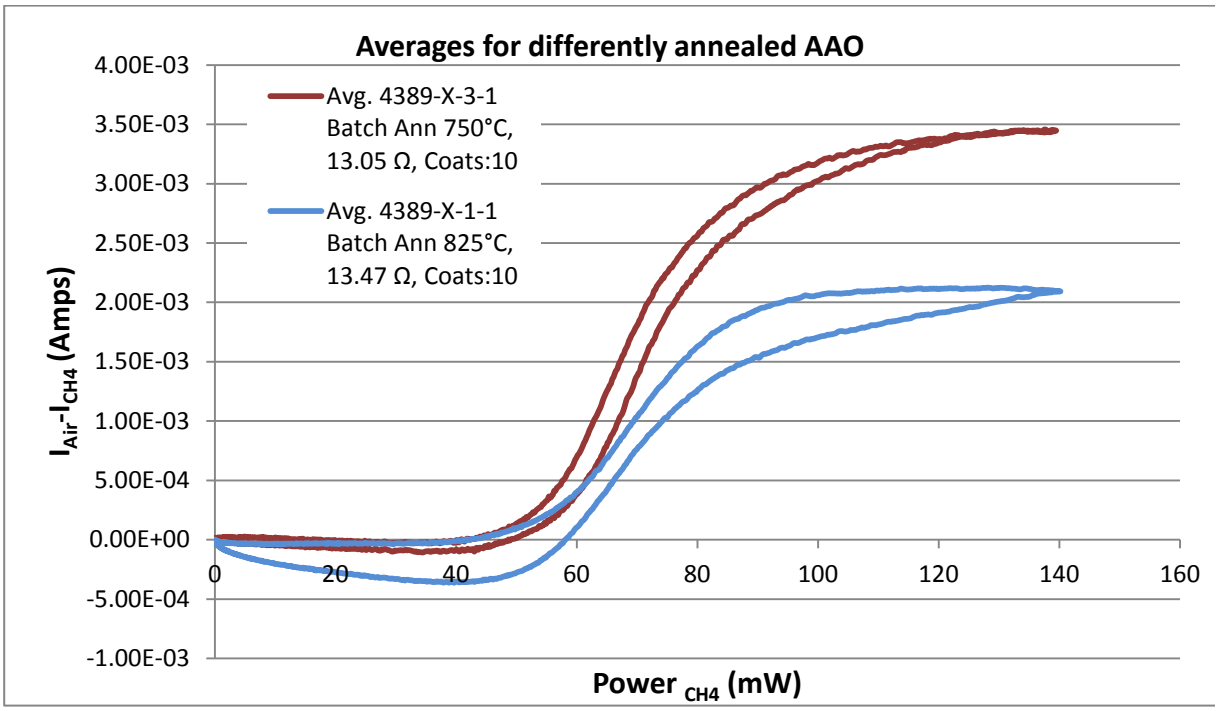

Figure 6: Comparison of the response for sensors with high and low surface area.

Additional details of the sensor development using intrinsic AAO is found in *Appendix C*.

B.4. SENSOR DEVELOPMENT – BEADED ELEMENTS

Ceramic beads, as are traditionally used with this type of sensors were considered following noted shortcomings using the intrinsic AAO as the catalyst support. The beads were applied to the sensor elements in order to improve the sensor response and lifetime. The application of a support bead provides substantially more catalytic surface area, thus increasing the sensor response, as more of the test gas is combusted. By changing the chemistry of the support material, the lifetime of the catalyst (and thus the sensor) can be extended. Two types of bead materials were examined. A high surface area alumina nanopowder was used to increase the surface area, with little to no change in the surface chemistry as compared to the AAO. A mixture of ceria-zirconia nanopowder was used to both increase the surface area compared to the AAO only, and to increase the amount of lattice oxygen accessible to the catalyst.

i) Fabrication

The alumina beads were formed using a ~4wt% □-Al_2O_3 powder in water suspension. The alumina powder has a surface area of 100 m^2/g, and particle size of 0.01 – 0.02 µm. The cerium-zirconia beads were made using a cerium (IV) oxide -zirconium (IV) oxide powder (Aldrich part number: 634174) with equimolar amounts of cerium and zirconium and a particle size of < 50 nm. Using water only, it was not possible to make a Ce-Zr suspension without precipitation issues. In order to keep the Ce-Zr powder in suspension, and retain reasonable fluid properties, it was mixed with ammonium citrate into a solution of 1M ammonium hydroxide. The dispersant (ammonium citrate) was always 2 wt% of the powder, and the amount of ammonium hydroxide used depended on the desired viscosity of the resulting suspension.

The suspension was applied to the entire length of the heater elements of the sensor using a brush under a microscope and letting the solution dry in air for a few seconds. The bead was built up by applying additional coats of the powder suspension, typically about 16 coats. For this method the bead size was made as consistently as possible, but differed in size based on the person making the bead. The element was then heated to 85mW to sinter the bead. The desired catalyst was then applied to the bead.

Due to the variation in bead sizes, and the inefficiency of the bead application method, a new method was explored to deposit beads quickly and reproducibly. This was done using a modified screen printing method. A screen was made such that it could be placed atop a snapstrate (4x4 sensor substrates connected together) and the holes lined up with the elements. A thicker paste like solution was then applied into the holes of the screen. This technique was easier to implement, and resulted in beads of a more consistent size. Additionally, it was far easier to create beads of smaller length, which covered only the heated zone. While this method was not optimized, feasibility was shown and with additional work should become a robust manufacturing process.

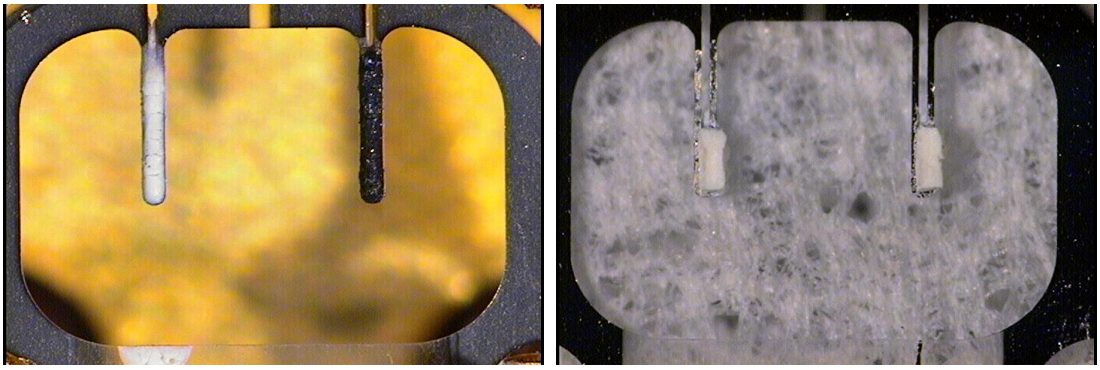

Figure 7: Sensor made using brush method to apply beads (L), beads made using screen method (R).

iii) Testing

About 20 groups of sensors were fabricated for testing. The variables included application method, bead material, catalyst, and amount of bead material and/or catalyst applied. A summary of the sensors is presented in Table 1.

Table 1: Beaded sensors produced and tested.

LttA	1st dual element cat on AAO
LttB	single element cat on AAO for CVs
LttC	2nd batch duel elements on AAO
	"baked" dual element cat on AAO as snapstrate, then oven fired
LttD	"activated" dual element cat on AAO
LttE	PhI beaed and companion duel element cat
LttF	Beaded replicates of LttE
LttG	Beaded from calcined Pd-Al2O3, single element
LttH	#1: fast bead - fast Pd-catalyst-12 coats
	#2: fast bead - fast Pd-catalyst-10 coats
	#3&4: fast bead - fast Pd-catalyst-10 coats
LttJ	fast process - 1:1 Pd: Pt (Pd/Pt#1) - 10 coats
LttK	fast process - 2:1 Pd:Pt (Pd/Pt#2) - 10 coats
LttL	fast process- 1.5:1 Pd:Pt - 10 coats - heater down
Ltt M	fast process- 3:1 Pd:Pt - 10 coats - heater down
LttN	fast process- Pd - 10 coats - heater up
LttP	fast process- 1.5:1 Pd:Pt - 10 coats - heater up
LttQ	fast process- Pt (tetraamine Pt-nitrate in 1M HNO3) - 10 coats - heater down
LttR	fast process-power supply- Pd - 10 coats
LttS	blank sensor for heater stability testing
LttT	Ce-ZrO2 beads with Pd cat; 12c fire after each 2c
LttU	Ce-ZrO2 beads with 2:1 Pd:Pt cat; 12c fire after each 2c
LttV	Ce-ZrO2 beads with 2:1 Pd:Pt cat; 12c fire after each 2c
Ltt W	As U & V with "thin" Ce-ZrO2 beads
LttX	As U & V with "ultra-thin" Ce-ZrO2 beads
LttY	As U & V with Ce-ZrO2 bulbs at end of element

Two different types of testing were performed on these dual element sensors: CV's (as described above) and bridge testing. CV's were used for sensor screening and bridge testing was used to thoroughly evaluate sensors. A Wheatstone bridge is typically used to measure the output of catalytic sensors. As shown in Figure 8, four circuit branches are arranged in a square. The source of the electrical current is connected, and between the other pair of opposite corners, the output measurement circuit is connected. In operation a balanced bridge has no output signal. When the gas burns on the active sensor surface, the heat of combustion causes the temperature to rise, which in turn changes the resistance of the sensor element with catalyst applied. As the bridge is unbalanced, the offset voltage is measured as the signal. It is important that the reference sensor or

bead maintains a constant resistance during the exposure to the combustible gas; otherwise, the measured signal will be inaccurate.

At different points in the development of the beaded, dual element sensors the best performing sensors to date were selected for characterization. Testing included: operating power, linearity, calibration, repeatability, hydrocarbon range, humidity, environmental temperature, and sulfur resistance. Long term stability was also performed on the sensors. These test reports are included as appendices:

- *Appendix D* – LttE
- *Appendix E* – LttH, LttJ, LttK
- *Appendix F* – LttM, LttN
- *Appendix G* – LttT, LttU

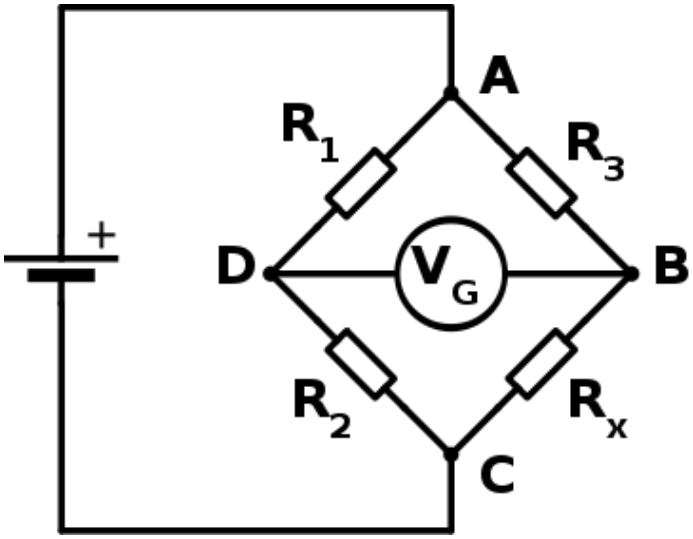

Figure 8: Wheatstone Bridge.

Through the development effort it has been determined that a palladium only catalyst on a cerium oxide/zirconium oxide bead is the desired system to move forward with. This system provided the best combination of low power consumption, gas response and sulfur resistance.

B.5. SENSOR PACKAGING

Because the sensors under development operate at high temperature (400-550°C) and they are used in environment where flammable gas mixtures may exist, the possibility of the sensor itself being an ignition source must be considered. While it may be possible that the small size and low power of the sensor being developed by Synkera could make it an intrinsically safe device, this is not certain and cannot be determined without extensive approval agency testing (that was not within the scope of the Phase II effort). Because of this, packaging the sensors in an explosion proof (XP) package was investigated. Gas sensors and instruments are typically made explosion proof through the use of sintered metal flame arrestors. By preventing the gas within the sintered metal housing, where the ignition source is contained, from burning back into the environment ignition is prevented. This works because the high thermal conductivity of the porous sintered metal flame arrestor cools the flame front or combustion wave by absorbing and dissipating the heat of the flame.

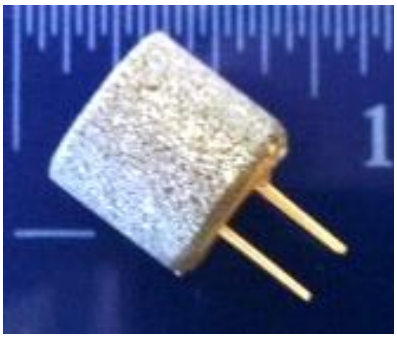

Figure 9: Sensor with sintered metal cap.

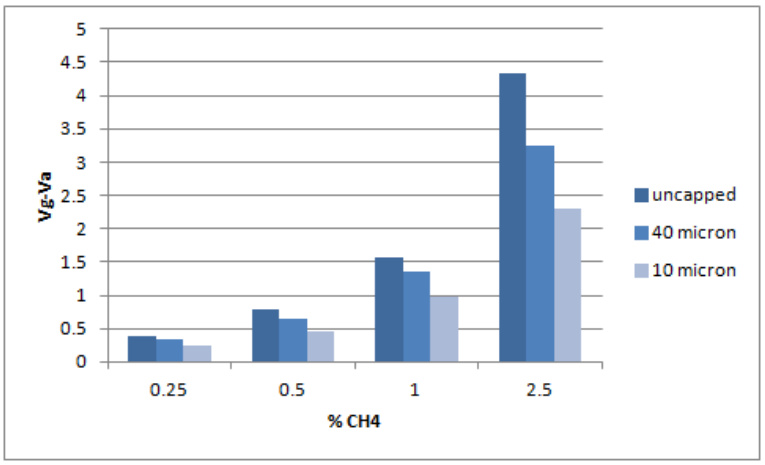

Figure 10: Effect of caps on magnitude of sensor response.

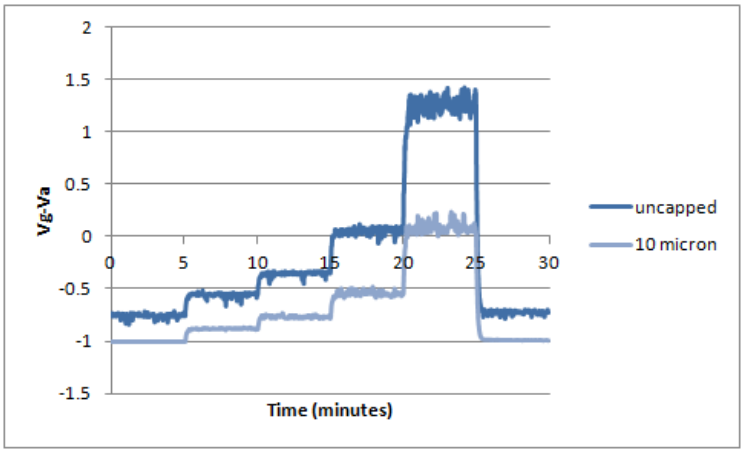

Figure 11: Effect of response time of sintered metal cap.

As part of this process Synkera acquired some porous sintered metal caps, of different media grade, packaged sensors using these caps, and performed some testing. A sensor packaged in this manner is shown in Figure 9. Comparisons were made between sensors packaged with standard caps (not porous metal), caps with 10 micron media, and caps with 40 micron media.

The two key performance characteristics considered were response magnitude (sensitivity) and response time, as these caps can influence both.

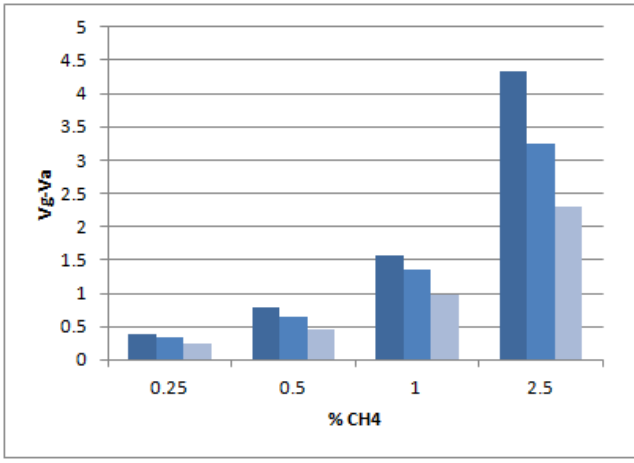

Figure 10 shows the response magnitude comparison for the different experiments and Figure 11 presents the response curves. While this testing indicates a slight decrease in response magnitude the response time is not significantly affected. Based on this information it should be possible to implement such packaging if necessary to make the sensors explosion proof.

B.6. ELECTRONICS DEVELOPMENT

A revised bridge circuit design was completed and built during Phase II. This redesign addresses many of the limitations associated with the original, analog circuit designed and implemented during Phase I. The aim of this circuit was a multifunctional tool that can be used as a stand-alone evaluation circuit, or integrated as discreet circuits as part of larger test systems. The requirements used to define the new module included:

- Microcontroller based to remove the need for large numbers of analog inputs through DAQ cards to enable easy scaling of test systems
- USB connectivity
- A small PCB footprint (2" x 3" max)
- A means to adjust the power delivered via the microcontroller for development flexibility (80 mW to 200mW to bridge, ~1% adjustable bridge bias, 200mV to 2.5 V)
- Ability to power sensor elements with individual heater resistances in the range of 10 to 25 ohms
- Accommodation to operate the sensor off the board (external sensor hookup)
- Analog outputs, in addition to the digital outputs, to allow monitoring directly from the circuit

In addition to the basis provided by the Phase I circuit, the redesign drew concepts from more recent circuit designed prepared by Synkera for operating other sensors in our product line. Descriptions of the key design aspects of the new bridge circuit follow.

i) Bridge Bias Control

In order to have an adjustable bridge excitation voltage a circuit was developed that will allow a PIC18F6J50 microcontroller to change the bridge excitation voltage based on feedback on the applied voltage, current, or power. To obtain the adjustable bridge voltage a LT3021 voltage regulator was used in conjunction with the MCP4152 digital rheostat. The IC's are configured per Figure 12.

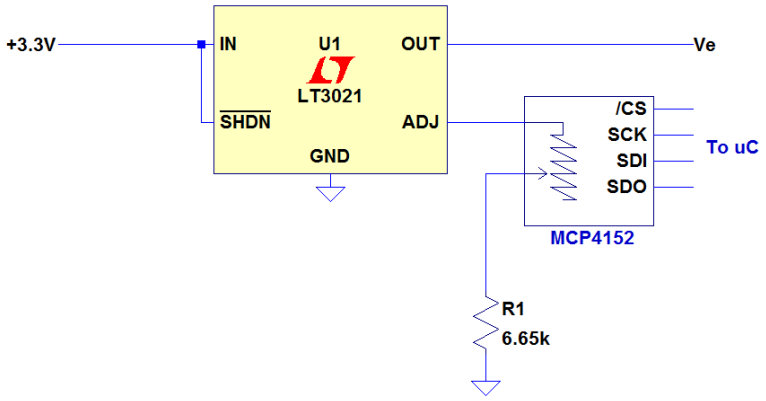

Figure 12: Circuit to produce a digitally controlled, adjustable voltage to the bridge.

The circuit uses an SPI interface with the microcontroller to change the rheostat's resistance from anywhere between 0 and 100 kΩ in steps of 390 Ω. This adjustable resistance allows the output voltage of the LT3021 to be changed digitally by the following equation:

$$\mathrm{Ve} = (0.2\mathrm{mV})[1 + \frac{\mathrm{R_{pot}}\ \Omega}{6.65\ \mathrm{k\Omega}}]$$

This sets the maximum, minimum, and step size:

$$\mathrm{Ve_{maximum}} = (0.2\ \mathrm{mV})\left[1 + \frac{100\mathrm{k}}{6.65\mathrm{k}}\right] = 3.21\ \mathrm{V}$$

$$\mathrm{Ve_{minimum}} = (0.2\ \mathrm{mV})\left[1 + \frac{0}{6.65\mathrm{k}}\right] = 0.2\ \mathrm{V}$$

$$\mathrm{Ve_{step}} = (0.2\ \mathrm{mV})\left[1 + \frac{100\mathrm{k}}{6.65\mathrm{k}}\right] - (0.2\ \mathrm{mV})\left[1 + \frac{99.61\mathrm{k}}{6.65\mathrm{k}}\right] = 11.7\ \mathrm{mV}$$

The LT3021 can deliver up to 500mA itself, although the actually limit in this circuit will be set by the current supply of the IC delivering the +3.3V to the LT3021. For this design the max current available to the bridge is about 130 mA.

iv) Bridge Current Sensing

In order monitor the power delivered to the bridge the current as well as the voltage (Ve) must be known. To measure the current entering the bridge a simple high side current sense resistor is used with a differential amplifier. This circuit is shown in Figure 13.

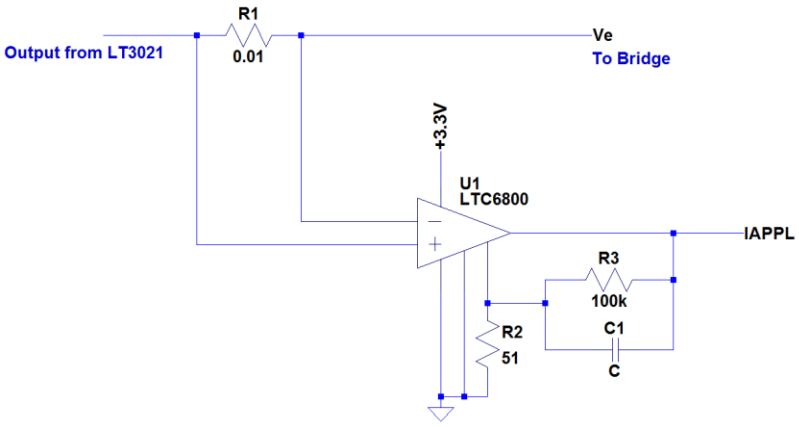

Figure 13: High side current sensing circuit.

In this design, using R1 of 10 mΩ as the current sense resistor adds a small error to the set voltage of the LT3021 so the actual voltage applied to the bridge is:

$$\mathrm{Ve_{error\_max}} = \mathrm{I_{bridge\_max}} * \mathrm{R_1} = 150\ \mathrm{mA} * 0.01\ \Omega = 1.5\ \mathrm{mV}$$

This maximum voltage drop across the current sensing resistor is negligible, as it is so small compared to the tolerance of the MCP4152 used to set the voltage in the first place.

The LTC6800 instrumentation amplifier measures the voltage drop across the current sense resistor and amplifies it before being converted by the analog to digital converter of the microcontroller. The gain of the amplifier is given by:

$$\mathrm{A_v} = 1 + \frac{\mathrm{R3}}{\mathrm{R2}} = 1 + \frac{100\mathrm{k}\Omega}{51\Omega} = 1962\frac{\mathrm{V}}{\mathrm{V}}$$

This gives a transfer function of the circuit as:

$$\mathrm{Vout} = \mathrm{A_v}(\mathrm{V_{+in}} - \mathrm{V_{-in}}) = \left(1962\frac{\mathrm{V}}{\mathrm{V}}\right)\left(\mathrm{I_{bridge}} * 0.01\ \Omega\right) = 19.62 * \mathrm{I_{in}}$$

With a maximum current that can be read as:

$$\mathrm{I_{in,max}} = \frac{\mathrm{V_{out,max}}}{19.62} = \frac{3\mathrm{V}}{19.62\ \Omega} = 153\ \mathrm{mA}$$

This means that the analog to digital conversion uses its full dynamic range while digitizing the value giving the best resolution that is attainable with the hardware on the PIC18F46J50 microcontroller.

v) Bridge Output

The sensing elements are placed in a Wheatstone bridge configuration. Using a bridge to sense the resistance change of the sensor gives two main advantages:

- Ambient temperature effects are essentially negated as both of the sensor elements shift resistance at the same rate and in the same direction, producing no change in the differential output of the bridge
- Very easy to sense small changes in resistance, automatically centered with a common mode voltage between VDD and GND.

In order to sense the output of the bridge a specialized IC was used, the MAX11213. This component uses a SPI interface to communicate to the microcontroller and has a large array of built in functions that greatly reduce the amount of components in the design. The circuit designed for this function is shown in Figure 14.

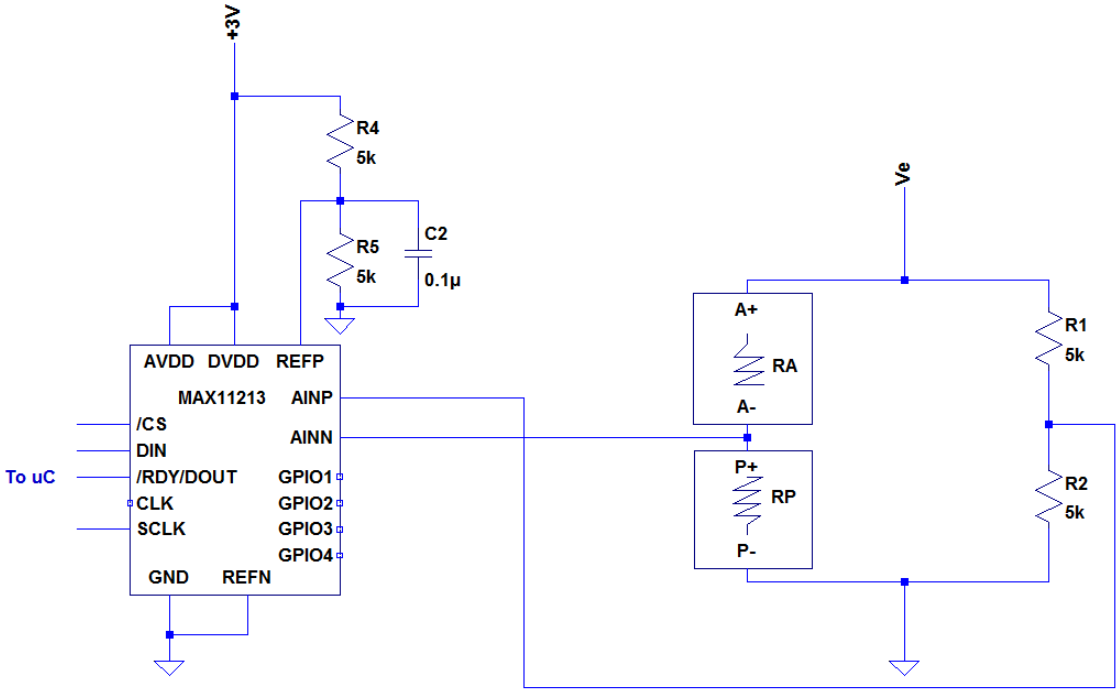

Figure 14: The sensing bridge and the MAX11213 16 bit ADC chip.

The bridge uses two 5.11 kΩ, 0.1% precision resistors for the non-element side. This value was chosen as it is high enough as to minimize current draw and thus power consumption on the one side of the bridge, but also small enough to keep any thermal noise reasonably low.

The MAX11213 has many functions which make it ideal for this application. The MAX11213 has a bipolar input setting which means that it can sense both positive and negative voltages that are present across its inputs. This is advantageous for development purposes as this allows both the active and the passive sensing elements to start at different resistances from each other in either direction and still be measured. The MAX11213 also has an internal digital offset register which will automatically correct for an initial difference in sensing elements before sending the result to the microcontroller. This means less firmware development needed for the module. Lastly, the MAX11213 has an internal programmable digital gain which further reduces the required components needed in the design.

The complete sensor module schematic is presented as *Appendix H*. An assembled, 2" x 3" prototype circuit card is shown in Figure 15.

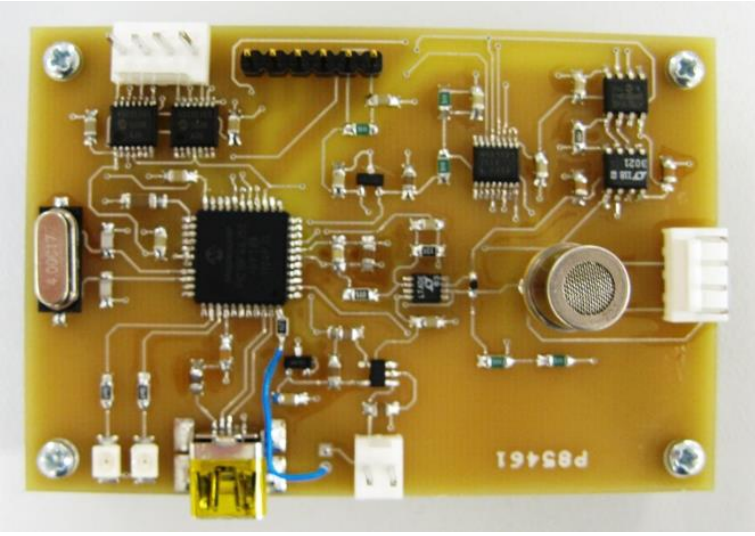

Figure 15: Circuit card.

B.7. MANUFACTURING, SCALE-UP AND COSTING

i) Manufacturing and Scale-up

The manufacturing process can be separated into the following major categories for sensor fabrication. Current status and recommended improvements are outlined.

1. AAO substrate fabrication
    - Current: Through this and related efforts the fabrication of 4 – 4x4 snapstrates on 6.5 x 6.5 cm aluminum substrates has been well established.
    - Future: For other AAO sensor products 4 - 5x5 snapstrates have been produced on the 6.5 x 6.5 cm aluminum substrates. Some AAO membrane products are produced on 10 x 10 cm aluminum substrates. These things indicate that further scaling of combustible gas microsensor substrates by increasing the snapstrate array size and/or aluminum substrate size should be feasible.
2. Pt sputtering
    - Current: A 2 x 2 array of 4x4 snapstrates are deposited on using a relatively small sputter chamber.
    - Future: A larger sputter chamber is being commissioned at Synkera, which will accommodate larger arrays and/or larger snapstrates.
3. Bead application
    - Current: Most Phase II work was performed by individually applying bead material to each element by hand, followed by applying a voltage to the elements to fire the material.
    - Future: Some effort was performed to print beads on snapstrates prior to mounting, and then firing the multiple beads at the same time in a furnace. This needs further development, but is expected to be a suitable process to utilize in manufacturing.
4. Catalyst deposition
    - Current: All Phase II work was performed by individually applying catalyst to each active element by hand, followed by applying a voltage to the elements to fire the material.
    - Future: Equipment is available to allow the semi-automated deposition of the catalyst solution. During Phase II conversations were had with MicroFab (http://microfab.com/) regarding their ink-jet dispensing technology. The impression is that this technology is suitable for the deposition of catalyst on Synkera's

combustible gas microsensors. Catalyst could be applied to snapstrates, before mounting, and fired in an oven if this method was used.

5. Sensor element mounting
    - Current: In Phase II sensor elements were mounted using silver epoxy to TO-39 headers and cured in an oven prior to bead and catalyst application.
    - Future: Other than improving efficiency through the above mentioned bead and catalyst application to snapstrates, prior to mounting, the current method is expected to be used for quantities up to at least 10,000 annually.
6. Capping
    - Current: Simple caps were super glued to headers to protect the sensor elements during Phase II.
    - Future: In production the capping method will depend whether XP is required. If it is a method for attaching the porous metal caps will need to be determined, either welding or use of an approved epoxy. If the sensors are intrinsically safe using superglue or the standard epoxy Synkera uses for other sensor products should be adequate.
7. Testing
    - Current: Bridge testing was performed on up to 8 sensors at a time using a development test system.
    - Future: For manufacturing a dedicated test system with larger capacity will be required. The first step will be a 64 position test system modeled on an existing manufacturing test system used for other sensor products at Synkera.

The fabrication of Smart Gas Cards includes the additional steps, with current ideas of how they will be carried out. For anything more than prototypes it is likely that the Smart Gas Card would be marketed and distributed by an established instrument manufacturer under their label. In this case some or all of the steps below could be performed by that company.

1. PCB fabrication and assembly
    - This will be outsourced to a local shop (such as Advanced Circuits) that specializes in this type of work.
2. Case fabrication
    - The outer case will be produced by injection molding. Many injection molding companies exist in Longmont, the state of Colorado, or elsewhere in the U.S. that will be able to meet at least initial needs at reasonable prices.
3. Assembly
    - Sensor will need to be paired with circuits, the case put around that assembly, and any labeling applied. For small quantities this will be done at Synkera. For larger quantities a contract manufacturer may be utilized.
4. Final Test/Calibration

- This will be performed in-house to ensure functionality and to assure quality. A multi-position test system for these functions (on the packaged device) will likely be designed and fabricated.

ii) Costing

Unfortunately, for the most part, the steps above described for manufacturing of the combustible gas sensors have not been developed to the point to allow for good estimates of all manufacturing costs (labor and materials). Recent analysis does indicate that blank microsensor substrates can be produced at <$2 each in volumes over 10,000/yr. Estimates for Pt sputtering indicate that the cost of Pt sputter in volumes over 10,000/yr will also be <$2 each. Packaging (non-XP) should be around $2 each in those quantities. Testing is estimated to be ~$0.50. The big unknown for this sensor is the materials deposition (bead and catalyst), as they are different than deposition methods used for other Synkera sensors. If an estimate of $3.50 each is used for the combination of these two steps (which is likely high), a total cost of manufacture of $10 each, in quantities of 10,000 sensors per year is reasonable.

C. FUTURE WORK

Continued work on the combustible gas microsensor is being performed under a DHS Phase III effort. After a successful DHS Phase II working to develop very small, low power metal oxide sensors for incorporation into mobile devices, Synkera received Phase III funding to produce a multi-gas detector specifically to protect fire fighters in the line of duty. Combustibles are included in the list of gases and the combustible gas microsensor, initially funded by NIH, is being considered for use.

i) Sensor Development

In order to enhance the sensor response, further work is recommended which builds upon the work done to date. The following table is a summary of the recommended future catalyst work and the ranking of importance.

Description	Ranking
Reliability: Batch to Batch	1
Catalyst Deposition: Pd Concentration in Solution	6
Catalyst Deposition: Calcining Rate	3
Catalyst Activation: Methane Treatment	4
Catalyst Activation: Hydrogen Treatment	5
Promoters: Mn, Re, Ru	8
Support Parameters: AAO Thickness	7
Support Parameters: Annealing Temperature	2

ii) Electronics Development

The module has been designed and a prototype built. Testing of the module has determined that a few changes need to be made to the schematic and layout. Further testing and firmware development still needs to be performed before the module is finalized and quantities of the boards are ordered.

Most of the necessary changes are minimal and will result in only small design alterations. If it is desired that the PCB is shrunk, then the layout of the new board will take some time, but is still a relatively easy job depending on the degree of reduction.

iii) Manufacturing

The processes discussed in C.7 (above) will need to be finalized and established in order to meet larger production quantities (e.g. 10,000 units annually).

D. CONCLUSIONS

This Phase II has established a viable route to new combustible gas microsensors using AAO as the base material. It has also set the foundation for producing instrumentation. Additional work is required for commercialization and scale-up, which is currently in progress. As part of a number of sensor development efforts recently completed and still in progress over the past couple of years at Synkera this Phase II has played a significant role in further advancing the state of the art for AAO based sensors and helped expand Synkera's sensor product line.

The Phase II Objectives are listed below, with comments regarding what was achieved with respect to them during the Phase II.

- *Achieve reliable and consistent sensor performance: power below 50 mW per element (active and reference), sensitivity of 50mV/% CH_4, drift <5% full scale/yr, and resistance to poisoning (10 ppm H_2S for 10 min)*

  Reliable sensor performance, and a sensitivity of 50 mV/% CH_4, was achieved for Phase II sensors at 70 mW per element. Further refinement of the AAO microheater geometry, and bead application (thinner, less massive beads) have the potential to reduce the power further. Power management schemes, such as duty cycling or operating the reference element at a lower temperature than the active element, could reduce the total power further.

  Long term drift still needs to be examined closely in further work. It is expected that additional work in the areas of better defining burn-in parameters and catalyst activation will minimize long term drift.

  The use of palladium only catalyst on a cerium oxide/zirconium oxide bead provides reasonable resistance to sulfur, as demonstrated with the "Ltt T" sensors.

- *Validate cost projections below $15 for dual-element sensors and below $50 for Smart Combustible Gas Card™ for projected volumes above 10,000/yr.*

  Based on work during Phase II and other related sensor efforts, a sensor cost of $15 for sensors in quantities of 10,000 per year is feasible. From work on other instrumentation efforts at Synkera, a cost of $50 for a Smart Combustible Gas Cardin those quantities is possible, but will depend on the required (and desired) features for the device.

- *Demonstrate 1 week continuous operation of Smart Combustible Gas Card™ prototype between battery recharges*

  A complete Smart Combustible Gas Card was not produced during Phase II, as more effort in the development of the sensor itself was undertaken. Based on the current power consumption, ~140 mW total for both elements (active + reference), it is unlikely that 1-week between charges is possible with the current sensor. In discussions with customers and end-users this may not be critical, as this type of instrument is typically charged at the end of every shift. Through additional development power reduction will still be a target, which will allow longer times between charges. Also, implementing different power management schemes, such as operating the reference element at a lower temperature or using duty cycling, could reduce the overall power consumption.

- *Secure partnerships and financial commitments in support of commercialization.*

  Under additional funding from the Department of Homeland Security for the development of a multi-gas instrument for use by fire fighters the combustible gas microsensor, as developed under this Phase II, is being considered for inclusion in that instrument.

List of Appendices

A: Product Requirement Specification (PRS)

B: Final Report on Modeling effort at University of Colorado

C: Summary of development of using intrinsic AAO

D: Evaluation of LttE

E: Evaluation of LttH, LttJ, and LttK

F: Evaluation of LttM and LttN

G: Evaluation of LttT and LttU

H: Sensor module schematic

Appendix A

Product Requirement Specification (PRS)

SYNKERA
Template: 001-000-085 Rev A

Sensor Product Requirement Specification (PRS)
Sensor: MikroKera Combustible

Item #	Category	Design Target Name/Class	Design Target Value	Design Target Units	Source of Design Target Value	Flexibility	Confidence	Top Five	Comments
1	Sensing	Sensitivity	> 100	mV per % methane	Proposal	G	3		E2V: >20 mV / % CH4 Could consider lowering due to benchmarking
	Sensing	Zero offset range	+/- 20	mV max	Benchmarking	Y	4		
2	Sensing	Range	0.1 to 5	% methane	Benchmarking	R	5		based on E2V VQ22
3	Sensing	Response Time	< 10	seconds to T50	Benchmarking	Y	4		Proposal said <2 s; ISA lists t50 <= 20s, t90 <=60s
4	Sensing	Linearity	0.95	R-value for curve match up to 3% methane	Synkera Opinion	Y	3		Note that e2V simply says "linear"
5	Sensing	Accuracy	+/-3% of full scale from 0-2.5% gas, +/-5% of full scale from >2.5% to 5% gas	% of full scale reading	Standard	Y	4		Among ISA, MSHA, CSA, most stringent is CSA: +/-3% of full scale from 0-2.5% gas, +/-5% of full scale from >2.5% to 5% gas
6	Sensing	Short-term Repeatability	+/-5% of full scale or +/-10% of reading, whichever is greater for 6 brief exposures to 45-55% LEL gas at 10 min intervals over 1 hr.	% of full scale reading or % of reading	Standard	Y	3	2	from CSA standard
7	Sensing	Selectivity	responds well to alkanes		Synkera Opinion	Y			testing to hexane
8	Sensing	Poison Resistance	10 ppm H2S	10 minutes	Proposal			3	
	Sensing	Maximum gas concentration	5%	CH4	Benchmarking	R	5		
9	Reliability/Life Expectancy	Stability (Sensitivity Drift)	<2.5%	full scale per month	Benchmarking	Y	4	4	e2V
10	Reliability/Life Expectancy	Baseline Drift	< 5	% per year	Proposal	Y		5	e2V: <0.75mV/month
11	Service/Maintenance	Calibration Frequency	> 6	months		Y			
12	Reliability/Life Expectancy	Lifetime	>12	months	Benchmarking	Y	3		
13	Environmental	Operating Temperature Range	-40 to 60	Celsius		Y			
	Environmental	Zero offset with temperature	<= 0.2	% CH4 from 20C to -10C and +40C	Benchmarking	Y			e2V
14	Environmental	Storage Temperature Range	-40 to 85	Celsius		Y			
15	Environmental	Operating Humidity Range	0 to 95	%RH non-condensing		Y			
16	Environmental	Storage Humidity Range	0 to 99	%RH non-condensing					
17	Electrical	Power Consumption	< 100	mW	Synkera Opinion	Y		1	for 2 elements
18	Electrical	Operating Mode (Always On, Cyclic)	Always On		Benchmarking	Y			
19	Electrical	Operating Current	33	mA	Synkera Opinion	Y			based on power consumption, note most competitors spec current, not power
20	Electrical	Bridge Supply Voltage	2.9 to 3.1	volts	Benchmarking	Y			e2V
21	Electrical	Warm-Up Time	Reads zero +/-5% of FS within 5 min	minutes	Synkera Opinion, Standard	G			CSA standard: allows manufacturer to specify time to read zero +/-5% of FS
22	Electrical	Heater Resistance	10	ohm	Synkera Opinion				
23	Electrical	Heater Variance	1	ohm	Synkera Opinion	Y			
24	Electrical	Heater Matching	0.5	ohm	Synkera Opinion	Y			
25	Packaging	Header Type	TO-39	Low profile Micro					
26	Packaging	Cap Type	fritted cup						as option if IS rating not achieved
27	Packaging	Element Attachement	Epoxy	P-1011					
28	Packaging	Cap Attachement	Epoxy						EN specified potting compound

Flexibility Specification

Green -- very flexible or no current specification

Yellow -- preferred, an estimate or can be changed to improve overall product

Red -- fixed specification unless some important factor forces a change.

Confidence Specification

1 low confidence (we think this is what the customer wants)
5 extremely high confidence (well supported by direct or indirect market research
Lower confidence rating encourages target to be re-evaluated as project is developed.

29	Packaging	Enclosure Material							
30	Market/Volume	Sinter Material							
31	Market/Volume	Pin-Out	1 - Active + 2 - Reference + 3 - Reference - 4 - Active -		Proposal				
32	Reliability/Life Expectancy	Warranty							
33	Cost	Initial Expected	$25		Proposal				
34	Regulatory	Projected Full Production	50,000	units/year					
35	Regulatory	Initial Expected Volumes	1000						
36		Projected Full Production Volumes	$15	each					
37	Regulatory	Relevant Standards	ISA, CSA, MSHA, ATEX, IECE						
38	Regulatory	Hazardous Location Certs.	Yes						

Appendix B

Final Report on Modeling effort at University of Colorado

FINITE ELEMENT BASED THERMAL MODELING OF ANODIC ALUMINIUM OXIDE BASED GAS SENSOR

Narasimha Boddeti and Martin L. Dunn,
Department of Mechanical Engineering,
University of Colorado at Boulder.

Objective

The goal of this study is to develop a parametric Finite Element (FE) based thermal model of Anodic Aluminium Oxide (AAO) based gas sensor developed by Synkera Technologies Inc. The primary objective is to understand the heat loss mechanisms from the micro-heater used in the sensor (Fig. 1) so as to optimize the power consumption and/or geometry of the micro-heater. This is important so as to ensure a robust, efficient and reliable design of the gas sensor without losing its sensitivity.

Gas Sensor Design

The design of the gas sensor used in this study has a square AAO die of side length 5.64 mm and thickness 50 μm (can vary) with the corners filleted (colored light gray in Fig. 1). A layer of sputtered platinum of thickness 600 nm, deposited on the AAO (shown in black in Fig. 1) acts as the electrical contact. Another layer of platinum with thickness 300 nm is deposited over the contacts as well as the red area shown in Fig. 1. The red area acts as the heater and is used to keep the sensor operating at a specific temperature (~ 500 ^{o}C) with a given power supply rate (50 mW – 100 mW).

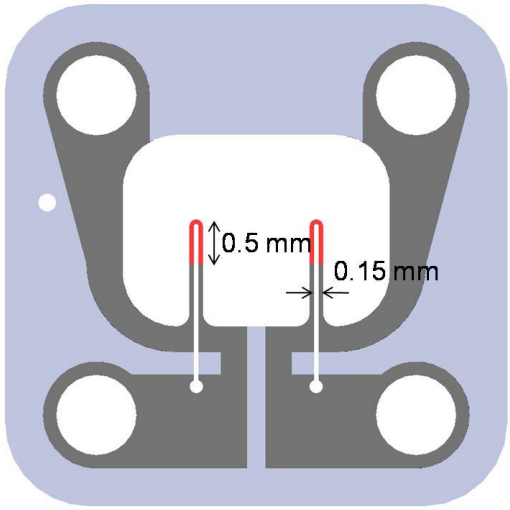

Fig. 1 – Gas Sensor Design (Revision 2.1)

Theory and Modeling

The finite element analysis software Abaqus has been used for modeling and simulating the gas sensor thermally. The finite element method solves the three dimensional heat transfer equation (Eqn. 1) numerically

at discrete points within a control volume subject to prescribed boundary conditions and initial conditions to give a temperature field. From the temperature field, other quantities like heat fluxes can be obtained.

$$\frac{\partial Q}{\partial t} = \nabla . k \nabla T + P \qquad (1)$$

Here in equation 1, Q is the heat energy, T is the temperature, t is time, k is the thermal conductivity and P is the heat source. The FE method can solve either the full transient problem or the steady state problem (steady state implies ∂Q/∂t term can be neglected). We solved the steady state problem, since the transient effects are assumed to be irrelevant as far as the primary objective is concerned. Also, the sensor being light weight, its capacitance should be small and hence the time required to reach steady state should be small too. It should be noted that the effect due to coupling of mechanical deformations with the thermal analysis is not considered in this study. In other words, we dealt with uncoupled steady state heat transfer problem in this study.

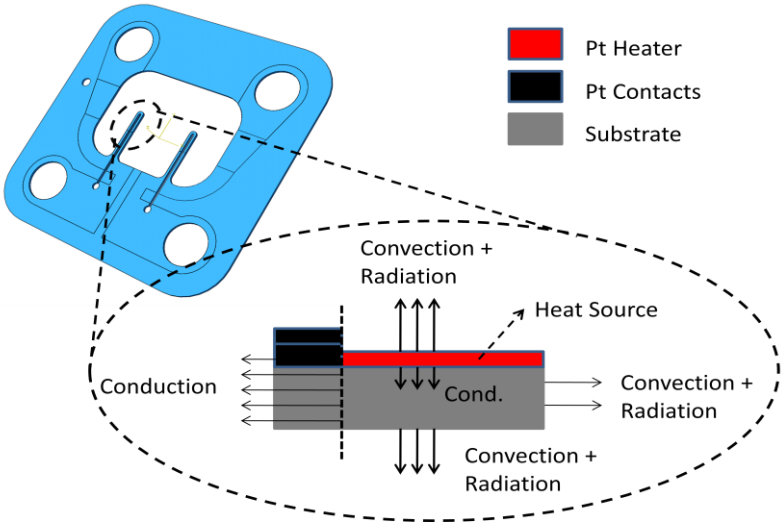

Fig. 2 - Schematic of the side view of the heater showing the heat loss mechanisms from the heater

The thermal load (or heat source) in the sensor is provided by the resistive heating of platinum micro-heaters (shown in red in Fig. 2). This thermal load is modeled as a uniform body heat flux coming out from the volume occupied by the heaters. The heat loss mechanisms from the micro-heater that have been identified in the model are free/natural convection and radiation to the ambient air from the heater and conduction to the rest of the sensor through the platinum contacts and AAO. In the FE model, the convection and radiation mechanisms are modeled as boundary conditions applied to the appropriate surfaces. In Abaqus, radiation boundary condition is implemented as,

$$q = \varepsilon\sigma(T^4 - T_0^4) \qquad (2)$$

This formula can be recognized as the Stefan-Boltzmann law, where q is the heat flux across the surface, T is the temperature at that particular point on the surface, T_0 (295 K) is the ambient temperature, ε is the emissivity of the material and σ is Stefan-Boltzmann constant. The convection boundary condition is implemented as,

$$q = h(T - T_0) \qquad (3)$$

where h is convection heat transfer coefficient of the material.

Literature Survey

It is now clear from the previous section that the material properties required for the uncoupled thermal simulations are thermal conductivities of sputtered Platinum (Pt) and AAO (kPt and kAAO), emissivities of Pt and AAO and convection heat transfer coefficient (h). From the experiments performed by Synkera, it has been observed that the electrical properties of sputtered platinum are close to those of bulk platinum which should indicate that thermal properties should be close to those of bulk platinum as well. Hence a value of kPt = 71.6 W/m/K, the bulk thermal conductivity of Pt has been used in the FE model. The emissivities have been obtained experimentally by Synkera to be 0.77 and 0.80 for Pt and Alumina respectively. The thermal properties of AAO are still an unknown and hence a literature survey has been done. It has been found that they depend on the method of preparation, porosity and the crystal structure. Thermal conductivity values ranging from 1.0 to 26.0 W/m/K have been found in the literature (see Table 1). Expectedly, amorphous alumina has a low thermal conductivity of about 1.0 W/m/K and crystalline alpha-alumina has a higher value of about 26.0 W/m/K.

Thermal Conductivity, k (W/m/K)	Comment	Source
0.5 – 1.0	Thick anodized aluminum coatings (25 - 90 μm).	Ogden et al. (1)
1.3 @ 300 K	Thermal conductivity of amorphous alumina templates along the nano-channel axis.	Borca-Tasciuc and Chen. (2)
1.4 @ 300 K, 1.71 @ 480 K	Amorphous anodic alumina film, 30% porosity, 30 nm pore diameter and 1.4-5.0 μm.	Cai, Yang et al. (3)
1.6 @ 300 K, 2.0 @ 340 k	Amorphous thin alumina films	Stark et al. (4)
26.0 @ 300 K	From, $k = k_0 \exp(-1.5\varphi/(1 - \varphi))$. k_0 is the thermal conductivity of solid crystalline alumina and φ is the porosity.	Zivcova et al. (5)

Table 1 - Thermal conductivity values for Alumina found in literature

It is not clear if the AAO used in the sensors consisted of crystalline alumina or amorphous alumina. Also, due to the high temperatures expected to be seen near the heater, the convection heat transfer coefficient (h) must be a function of the temperature of the heater surface. Hence, convection heat transfer coefficient (h(T)) and thermal conductivity of AAO (k_{AAO}) are both unknowns in this model.

Thermal Properties from Experiments

To determine the unknowns in the model, Synkera conducted experiments in both vacuum and ambient air. The average surface temperature of the heater as a function of the input power is obtained through these experiments. In the FE analyses, kAAO and h are varied systematically so as to identify their values by comparing the FE results with those from experiments. A reasonably fine mesh (see Fig. 3) has been used for all the FE analyses. Three dimensional quadratic heat transfer (DC3D20) hexahedron elements have been used. Each element has 20 nodes, 8 at each corner and 12 at the centers of each edge of the hexahedron. A fine mesh of characteristic element size 0.01 mm in the XY-plane is used for

the heater and a coarse mesh of characteristic element size 0.05 mm in the XY-plane is used for the rest of the sensor. Along the thickness direction, the characteristic sizes of the elements are 10 μm and 300 nm for the AAO die region and Pt region respectively.

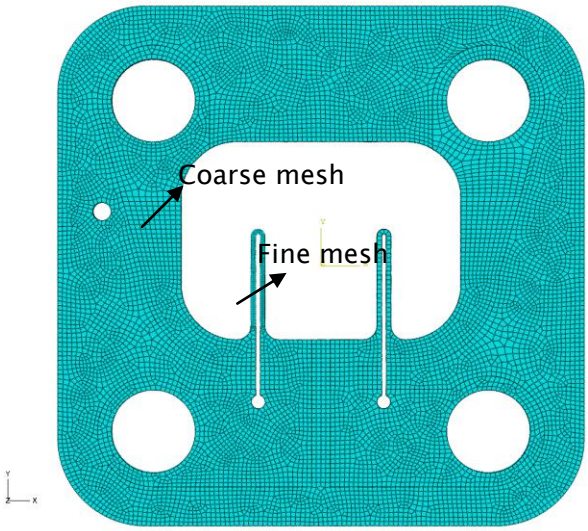

Fig. 3 - Meshing of the sensor as used in the simulations

For the experiments that are conducted in vacuum, heat loss through convection should be zero. Hence, accounting for just heat loss through radiation and conduction and parametrically changing the thermal conductivity of AAO in the FE model from 1.3 W/m/K to 20 W/m/K, we should be able to identify the actual thermal conductivity of AAO. The results are shown in Fig. 4, which shows the variation of average temperature on the heater top surface with the input power being supplied to it. It can be seen from the plots that for k_{AAO} = 5 W/m/K compares well with the experiment but tends to diverge away from experiment at higher powers (at about 25 mW). This can be attributed to slight increase in the thermal conductivity of AAO with temperature which is not uncommon in amorphous form of alumina (Ref. 3, 4).

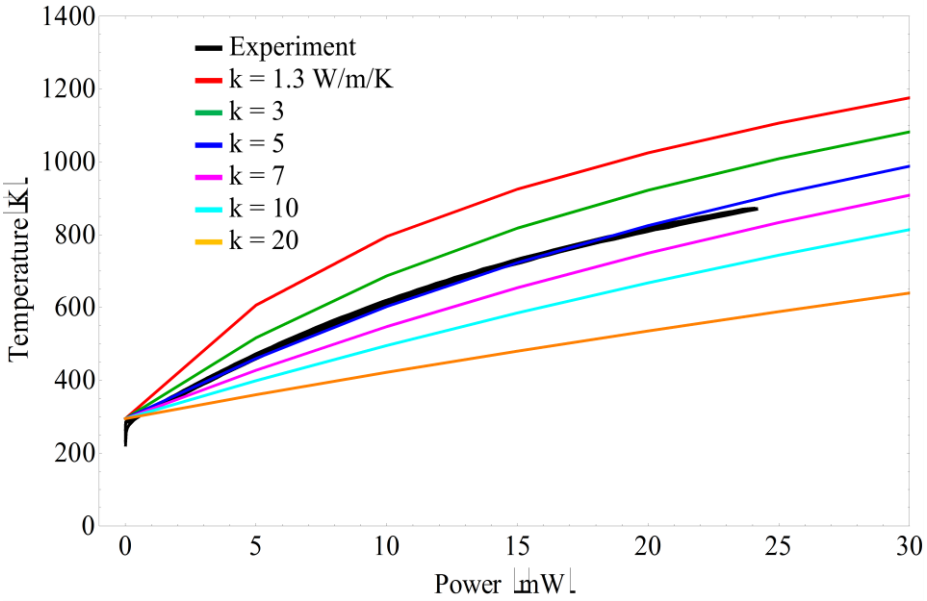

Fig. 4 - Fitting k_{AAO} using Temperature vs. Power variation in vacuum

The convection heat transfer coefficient (h) is still an unknown. To find it, we now changed h in the FE simulations parametrically from 200 to 500 W/m^2/K keeping k_{AAO} fixed at 5 W/m/K and compared the FE results with the results from experiments done in air. The comparison is shown in Fig. 5 (left). It is clear that h is temperature dependent. So, we used the points where the FE analysis curves intersect with the experiment and used them to interpolate h as a polynomial function of temperature, T as shown below.

$$h(T) = 985.292 - 5.423\,T + 0.015\,T^2 - 0.172e-4\,T^3 + 7.502e-9\,T^4 \qquad (4)$$

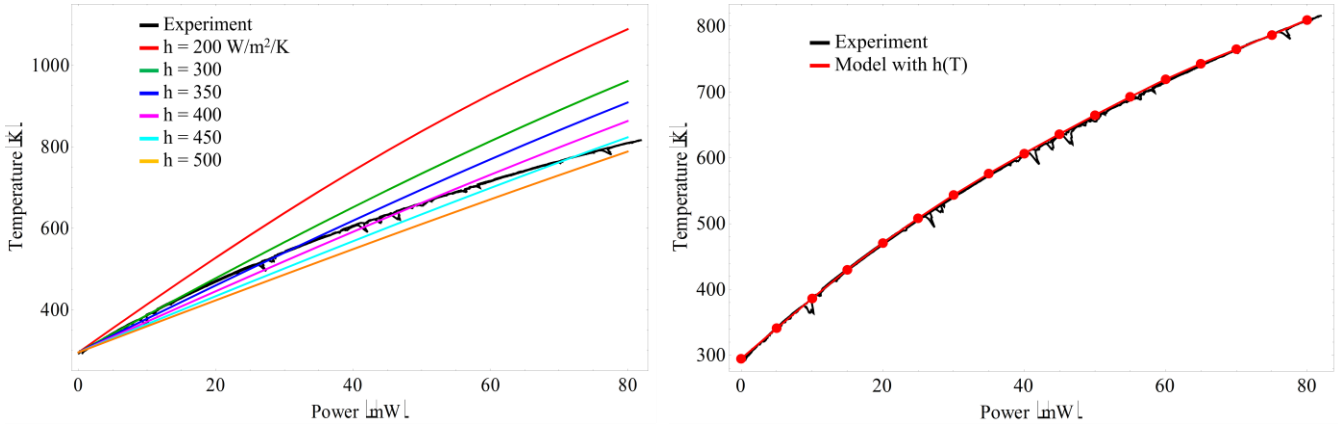

Fig. 5 - (Left) FE results with 'h' value fixed at different values, (Right) FE results with fitted h(T) compared with experiment

The plot on the right in Fig. 5 shows a comparison of the experiment with the results from the FE model with k_{AAO} = 5 W/m/K and h as a polynomial function of temperature (equation 4) (h values range from about 300 W/m^2/K at 300 K to about 480 W/m^2/K at 800 K). It is clear that we obtained a very good fit from our simulations for the convection heat transfer coefficient, h and thermal conductivity of AAO, k_{AAO}.

Results

Now, we used the developed model with the inferred thermal properties to simulate the thermal behavior of three different geometries and evaluate their performance. Apart from the original 50 μm design used in developing the model, 25 μm and 75 μm designs were evaluated.

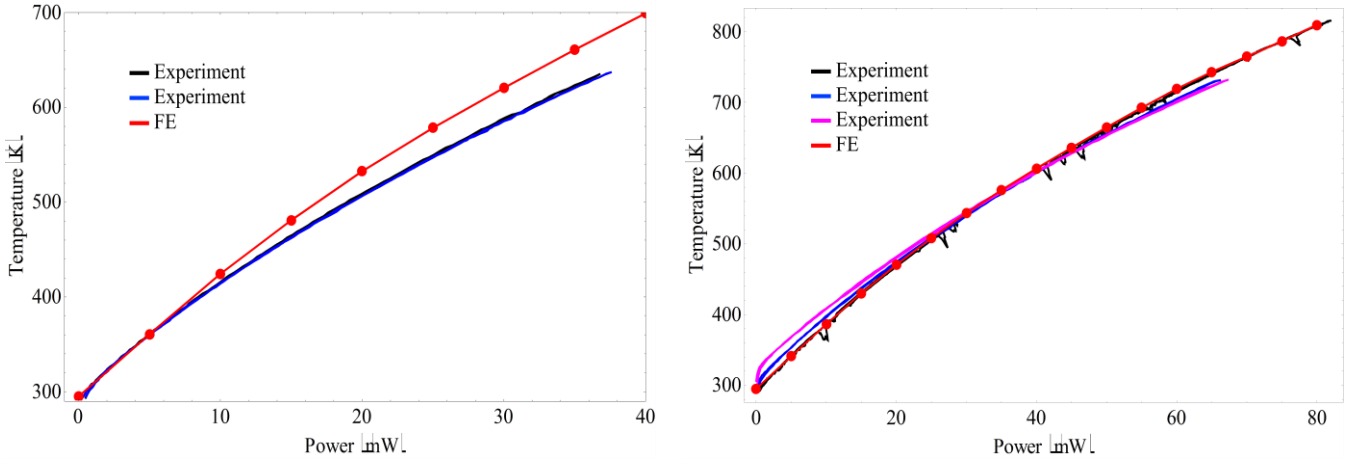

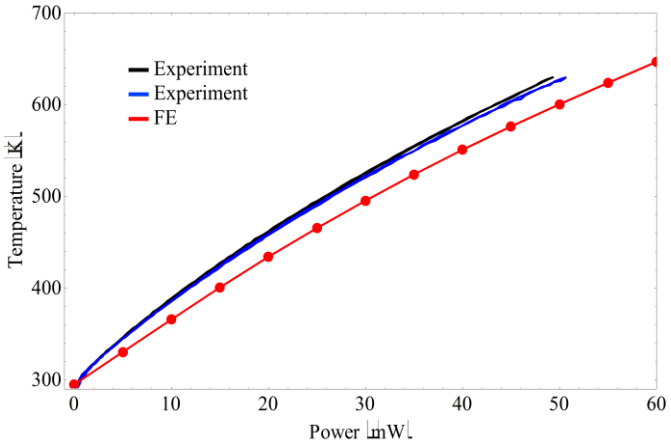

Fig. 6 - Thermal behavior of 25 µm design (top left), 50 µm design (top right) and 75 µm design (bottom)

It should be noted that 25 µm, 50 µm and 75 µm here refer to the thickness of the AAO die used in each design. The results of the FE simulations along with the experimental data are as shown in Fig. 6. It can be seen that the model predicts the behavior of the 50 µm design very well and reasonably well for 25 µm and 75 µm designs. For the 25 µm design, the model over predicts the temperature, while for 75 µm design it under predicts. We post-processed the FE results to obtain the amount of heat lost through each different heat loss mechanism. The predicted heat loss through each mechanism for each different design is compared in figure 7.

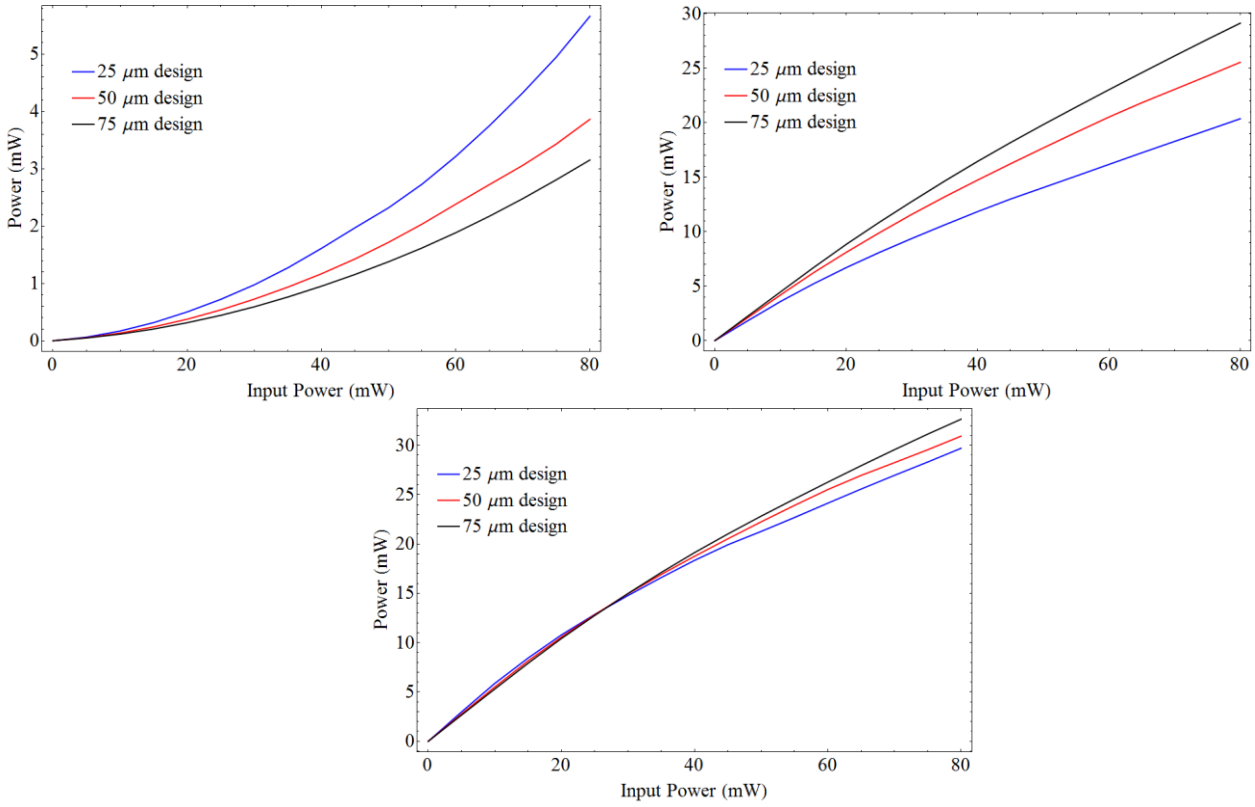

Fig 7 - Predicted heat loss through different mechanisms for radiation (top left), conduction (top right) and convection (bottom)

It can be seen that for each design, the predicted heat loss through convection roughly remains the same, whereas heat loss through conduction increases with thickness. This is to be expected as the surface area changes only slightly with the change in thickness thus causing only small changes to the convection heat loss for the different designs. But the change in thickness changes the cross-sectional area available for conduction significantly and thus the predicted trend.

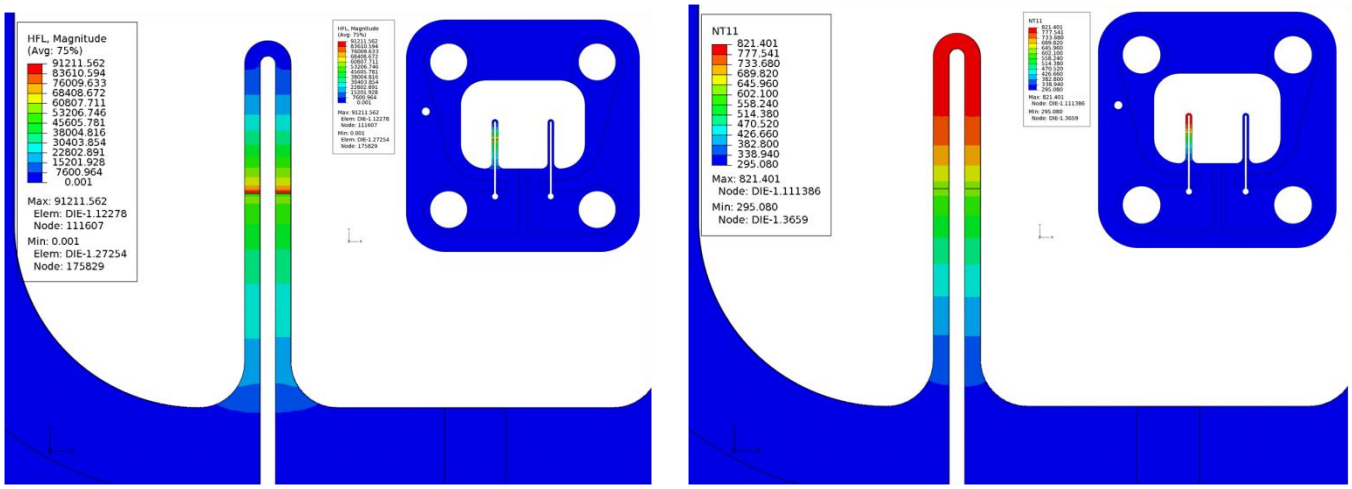

Fig. 8 - (Right) Zoomed-in Heat Flux magnitude distribution, (Left) Zoomed-in Temperature distribution for 25 μm design; Inset shows the complete distribution

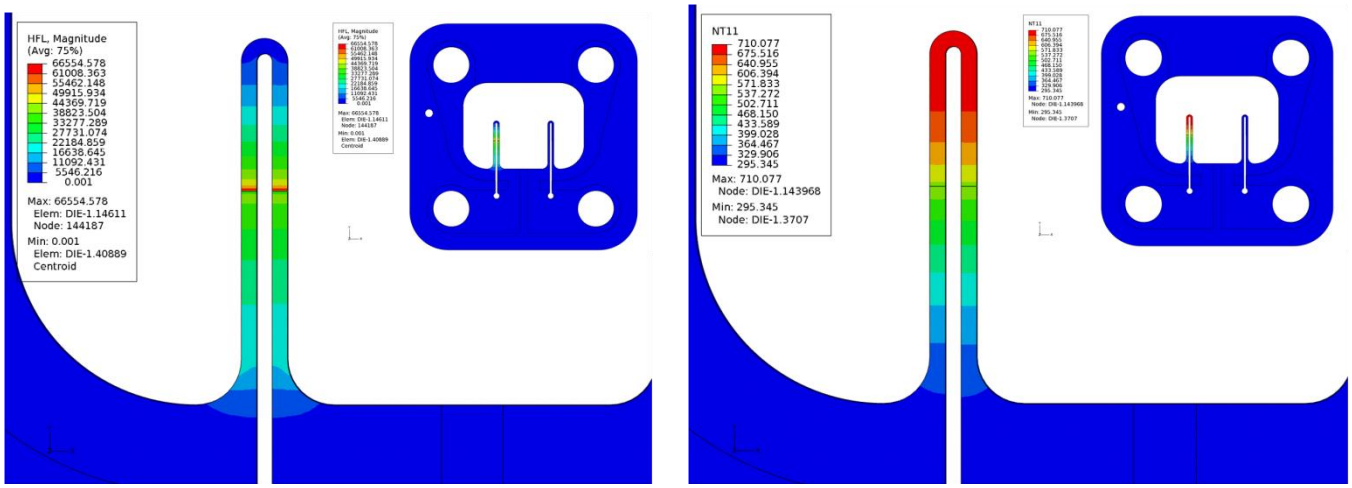

Fig. 9 - (Right) Zoomed-in Heat Flux magnitude distribution, (Left) Zoomed-in Temperature distribution for 50 μm design; Inset shows the complete distribution

The images in Fig. 8, 9, and 10 show the temperature distribution and heat flux distribution near the heater for each design when the input power is set at 50 W. The inset in each image shows the temperature distribution or heat flux magnitude distribution. It can be clearly seen from the insets that the most of the sensor is nearly at the ambient temperature while the most interesting thermal behavior is all near the heater. Also, it is clear that the tip of the heater is the hottest part of the sensor when the device is in operation and that we find the heat flux is a minimum near the same. The same information is conveyed through the plots in Fig. 11 where the temperature and heat flux variation for the three different designs at an input power of 75 mW along the heater

length starting from the base (Point A) to the tip (Point B) is shown. Since, the heat flux components in the x and z directions are negligible compared to heat flux in y-direction (shown in inset in Fig. 11), only the y-component is plotted. Due to the step in the deposited Pt film, it can be seen from Fig. 11 that there is a small jump in the temperature at about 0.55 mm distance from Point A. Though it is a small jump in terms of temperature, the temperature gradient is high enough to be seen as a sharp jump in the heat flux variation.

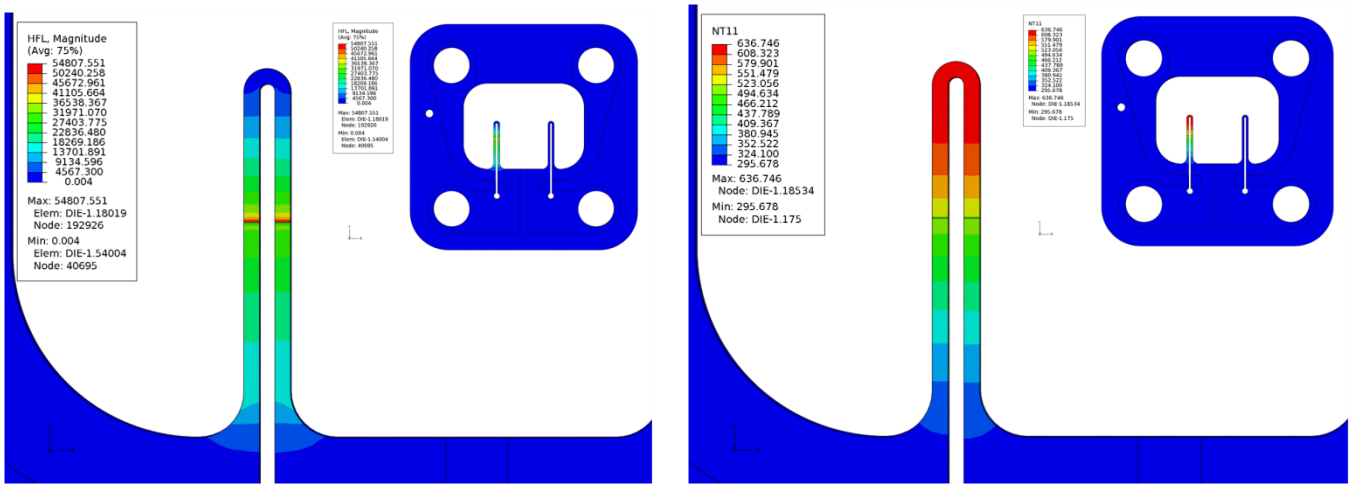

Fig. 10 - (Right) Zoomed-in Heat Flux magnitude distribution, (Left) Zoomed-in Temperature distribution for 75 μm design; Inset shows the complete distribution

The maximum temperature and the average top surface temperature of the heater seen in each design is tabulated as follows,

Design	Max. Temperature (K)	Avg. top surface Temp. (K)
25 μm	821.401	763.872
50 μm	710.077	664.782
75 μm	636.746	600.602

Table 2 - Comparison at 50 mW input power

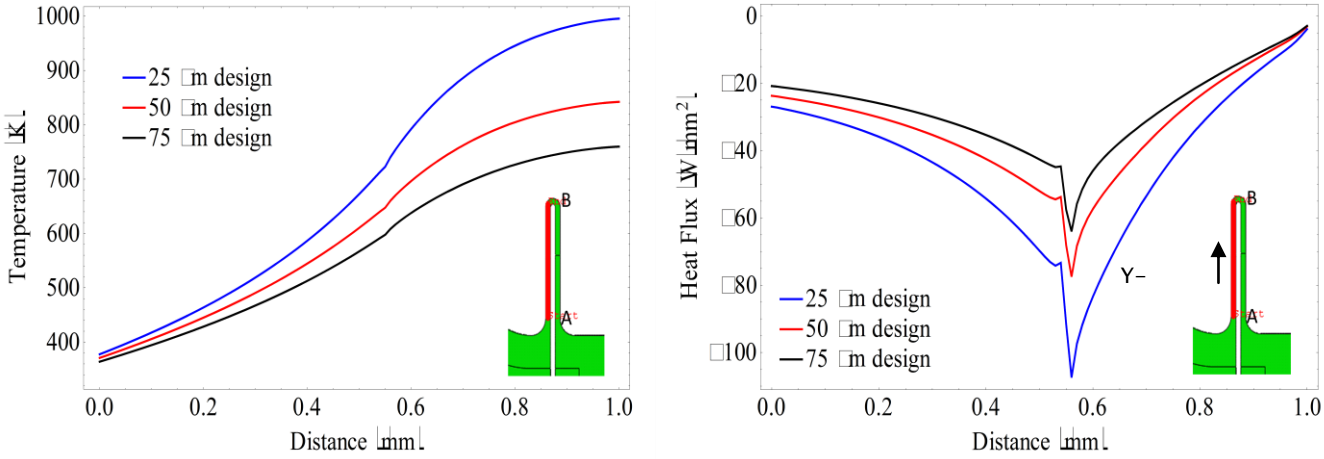

Fig. 11 - (Right) Temperature and (Left) Heat Flux (y-direction) along the length of heater at 75 mW input power, Inset shows the path used highlighted in red color (A = 0.0 mm, B = 1.0 mm)

Hence in conclusion, the 25 μm design outperforms the other two designs and based on its mechanical performance it should be the preferred design for the gas sensor.

Summary

A reasonably good thermal model of the gas sensor has been developed with the help of the experiments and finite element analyses. The finite element model has been used to extract the thermal properties of anodic aluminum oxide and predict the thermal behavior of different designs. The flexible nature of the finite element model should allow for a future detailed parametric study of the geometry so as to optimize the power consumption of the device and be able to predict the thermal behavior of a new design. Also, a future study on the effect of forced convection on the device operation is very important since heat loss in such conditions is accelerated and this may severely affect the functioning of the sensor.

References

1. Ogden, T. R.; Rathsam, A. D.; Gilchrist, J. T.; “Thermal Conductivity of Thick Anodic Oxide Coatings on Aluminum,” Mater. Lett. 1987, 5, 84– 87.
2. Borca-Tasciuc, D. A.; Chen, G.; “Anisotropic thermal properties of nanochanneled alumina templates,” J. Appl. Phys. 2005, 97, 9.
3. An Cai, Li-ping Yang, Jiang-ping Chen, Tong-geng Xi, Shi-gang Xin and Wei Wu, “Thermal Conductivity of Anodic Alumina Film at (220 to 480) K by Laser Flash Technique,” J. Chem. Eng. Data, DOI: 10.1021/je100437j, July 6, 2010.
4. I Stark, M. Stordeur and F. Syrowatka, “Thermal conductivity of thin amorphous alumina films,” Thin Solid Films, Volume 226, Issue 1, 15 April 1993, Pages 185-190.
5. Z. Zivcova, E. Gregorova, W. Pabst, D.S. Smith, A. Michot and C. Poulier, “Thermal conductivity of porous alumina ceramics prepared using starch as a pore-forming agent,” J. Eur. Ceram. Soc. 29 (2009), pp. 347–353.

Appendix C

Summary of Development of Using Intrinsic AAO

EXECUTIVE SUMMARY

Numerous catalyst formulations were tested on the same sensor platform and in the same conditions in order to provide a side-by-side comparison of the catalyst formulations only. ***The best performing*** (based on highest response at the lowest power) formulation for combustible gas sensors is saturated ***palladium nitrate in 1M nitric acid.***

When this catalyst formulation was tested on heaters annealed to different temperatures, it was found that the ***annealing temperature has a substantial effect*** on the performance of the sensor, with the 750°C annealed samples performing better than those annealed to 825°C.

Further tests planned include: testing the current formulation on 50µm sensor platforms, confirming batch to batch reliability, and improving catalyst performance via activation methods.

Summary Table of Results:

Formulation	Min Power @ 0.001 Amps	@ Catalyst Coat	Max Amps @ 100 mW	@ Catalyst Coat	# of Samples Tested
Pd Nitrate in Nitric Acid	62.9	10	3.2e-3	10	2
Pd Nitrate in Methanol	69.7	2	2.1e-3	2	2
Pd Nitrate & Citric Acid in Methanol	87.2	20	1.5e-3	20	1
Pd Acetate in Methanol	71.9	8	2.3e-3	8	4
Pd Acetate & Citric Acid in Water	76.2	10	2.0e-3	10	1

Note: All data in table and graph are averages for the given catalyst type tested on sample batch 4389-X-3-1: 150µm design, 40V, 50µm thick, annealed to 750°C.

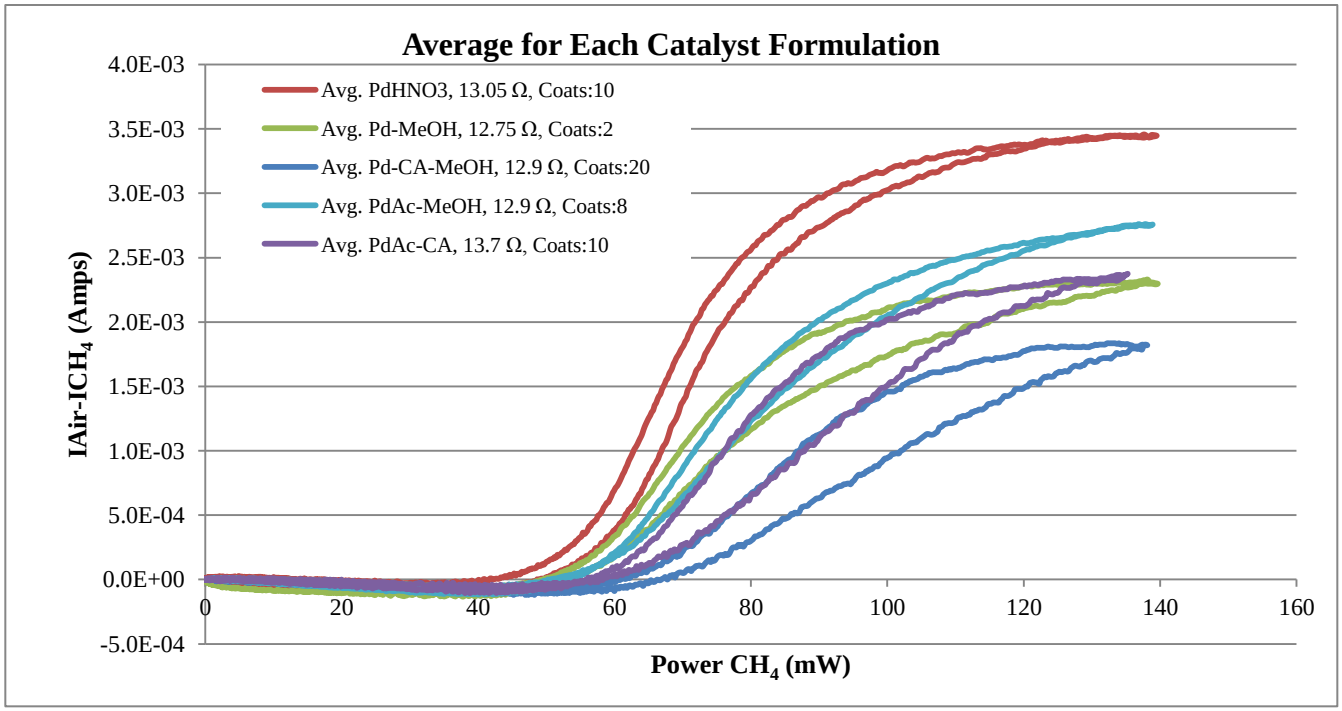

CATALYST FORMULATION TESTING RESULTS

CATALYST FORMULATION RESULTS SUMMARY

In order to minimize variables for side-by-side catalyst comparisons, the same sensor platform and testing procedure was used. Each formulation was tested on a sample from batch 4389-X-3-1: 150µm design, 40V, 50µm thick, annealed to 750°C. When making the solutions, it was attempted to maintain the same concentration (~6 wt%) of palladium, however due to solubility limitations some solutions contained lower concentrations. Details on each catalyst formulation, application procedure, and testing method are discussed in following sections.

To date, the best performing catalyst is saturated palladium nitrate in 1M nitric acid. This formulation has the highest response at a given power. It is also the easiest to apply in a consistent manner, and has the longest shelf life. It is recommended that this formulation be used in future research and for fabrication. An improvement on the catalytic activity of this formulation may be achieved through further work including: varying the palladium concentration in the solution and catalyst activation procedures.

All other formulations had a significantly lower response, at best only 75% of the response of the palladium nitrate in nitric acid. Solutions which used methanol as the solvent were very difficult to work with. The palladium would begin to immediately reduce causing particulates and an ever changing palladium concentration in the solution. After roughly 8 hours the palladium reduces to such an extent that large black “chunks” form and the solution turns clear. ***It is NOT recommended to use methanol based solutions*** for manufacturing.

The average values □R value for each catalyst formulation versus catalyst coats is shown in the figure below. The plot of amps (I_{Air}-I_{CH4}) at a constant power vs # coats has the same trends. All of the average data and numerous other plots can be found in the catalyst formulation comparison file.

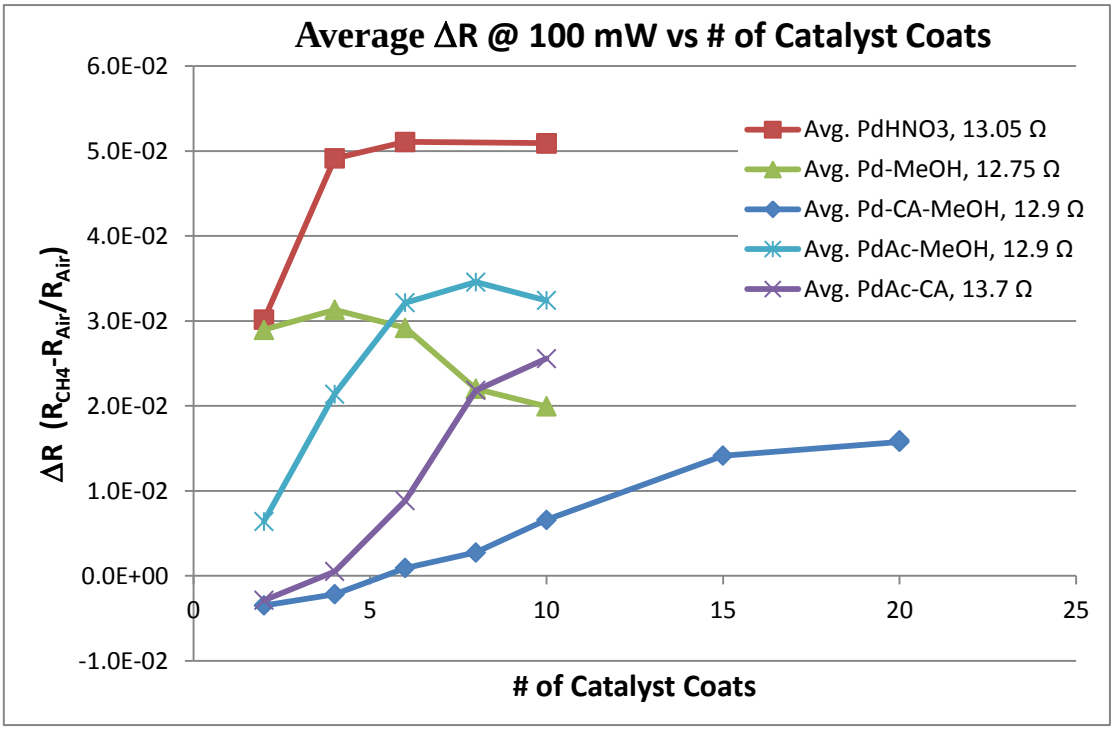

PD NITRATE IN NITRIC ACID – BEST TO DATE

Palladium nitrate in 1M nitric acid was the catalyst formulation used in Phase I of this research, and thus was used as the baseline to which all other formulations were compared. To date this is still the best performing catalyst formulation based on response at a given power. This solution is also the easiest to work with, as it is more concentrated than any other (based on visual color and amount of undisolved salt), and does not reduce over time to form a black precipitate.

For the specific platform used, the optimal number of catalyst coats is 6-10. The performance begins to decline slightly with subsequent coats.

It is recommended that this formulation be used for subsequent research and development, and for fabrication.

PD NITRATE IN METHANOL

Due to its low surface tension, methanol was tested as a solvent in order to enable a conformal distribution of the catalyst into the pores. It was thought that aqueous based solutions would be pulled out of the pores as the support was heated, and thus methanol may improve the catalyst distribution.

The methanol solution was difficult to work with, as the palladium immediately began to reduce and precipitate out of solution. Due to the constant precipitation, it was impossible to keep the solution clear of small particulates. When applying the catalyst, much care was required to avoid applying the Pd precipitate. When the particles were applied, the surface would become metallic and the response would decline.

For the specific platform used, the optimal number of catalyst coats is 4. The performance is much lower (almost half) of the baseline catalyst. With increasing catalyst applications, the response drops significantly.

This formulation poses too many difficulties, and it is not recommended for use in further work nor in fabrication.

PD NITRATE AND CITRIC ACID IN METHANOL

An organic gel method was suggested, as it was thought that the oxygen in the organic would bind to the palladium thus competing with the nitrates. The isolated Pd ions would then form many nucleation sites upon calcining. A 2:1 molar ratio of organic to palladium was recommended along with using citric acid as the organic and methanol as the solvent. It was also recommended that for this technique the ramp rate for calcination be no more than 5°C/min in order to avoid problems with HNO_3. For this specific test, the standard calcinations profile was used.

This solution, as with all of the methanol based solutions, was difficult to work with due to the rapid reduction of palladium. The reduced solubility of palladium nitrate in methanol also resulted in a much higher organic to palladium ratio than was desired, but the exact ratio is not known. Based on color, the solution had least Pd dissolved of all the formulations.

The optimum number of coats is unknown, as after 20 applications, the response was still increasing. The best response achieved was only around 25% that of the baseline catalyst. Due to the low response, high number of applications required, and shelf life, this formulation is not recommended for use in further work nor in fabrication.

PD ACETATE IN METHANOL

Palladium acetate was not originally on the formulation test plan, but due to the unavailability of palladium nitrate for two months, palladium acetate formulations were explored. As with the other methanol based solutions, this one began to reduce immediately.

For the specific platform used, the optimal number of catalyst coats is 8. The performance begins to decline with additional coats. This formulation has a best response similar to the palladium nitrate in methanol solution, which suggests that the catalytic effects of using palladium nitrate and palladium acetate are not substantially different.

As with the other methanol solutions, due to the short shelf life and limited response, this formulation is not recommended for further work.

PD ACETATE AND CITRIC ACID IN WATER

This formulation was also not originally on the formulation test plan and only tried due to the unavailability of palladium nitrate. This was the first attempt with the organic acid technique, and the methanol solvent was not used.

The non-methanol solvent allowed for the organic:Pd ratio to be closer to that actually desired, as the Pd is more soluble in water, and does not begin to reduce immediately. Based on color, this solution had slightly less Pd than the Pd Nitrate in nitric acid, and was similar to the methanol based solutions.

For this formulation only, the calcining rate was significantly lower than the standard procedure. The recommended rate was 5°C/min, but due to time constraints, a rate closer to 15°C/min was used (0-2.2V-0, at 0.0006V/s).

The optimal number of coats is unknown, as the response was still increasing after 10 applications. The maximum response, however, was only half that of the baseline solution. This formulation has a longer shelf life than the methanol based, and though it had a lower response than the baseline, it may be of interest for further exploration, such as varying the organic:Pd ratio.

EFFECT OF AAO ANNEALING TEMPERATURE

The standard Pd nitrate in nitric acid catalyst precursor was applied to two different batches of sensors. The only difference between the batches was the temperature at which the AAO was annealed. One batch (4389-X-1-1) was annealed to 825°C, which (according to previous BET work) results in a high surface area crystalline alumina phase. The second batch (4389-X-3-1) was annealed to 750°C, which results in a low surface area amorphous alumina phase.

Multiple samples from each batch were tested per the standard methods. The ***low surface area (750°C annealed) sensors had a statistically higher response*** than the high surface area (825°C) annealed sensors. A possible explanation is that the catalyst inside the small secondary pores of the high surface area sample is not available for the reaction. Even though the BET surface area is higher for the 825°C sample, the lower surface area sample results in more active catalytic sites.

These results have not yet been confirmed, which is necessary to determine whether this is truly a surface area effect, or simply a variation from sensor batches.

The average responses for each annealing temperature can be seen in the following graphs.

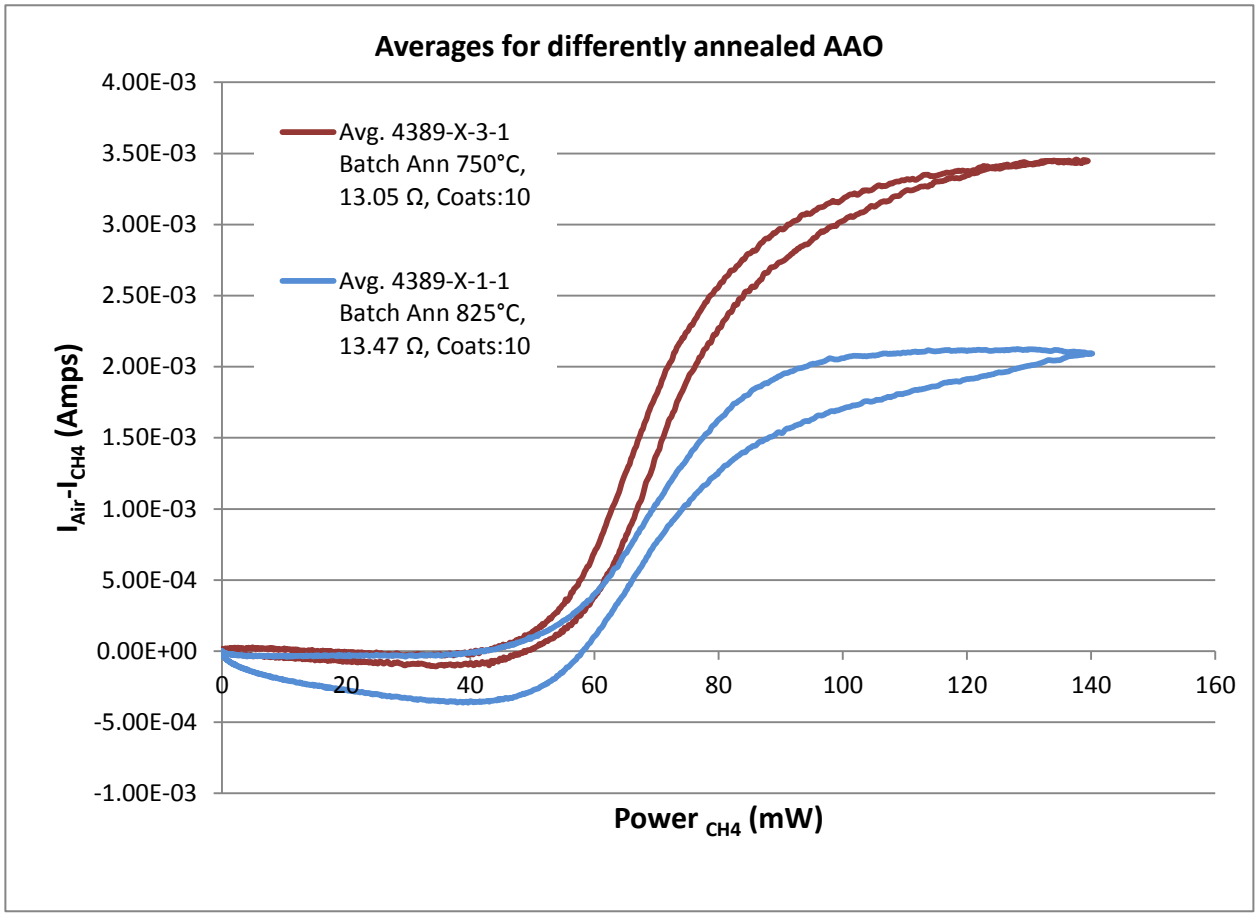

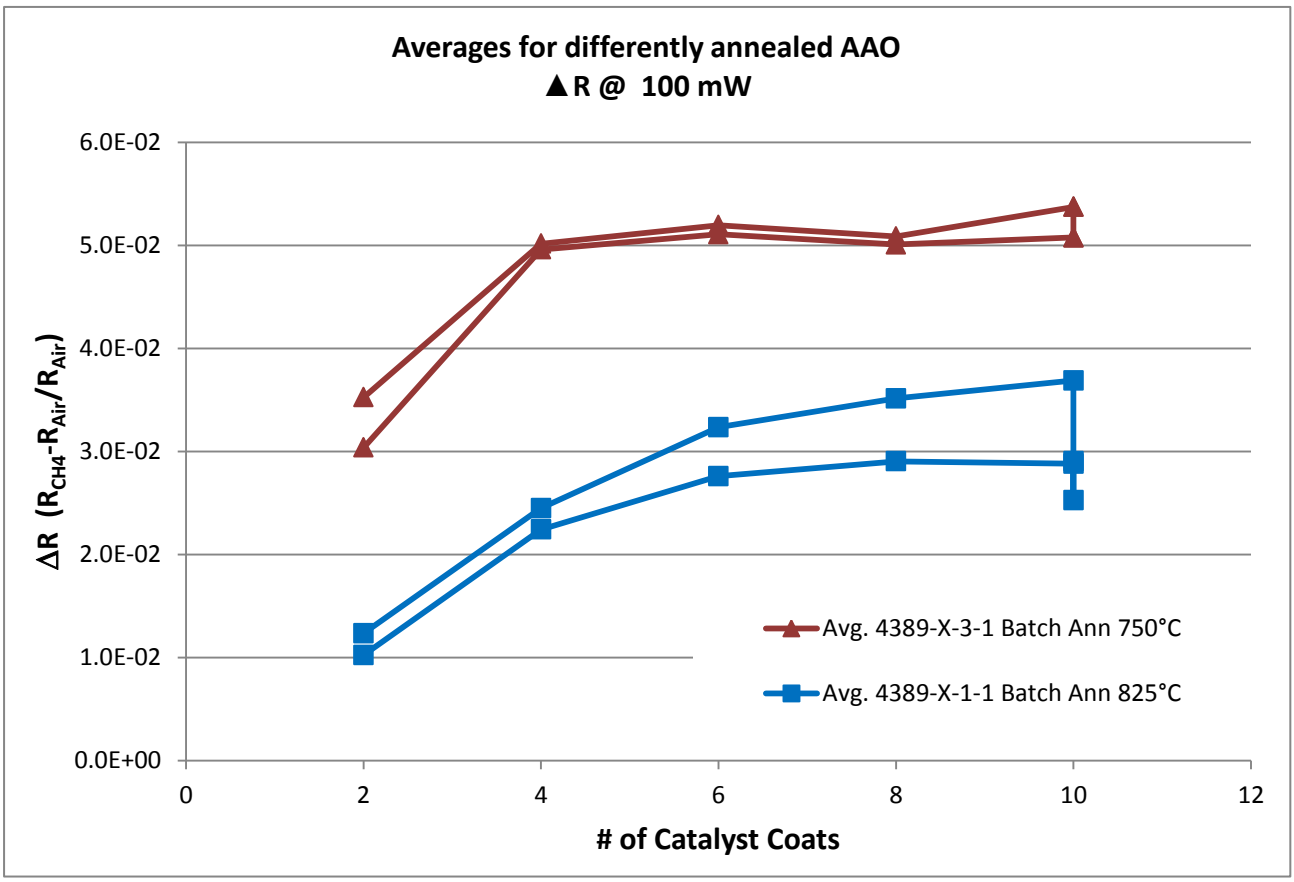

REPRODUCIBILITY OF TESTING PROCEDURES

Using the standard catalyst formulation, 7 sensors were tested to determine the reproducibility of the procedures. For the same catalyst formulation on the same heater platform, t***he reproducibility of the procedures is excellent.***

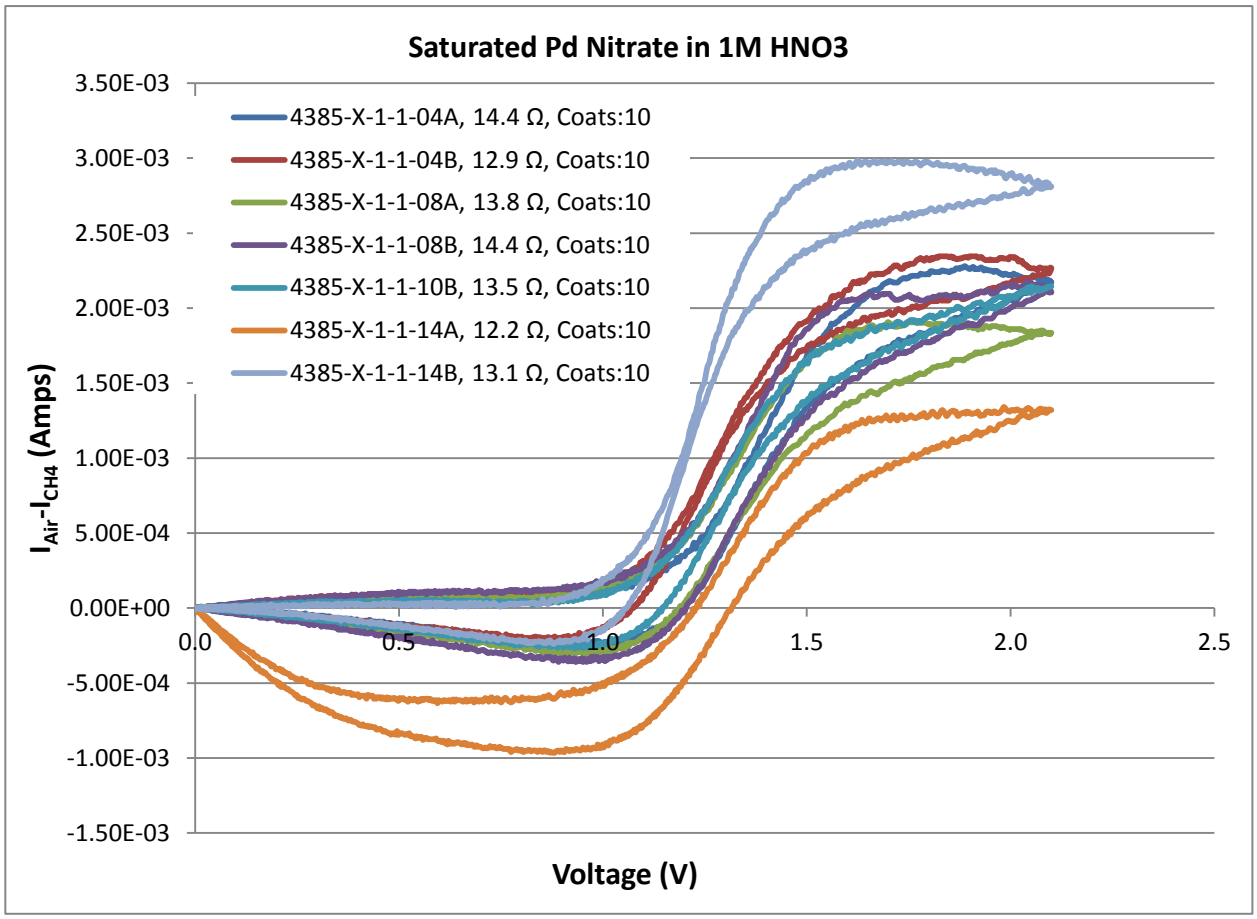

RECOMMENDED FUTURE CATALYST WORK

In order to enhance the sensor response, further work is recommended which builds upon the work done to date. The following table is a summary of the recommended future catalyst work and the ranking of importance.

Description	Ranking	Estimated Time for Task (not man-hours)
Formulation: Pd Acetate in 1M Acetic Acid	11*	2 days
Formulation: Pd Nitrate & Citric Acid in Water	10*	2 days
Platform: Current 50 µm design	1	10 days
Reliability: Batch to Batch	2	5 days
Catalyst Deposition: Pd Concentration in Solution	7	10 days
Catalyst Deposition: Calcining Rate	4	5 days
Catalyst Activation: Methane Treatment	5	2 days
Catalyst Activation: Hydrogen Treatment	6	2 days
Promoters: Mn, Re, Ru	12	15 days
Support Parameters: AAO Thickness	8#	5 days

Support Parameters: AAO Pore Size	9#	5 days
Support Parameters: Annealing Temperature	3	5 days

* If these tests are performed, they should be done before continuing with the catalyst deposition and activation parameters, as the results might change the catalyst choice

Details on which parameters to test are dependent on the modeling effort at CU

OTHER POTENTIAL CATALYST FORMULATIONS TO TEST

The baseline solution, Pd nitrate in nitric acid, has already been shown to be a responsive and the best formulation to date. If time permits, additional formulations are recommended for screening. If it is desired to test these solutions, it is recommended that they are tested before continuing on with more catalyst deposition and activation parameters, as the catalyst formulation should be decided upon before proceeding with those tests.

Pd Acetate in 1M Acetic Acid Reasoning: The acetate salt showed similar performance as the nitrate salt when methanol was used as the solvent, as well as when it was tested using the organic gel method. The purpose for testing the organic gel method was to isolate nitrates and prevent them from interfering with the Pd. Since the acetate salt does not contain nitrates, they cannot cause interference, and therefore the acetate may be a potentially better formulation.

Pd Nitrate & Citric Acid in Water Reasoning: Methanol is clearly not an ideal solvent as the solubility of the Pd nitrate is lower, and the Pd begins to reduce and precipitate out immediately. The organic gel capture is intended to isolate the nitrates and prevent them from interfering with Pd, while the methanol was intended to reduce the surface tension of the liquid. The problem with reduction of the Pd in methanol may be avoided, while still reducing the Pd-N interference. Additionally, the Pd Acetate & Citric Acid in water showed substantially better results than the Pd nitrate & citric acid in methanol, thus indicating that the non-methanol gel is better.

50µM PLATFORM

The ultimate goal of this project is to develop a sensor which operates at less than 50 mW. The current 150 µm platform requires much higher power, but due to the size and durability was the preferred platform for catalyst formulation screening.

The best catalyst formulation needs to be tested on the 50 µm design to determine if the response is sufficient for sensor use, or if additional catalyst (in the form of a bead or otherwise) is necessary.
Preliminary tests have already been conducted on the 50 µm design and show promising results. These tests were done on samples which were not properly prepared (open AAO pores side down, or heat side up), yet the sensors did show a noticeable response. Therefore it is believed that using a properly made sample will results in a substantially higher response.

Additionally, further testing on improving the catalyst, through activation or otherwise, should be done on this platform whenever possible. Due to the substantially reduced size of these sensors, what may be an unnoticeable result on the 150µm may be a substantial improvement on the 50µm, or vice versa.

BATCH TO BATCH RELIABILITY TESTING

The side-by-side catalyst formulation screening done to date was conducted using a single batch of sensors. When the standard catalyst was tested on a separate batch, the response was significantly different. Currently this difference is attributed to the annealing temperature of the AAO.

In order to confirm that the annealing temperature is truly the determining factor and that there is consistency in sensor fabrication, additional batches need to be tested. The baseline catalyst formulation should be used, as more data on this formulation is available than on any others.

The additional batches to test should be sensors made with the same parameters and in the same manner as those previously tested in order to avoid causing complications and uncertainty by adding additional variables. Both annealing temperatures should be tested in order to confirm the previous results and prove that the differences seen are not due to an anomaly in the fabrication of a batch.

CATALYST DEPOSITION CONDITIONS

The catalyst deposition procedure itself may result in overall response improvements of the sensors. The following are some methods to try in order to increase the response. Again, these developments should be done using only the chosen catalyst formulation.

Palladium Concentration in Solution

Currently a saturated solution is used for the catalyst deposition. By reducing the amount of palladium in the solution, the amount of palladium deposited per application is also reduced. The reduction in palladium may provide a means for increasing the number of active sites, as there will be less palladium nearby for islands to form with. On the other hand, this process may result in the need to substantially more catalyst applications. The number of applications should be taken into consideration in terms of future fabrication. It is recommended that the initial concentration tested be half that of the solution used in the catalyst screening. This should be sufficiently low to show improvements based on concentration change, and require no more than double the amount of applications.

Calcining Procedures

Calcining can be an important variable in terms of the number of active catalyst sites formed. The main variable to adjust is the temperature ramp rate. Currently a moderately aggressive ramp rate is used. Two additional rates are suggested for testing:

Step Change: In this technique, the sensor is brought temperature is brought almost instantaneously. The theory is that this rapid change in temperature does not allow the metal to conglomerate, thus creating more and smaller islands and hence more active sites.

Slow Ramp Rate: In this method a very slow ramp rate ~5°C/min is used. This is essentially the opposite extreme of the step change. For certain formulations, this slow rate allows for a complete burning off of the organics, and also prevents boiling of the solution out of the pores.

No Calcining Between Applications: It is unlikely that this technique will provide substantial improvement on the catalyst activity. However, this is an important procedure to look into, as it has a tremendous impact on future fabrication. By calcining only once after all the catalyst applications have been completed, will reduce the time and complexity of the fabrication process. This procedure needs to be tested to ensure that the catalyst activity remains adequate.

CATALYST ACTIVATION

The catalyst activity and lifetime can be significantly influences by activation procedures. The more available reaction sites, the higher the response of the sensor. By exposing the catalyst to different gases and corresponding conditions, the number of sites may be increased. Though the actual catalyst in the combustible gas system is PdO, reducing the palladium first may provide a means for increasing site through the recrystalization process. Both hydrogen and methane should be tested as reducing agents. Hydrogen is commonly used, and methane has been shown to enable better recrystalization than hydrogen for PdO systems.

PROMOTERS

The addition of a promoter may increase the response of the sensor. Manganese, rhenium, and ruthenium are the top three metals to test. Based on discussions with consultant Heinz Robota, there was no indication in the literature that a promoter would enhance the sensor response. If it is desired to test promoters, the promoter should be applied after all palladium applications, and a ratio of no more than 1:20 promoter to Pd should be used. It is suggested that other activity improvements be explored before the use of promoters.

SUPPORT PARAMETERS

The support itself plays a crucial role in the catalyst activity and sensor response. It dictates the heat and mass transfer of the system, as well as the available surface area. Increases in the sensor response may be achieved through changes in the AAO parameters. These should be explored, but only in conjunction with the CU modeling effort.

AAO Thickness

By increasing the thickness of the AAO platform, the surface area available for catalyst deposition increases. There will be an optimum thickness in which diffusion is not an issue, and the heat losses are not too great. The modeling should help define a reasonable range of thicknesses to test.

AAO Pore Size

Changing the pore size may also improve the sensor response. The change in pore size will vary available surface area for the catalyst to be deposited onto, and can also affect diffusion into the pores. Again there are competing issues including mechanical strength, heat loss, surface area, and diffusion and an optimum must be found in conjunction with the modeling effort.

Annealing Temperature

Current data indicates that the annealing temperature has a large impact on the sensor response. The lower annealing temperature (and thus lower surface area) samples show a statistically significant increase over the high annealing temperature (high surface area) samples. These results need to be confirmed. It is unlikely that additional annealing temperatures will result in improvements of the activity, as the activity is most likely dependant on the alumina phase.

APPENDIX C/A: CATALYST FORMULATIONS

This section discusses in detail the method by which the catalyst formulations were made. For more extensive notes, consult Esther Wilcox's µCGS lab notebook.

TABLE OF SOLUTIONS MADE

Those in **bold blue** are still in the chemical cabinet; those in black have been disposed of.

Solution Description	Date Made On	Pg #	Comments
Pd Nitrate in Nitric Acid	**12/28/09**	**7**	**Still looks good, is being used.**
Pd Nitrate in Methanol	2/2/10	24	After a few days, large black chunks had precipitated, and the rest of the solution was clear.
Pd Acetate in Methanol	5/19/10	39	Used for 2 days, then began to see the black chunks as with the Pd nitrate.
Pd Acetate in Methanol	6/2/10	43	Same as previous
Pd Acetate in Methanol	6/7/10	46	Same as previous
Pd Acetate & Citric Acid in Water	**6/9/10**	**48**	**Solution lighter in color than other Pd solutions made to date. Still looks good.**
Pd Nitrate in Methanol	7/2/10	54	Disposed of the next day due to precipitation
Pd Nitrate in Citric Acid in Methanol	7/21/10	55	Disposed of the next day due to precipitation

CATALYST SOLUTION RECIPES

The following recipes are based on procedures used and developed throughout the work of this phase of the project. For details on the history of individual formulation development and specifics for each individual batch made, refer to Esther Wilcox's lab notebook. The page numbers for each solution made are given in the preceding table.

SATURATED PALLADIUM NITRATE IN 1 MOLAR NITRIC ACID

As was previously determined by Oleg Polyakov, using roughly 6wt% of Pd nitrate results in a saturated solution with minimal Pd nitrate left undissolved. This procedure was based on work conducted in Phase I of this project. This solution is currently the best performing, and longest lasting.

- Weigh **16 g** of previously mixed **1 molar nitric acid** solution in a flask.
- Add **1 g** (~6wt% of final solution weight) of **Pd(II) Nitrate Dihydrate** to the flask.
- Sonicate for 30 minutes to ensure as much salt is dissolved as possible and that the solution is well mixed.
- Let solution rest for at least 2 hours, preferably overnight in order to let the undisolved Pd settle out.
- Using a pipette, pull off the clear liquid at the top of the solution and transfer to another container.

SATURATED PALLADIUM NITRATE IN METHANOL

The exact amount of palladium nitrate to give a saturated solution has not yet been determined. It has been seen that using 6wt% of palladium nitrate results in a saturated solution with undissolved salt.
This solution has a very limited lifetime. After only a day, the color begins to lighten, and black chunks of precipitate appear. After about 2-3 days, the solution is completely clear with large black chunks in the bottom. It is presumed that the palladium is reduced which results in the black precipitate, and the clear solution is methanol only.

- Weigh **1 g** of **methano**l in a vial.
- Add **0.065 g** (~6wt% of final solution weight) of **Pd(II) Nitrate Dihydrate** to the vial.
- Sonicate for 30 minutes to ensure as much salt is dissolved as possible and that the solution is well mixed.
- Let solution rest for 15 minutes in order to let the undissolved Pd settle out. Leaving the solution sit too long will result in large precipitate chinks forming.
- Using a pipette, pull off the clear liquid at the top of the solution and transfer to another vial. ALTERNATIVELY: pour the solution through a filter to remove the undissolved salts. NOTE: It is possible to use the original solution if caution is used when dipping the brush in order to avoid picking up undissolved particles.

2:1 CITRIC ACID AND PALLADIUM NITRATE IN METHANOL

The exact amount of palladium nitrate dissolved in the solution is unknown, and thus the actual ratio of organic acid to palladium is likewise unknown, though assumed to be greater than 2:1, as the citric acid appeared to dissolve completely, but the palladium nitrate did not.
This solution, like the other methanol based solutions, has a limited lifetime. After only a day, the color begins to lighten, and black chunks of precipitate appear. After about 2-3 days, the solution is completely clear with large black chunks in the bottom. It is presumed that the palladium is reduced which results in the black precipitate, and the clear solution is methanol only.

- Weigh **1 g** of **methano**l in a vial.
- Add **0.065 g** (~6wt% of final solution weight) of **Pd(II) Nitrate Dihydrate** to the vial.
- Add **0.095 g** (2:1 mole Organic to Pd) of **citric acid** to the vial.
- Sonicate for 30 minutes to ensure as much salt is dissolved as possible and that the solution is well mixed.
- Let solution rest for 15 minutes in order to let the undisolved Pd settle out. Leaving the solution sit too long will result in large precipitate chinks forming.
- Using a pipette, pull off the clear liquid at the top of the solution and transfer to another vial. ALTERNATIVELY: pour the solution through a filter to remove the undisolved salts. NOTE: It is possible to use the original solution if caution is used when dipping the brush in order to avoid picking up undissolved particles.

SATURATED PALLADIUM ACETATE IN METHANOL

The exact amount of palladium acetate required for a saturated solution in methanol has not yet been determined. Based on the palladium nitrate, a 6wt% palladium acetate solution is used. This results in a slightly lighter looking solution than the palladium nitrate, indicating that the amount of palladium salt dissolved is less. It has been seen that not all of the palladium salt is dissolved, indicating that a saturated solution has been made.
As with the Palladium nitrate in methanol, this solution has a limited lifetime. After only a day, the color begins to lighten, and black chunks of precipitate appear. After about 2-3 days, the solution is completely clear with large black chunks in the bottom. It is presumed that the palladium is reduced which results in the black precipitate, and the clear solution is methanol only.

- Weigh **1 g** of **methanol** in a vial.
- Add **0.065 g** (~6wt% of final solution weight) of **Pd(II) Acetate** to the vial.
- Sonicate for 30 minutes to ensure as much salt is dissolved as possible and that the solution is well mixed.
- Let solution rest for 15 minutes in order to let the undisolved Pd settle out. Leaving the solution sit too long will result in large precipitate chinks forming.
- Using a pipette, pull off the clear liquid at the top of the solution and transfer to another vial. ALTERNATIVELY: pour the solution through a filter to remove the undisolved salts. NOTE: It is possible to use the original solution if caution is used when dipping the brush in order to avoid picking up undissolved particles.

2:1 CITRIC ACID AND PALLADIUM ACETATE IN WATER

The exact amount of palladium nitrate dissolved in the solution is unknown, and thus the actual ratio of organic acid to palladium is likewise unknown, though assumed to be greater than 2:1, as the citric acid appeared to dissolve completely, but the palladium nitrate did not. This solution does not have problems with precipitation or immediate reduction occurring.

- Weigh **1 g** of **water** in a vial.
- Add **0.065 g** (~6wt% of final solution weight) of **Pd(II) Nitrate Dihydrate** to the vial.
- Add **0.095 g** (2:1 mole Organic to Pd) of **citric acid** to the vial.
- Sonicate for 30 minutes to ensure as much salt is dissolved as possible and that the solution is well mixed.
- Let solution rest for 15 minutes in order to let the undisolved Pd settle out. Leaving the solution sit too long will result in large precipitate chinks forming.
- Using a pipette, pull off the clear liquid at the top of the solution and transfer to another vial. ALTERNATIVELY: pour the solution through a filter to remove the undisolved salts. NOTE: It is possible to use the original solution if caution is used when dipping the brush in order to avoid picking up undissolved particles.

APPENDIX C/B: CATALYST DEPOSITION & TESTING PROCEDURES

In general the following procedures are used for preparing and testing each sensor. Consult the data analysis file or the lab notebook for specifics regarding a particular sensor.

HEATER IDENTIFICATION

Since each "sensor" has two heaters, each one is used individually for the catalyst testing. The tab on the sensor is placed either down or to the right (which ever leads to the heater elements aligning as shown in the figure). The heater on the left is denoted: A, and to the right is: B.

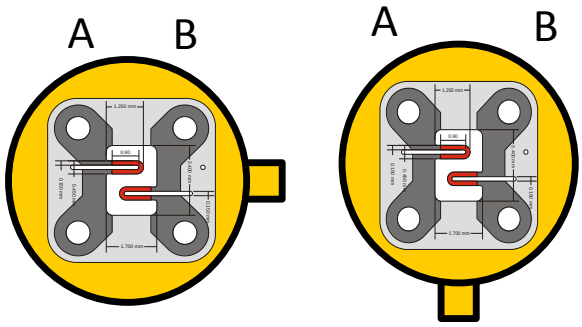

TEST SYSTEM & SETUP

Connecting to Potentiostat:

Before connecting any leads, place the sensor onto the top of the flow through cell holder. Ensure that the pins are firmly in the holes and will not fall out when turned up-side-down. The potentiostat must be turned on before connecting leads to the heaters; otherwise the heater will burn out upon turning on the potentiostat. The red and white leads from the potentiostat are connected to one end of the desired heater, and the green lead to the other end. Leave sensor on the holder top, the leads connected, and the potentiostat on during the entire catalyst application and testing procedure. When done, remove the leads before turning off the potentiostat.

CATALYST APPLICATION

Painting on the catalyst:

Place the holder top (with attached sensor) under the microscope. It is easiest to rest the holder top on a Styrofoam support with a notch cutout for the wire to run through. This method keeps the holder top stable and prevents the wires from snapping.

The brush is dipped into the desired catalyst solution. The solution is then carefully painted on to the heater. Sufficient solution is put on to wet the entire surface. This is seen by a round drop of liquid on the heater area only. Consistent deposition is achieved through patience and practice.

The following figures attempt to show this concept.

Heater with no solution on it Heater with uniform coating of solution on it

The AAO will absorb the solution rapidly. For consistency, it is important to apply the correct amount at one time and not reapply after the solution has been soaked into the support.

The brush is then rinsed in DI water, and gently wiped dry using a kimwipe.

The brush:

An artist's brush is trimmed to reduce the amount of bristles and their length. Then nail polish is applied to the base of the bristles, and the metal band holding them on. The nail polish acts as a chemical barrier to prevent the metal on the brush from interfering with the catalyst solution. The number of bristles and their length is a matter of personal preference and it is recommended that a sensor be used to test the bristles on before the nail polish is applied.

Calcining:

Currently, the heater is calcinced after each catalyst deposition. The final voltage (and temperature) is higher than the operating voltage. For the 150 µm sensors the calcining profile is: 0-2.2V-0, at 0.035V/s, for the 50 µm sensors it is: 0-1.5V-0 at 0.023V/s. When different maximum voltages are used, it is best to change the ramp rate so that the total time remains the same, this corresponds to keeping a constant temperature ramp rate.

NOTE: This procedure may change as further work is conducted.

TEST PROTOCOL

The sample is tested in the combustible gas stream before any catalyst has been applied, and then after every other application. This enables response vs catalyst coats to be generated. The sample is kept on the holder top at all times. Before testing, it is carefully inserted into the holder and secured.

Gas flow:

- ~ 100 ccm of Air for 5 minutes, then CV sweep
- ~ 100 ccm of 2.5% CH4 in Air for 5 minutes, then CV sweep
- ~ 100 ccm of Air for 5 minutes, then CV sweep

CV Sweep:

The CV sweep parameters must be changed for each sensory platform. The maximum voltage is based on temperature calibration curves and set to a voltage that corresponds to roughly 650°C. The sweep rate corresponds to roughly 625°C/min. For the current platforms this corresponds to:

- 150 µm: 0-2.1V-0 @ 0.035V/s
- 50 µm: 0-1.4V-0 @ 0.023V/s

Appendix D

Evaluation of LttE

SENSOR INFORMATION

- **CGmS-004-02 (a.k.a. LttE)**
- **2.1 design (longer heater)**
- **Beaded**
- **Pd catalyst**
- **On power (~50 mW/element) for 3+ weeks prior to evaluation**
- **Operated at ~50 mW/element for evaluation**
- **Data presented on representative sensor (#2) with notes regarding other sensors**
- **Bridge testing**
- **Evaluation data and this write up are located in \\Hera\ZeusPublic\RD&E\Research Projects\Current Projects\7057 - CGµS - NIH PhII (DR)\1. Results\5. Testing\Analysis\Evaluation_0311**
- **Data work up on sensor #2 is in this file**

POWER

Sensors tested at 40 and 50 mW/element

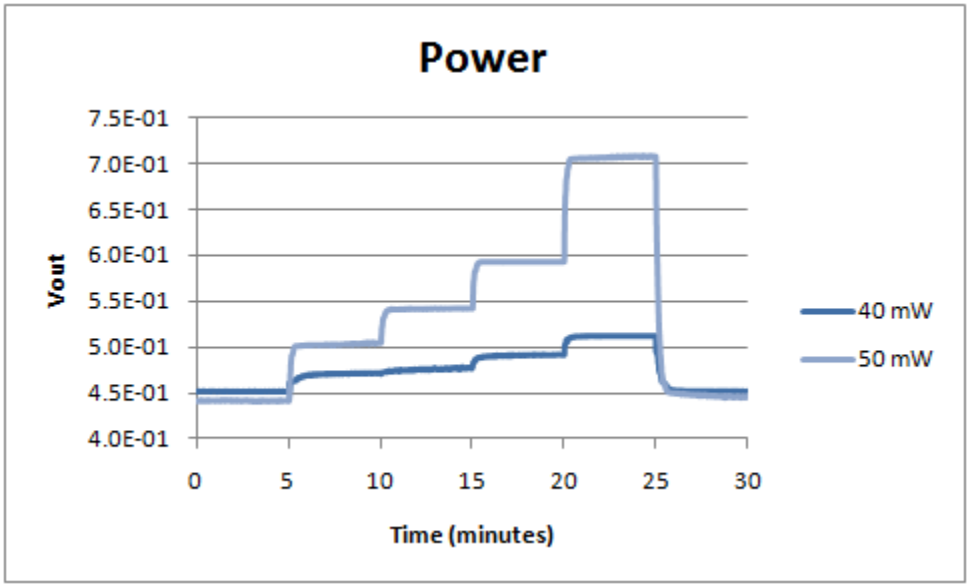

F. LINEARITY

Methane: 0.25, 0.5, 1, 2.5%

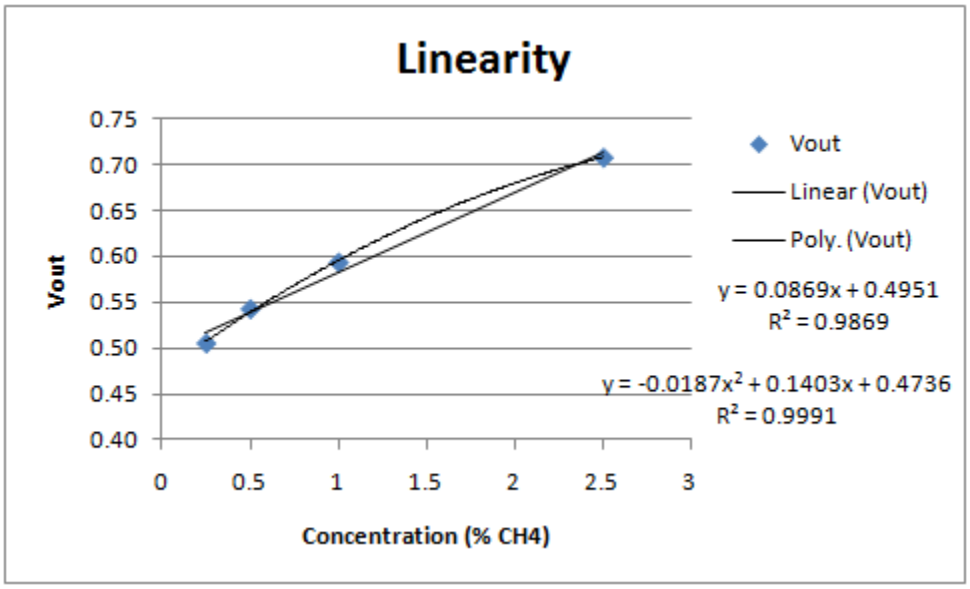

- It should be noted that the LttF sensors, which have a larger beaded area, seem to exhibit better linearity.

CALIBRATION

Methane: 0.35, 0.75, 1.25% (accuracy based on linearity data, both linear and polynomial fit)

Concentration (% Methane)	Error (linear fit)	Error (polynomial fit)
0.35	3.5%	-0.3%
0.75	-4.9%	-0.8%
1.25	-11.4%	0.1%

REPEATABILITY

6 exposures to 2.5% CH4 (5 min. exposure, 5 min. off)

- Sensor #1 had -0.1% error on the last exposure compared to the first exposure
- Sensor #2 had 0.3% error on all 5 exposures following the initial exposure
- Sensor #3 had -1.8% error on the last exposure compared to the first exposure
- Sensor #7 had 4.2% error on the last exposure compared to the first exposure

HUMIDITY

Methane linearity dry (0.25, 0.5, 1, 2.5%), 5 minute steps
Methane linearity @ 45%RH (0.25, 0.5, 1%), 5 minute steps
0-15-50-85-0 %RH, 10 minute steps

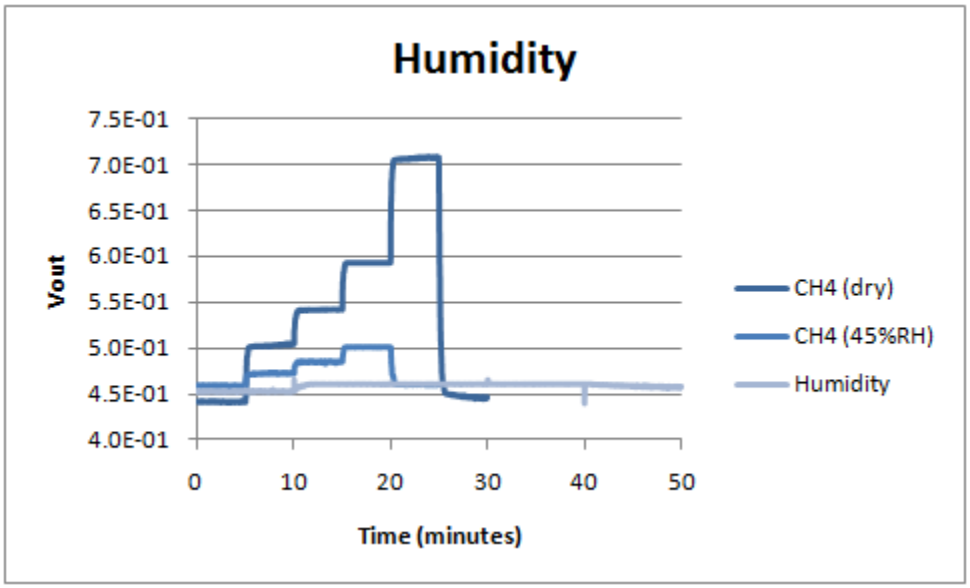

HYDROCARBON RANGE

Methane: 0.25, 0.5, 1.0, 2.5%
Propane: 0.1, 0.25, 0.5, 1%
Pentane: 250, 1000, 5000, 7500 ppm
Hexane: 250, 500, 1000, 5000 ppm

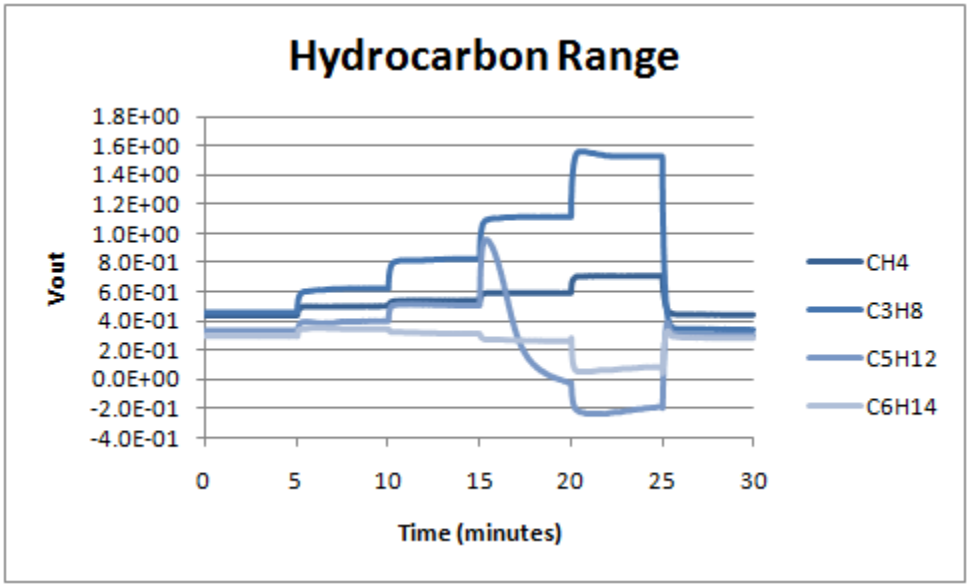

- Sensors #3 and #7 showed similar “negative” response to higher hydrocarbons
- Sensor #1 did not show this “negative” response (this sensor has a smaller beaded area than #7)

TEMPERATURE

Room Temperature (24°C) and 40°C

- Noise created by temperature chamber makes for poor data and specifically overwhelmed signal in test at -40°C

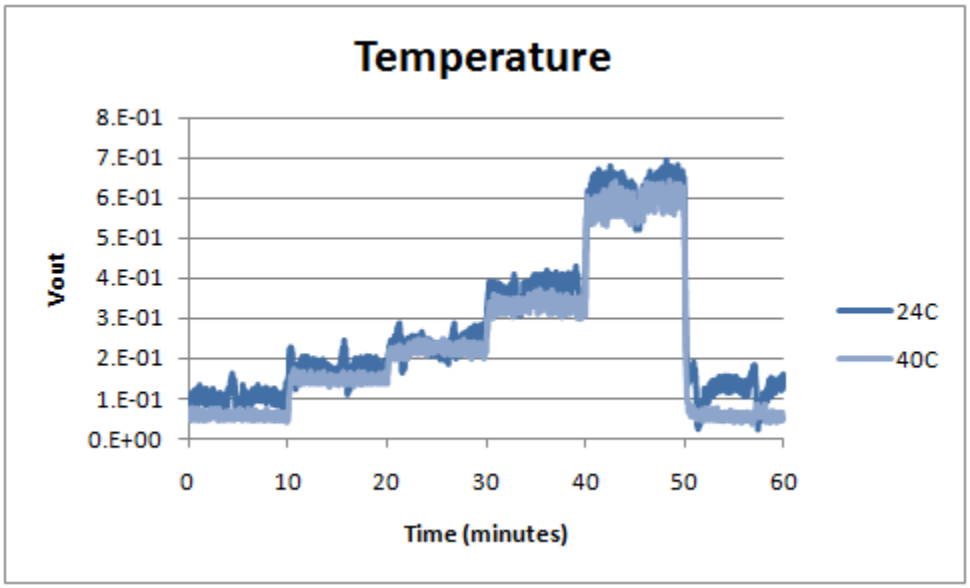

SULFUR RESISTANCE

Methane linearity (0.25, 0.5, 1, 2.5%)
Expose sensor to 10 ppm H_2S for 10 minutes (per proposal)
Methane linearity (0.25, 0.5, 1, 2.5%)

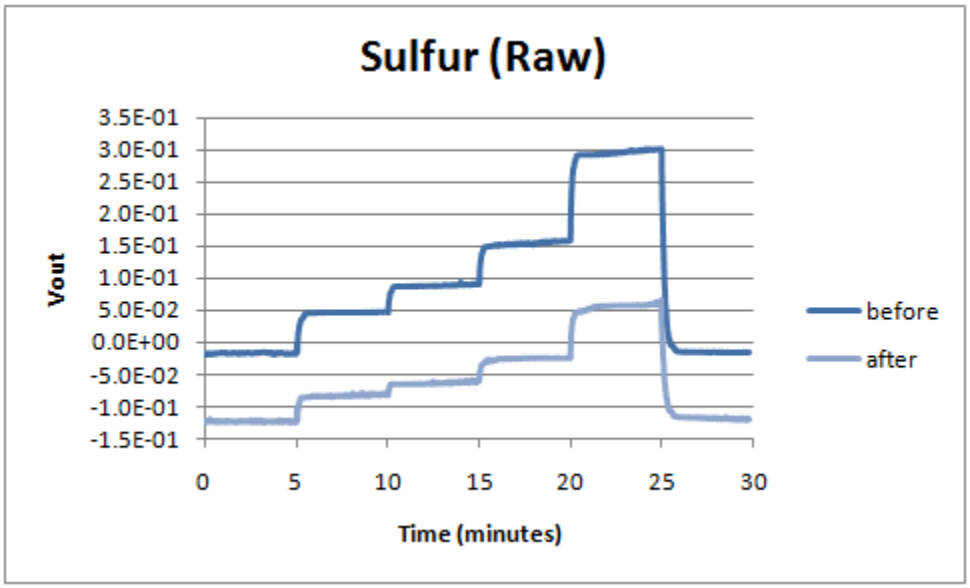

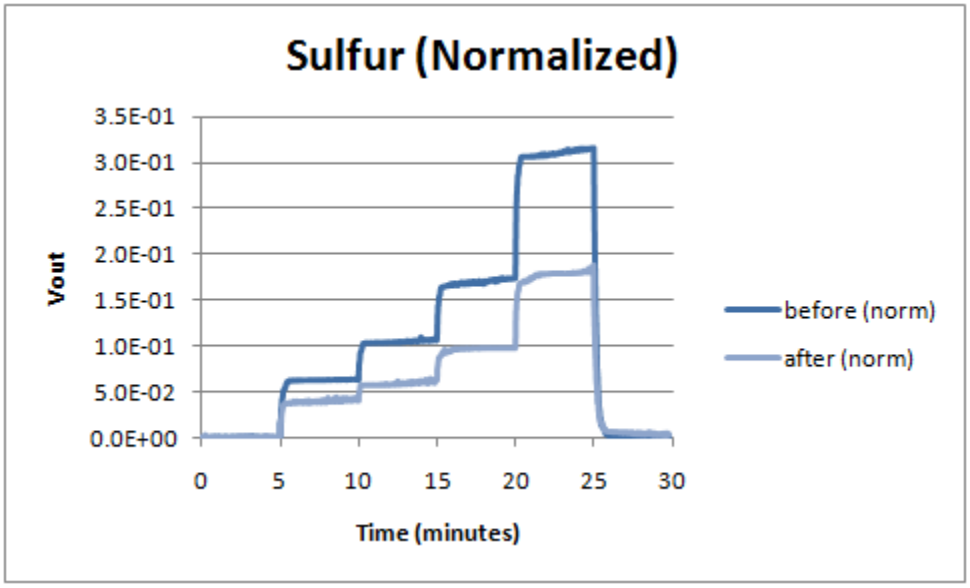

- Baseline normalized for easier comparison the magnitude of response before and after exposure to H_2S

LONG TERM STABILITY

Sensors power continuously at ~50 mW/element
CVs run periodically in air and 2.5% methane
Ig-Ia used as comparison for burn-in/degradation
Day 0 is 2/2/11

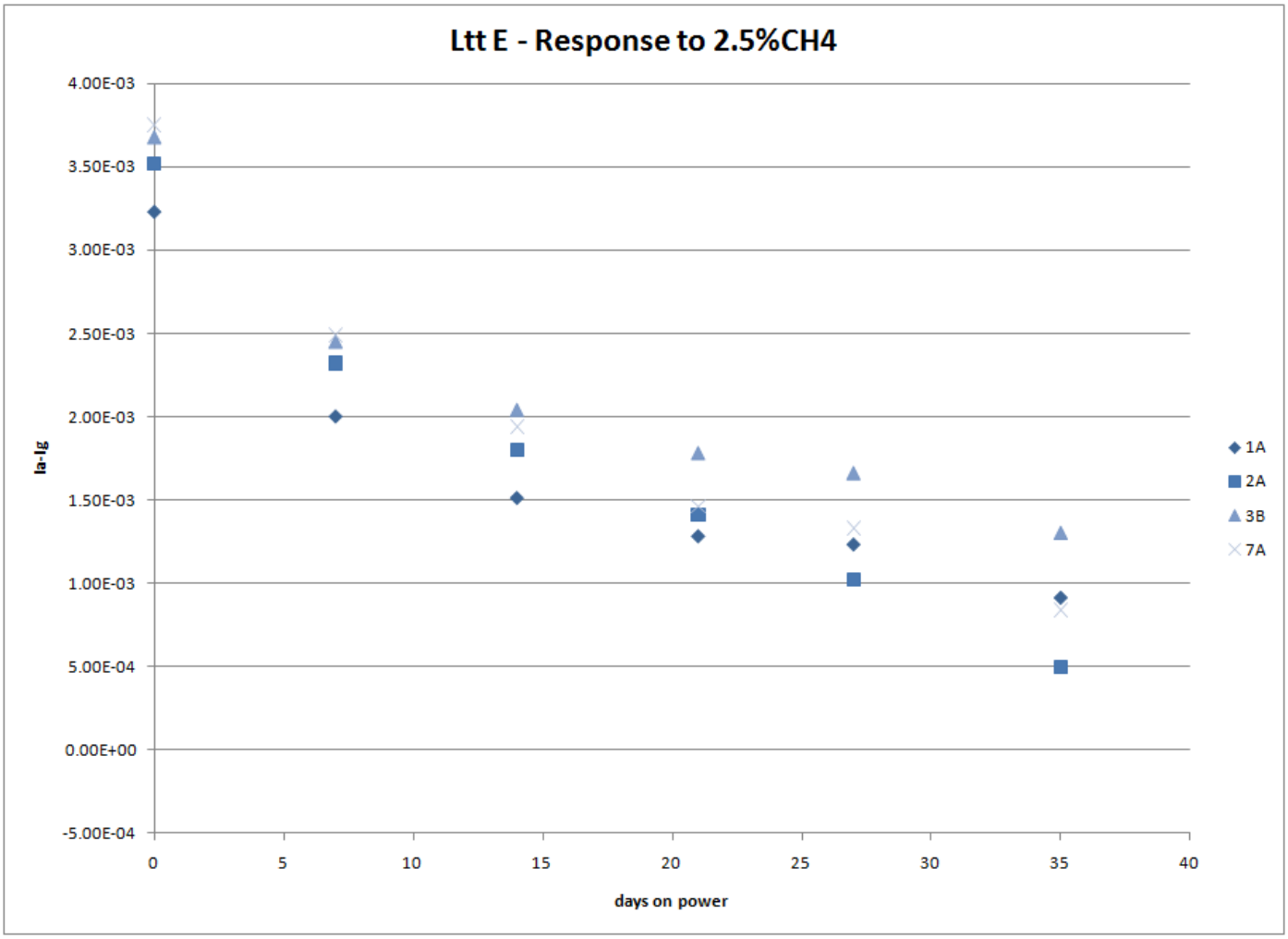

SUMMARY

F.1. POSITIVES

- Strong response at ~50 mW/element
- Good repeatability
- Short term calibration data is good, based on a polynomial curve fit

F.2. NEGATIVES

- Output is non-linear, trailing off at higher concentrations
- “Negative” response to higher hydrocarbons
- Significantly diminished response following exposure to H_2S
- Sensors taking more than 2 weeks to burn-in/stabilize

F.3. STILL TBD

- Humidity – response is significantly diminished between dry cylinder gas and a humidified gas stream at 45%RH, but we do not know the effect over the real range of humidity (5-95%RH).
- Temperature

Appendix E

Evaluation of LttH, LttJ, and LttK

Following the March 2011 evaluation of Pd only catalyst on beaded sensors an investigation of Pd/Pt co-catalyst ensued. This report covers the evaluation of two co-catalyst compositions and also Pd only catalyst as a reference.

SENSOR INFORMATION

	Ltt H	Ltt J	Ltt K
Composition	**Pd only**	**1:1 Pd:Pt**	**2:1 Pd:Pt**
Continuous Power	**70 mW/element**	**70 mW/element**	**70 mW/element**
Testing Power	**70 mW/element**	**110 mW/element**	**110 mW/element**

- **All sensors were on power > 1 month prior to the evaluation, during which time burn-in/stability data was being acquired**
- **2.1 design (longer heater)**
- **Beaded**
- **Bridge testing**
- **Evaluation data and this write up are located in \\Hera\ZeusPublic\RD&E\Research Projects\Current Projects\7057 - CGµS - NIH PhII (DR)\1. Results\5. Testing\Analysis\Evaluation_0511**
- **Data and work up is in this file**

POWER

The operating power was determined from CV experiments performed several days before the evaluation. The input was selected in order to operate the sensors on the plateau. The fact that the Pt containing catalysts require a higher operating temperature (power) is expected based on conversations with our consultant in catalyst development, Jim Miller.

LINEARITY

Methane (dry): 0.25, 0.5, 1, 2.5%

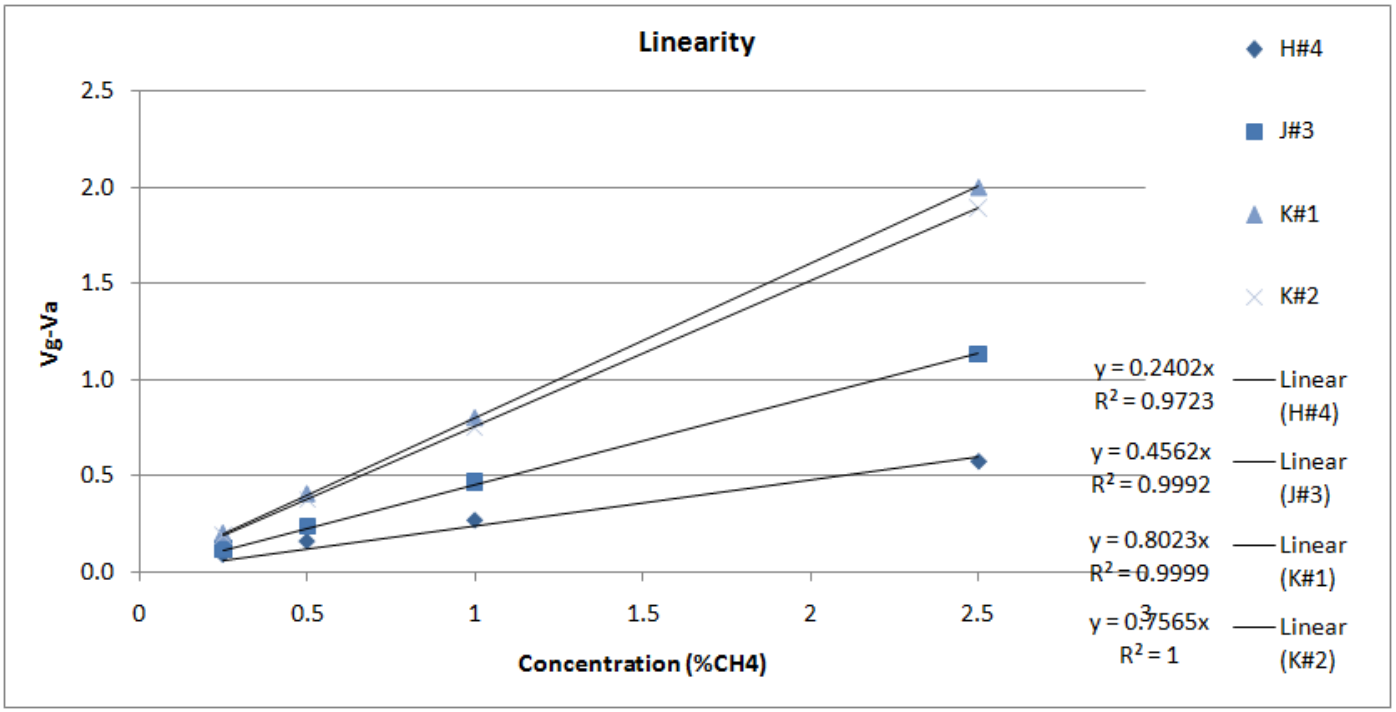

CALIBRATION

Methane: 0.35, 0.75, 1.25% (accuracy based on linear curve fit above)

Concentration (% Methane)	H4 (error)	J3 (error)	K1 (error)	K2 (error)
0.35	30.4%	16.1%	13.7%	6.9%
0.75	12.8%	8.5%	8.4%	4.4%
1.25	-0.5%	5.0%	5.1%	2.7%

H.

REPEATABILITY

6 exposures to 2.5% CH4 (5 min. exposure, 5 min. off)

Exposure	H4 (error)	J3 (error)	K1 (error)	K2 (error)
2	3.0%	-0.3%	-1.1%	-0.1%
3	5.2%	-0.4%	-1.5%	-0.4%
4	6.7%	-0.3%	-1.9%	-0.5%
5	7.8%	-0.3%	-1.9%	-0.6%
6	9.6%	-0.3%	-2.1%	-0.2%

HUMIDITY

Methane linearity dry (0.25, 0.5, 1, 2.5%), 5 minute steps
Methane linearity @ 45%RH (0.25, 0.5, 1%), 5 minute steps
0-15-50-85-0 %RH, 10 minute steps

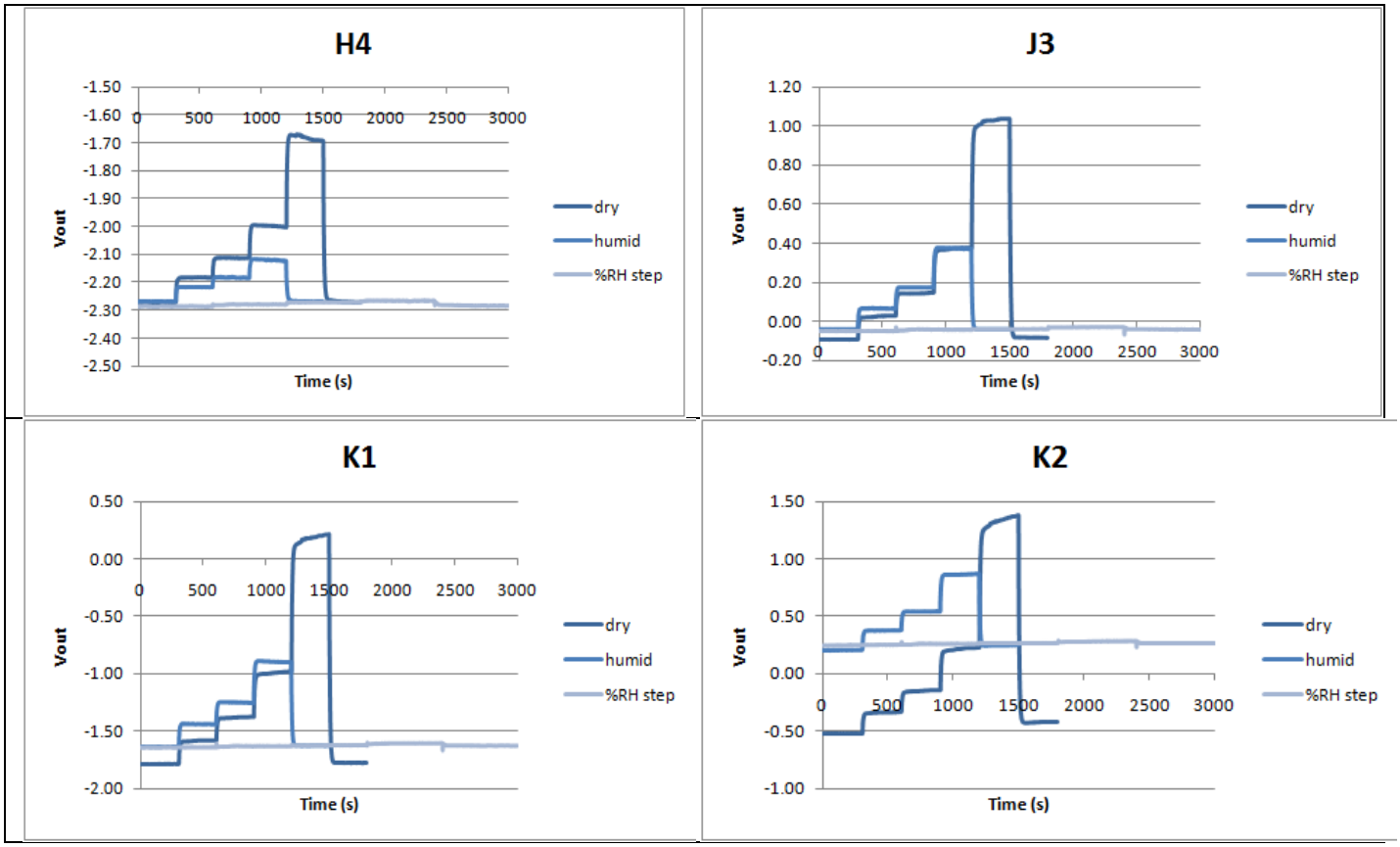

HYDROCARBON RANGE

Methane: 0.25, 0.5, 1.0, 2.5%
Propane: 0.1, 0.25, 0.5, 1%
Pentane: 250, 1000, 5000, 7500 ppm
Hexane: 250, 500, 1000, 5000 ppm

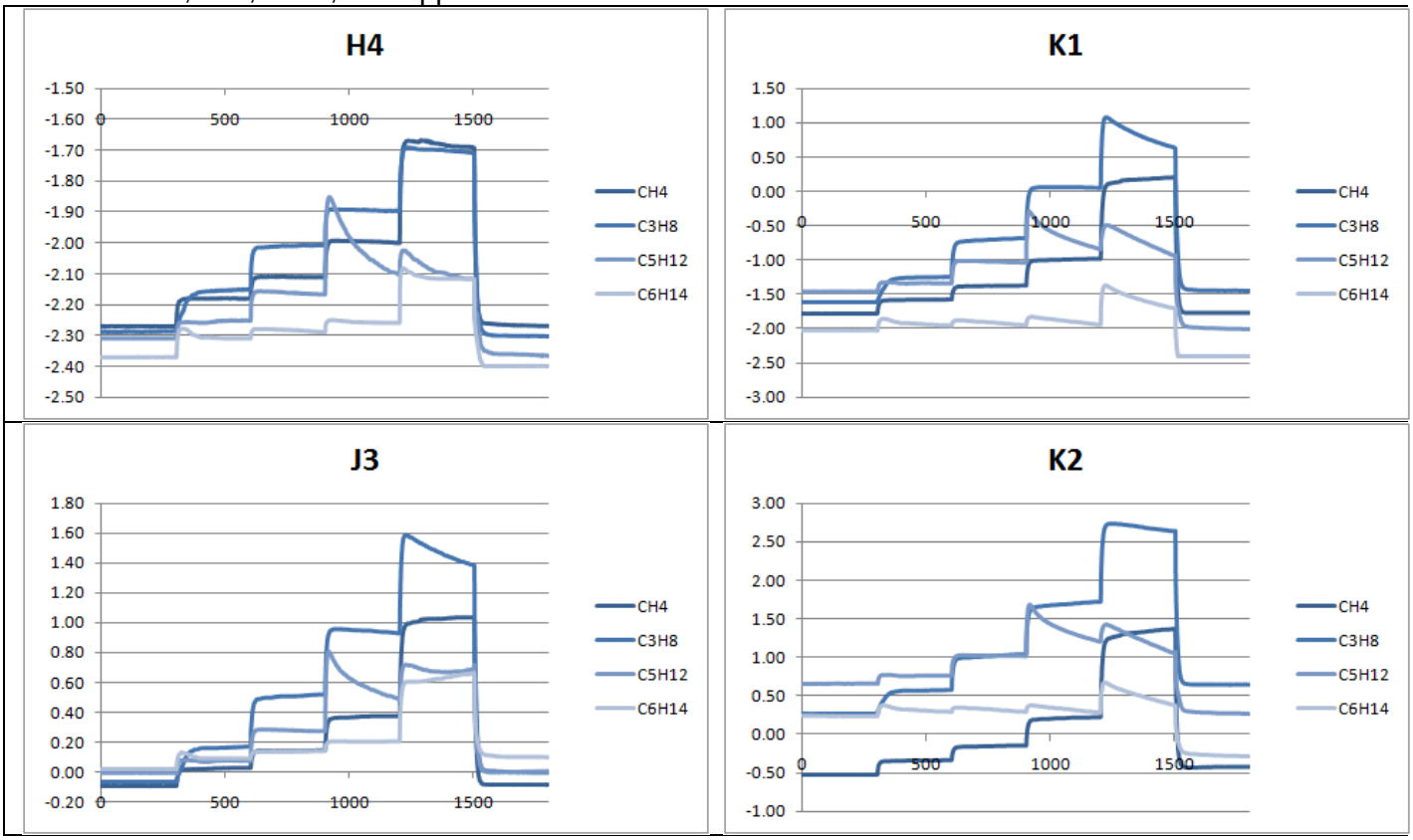

TEMPERATURE

Temperature testing was not performed due to the difficulties with noise when previously trying to using the existing temperature chamber to test the combustible gas sensors.

SULFUR RESISTANCE

Methane linearity (0.25, 0.5, 1, 2.5%)
Expose sensor to 10 ppm H_2S for 10 minutes
Methane linearity (0.25, 0.5, 1, 2.5%)

H4 did not undergo this testing, so data from the previous analysis of the Pd only sensors is included for reference (“Sulfur (Raw)”).

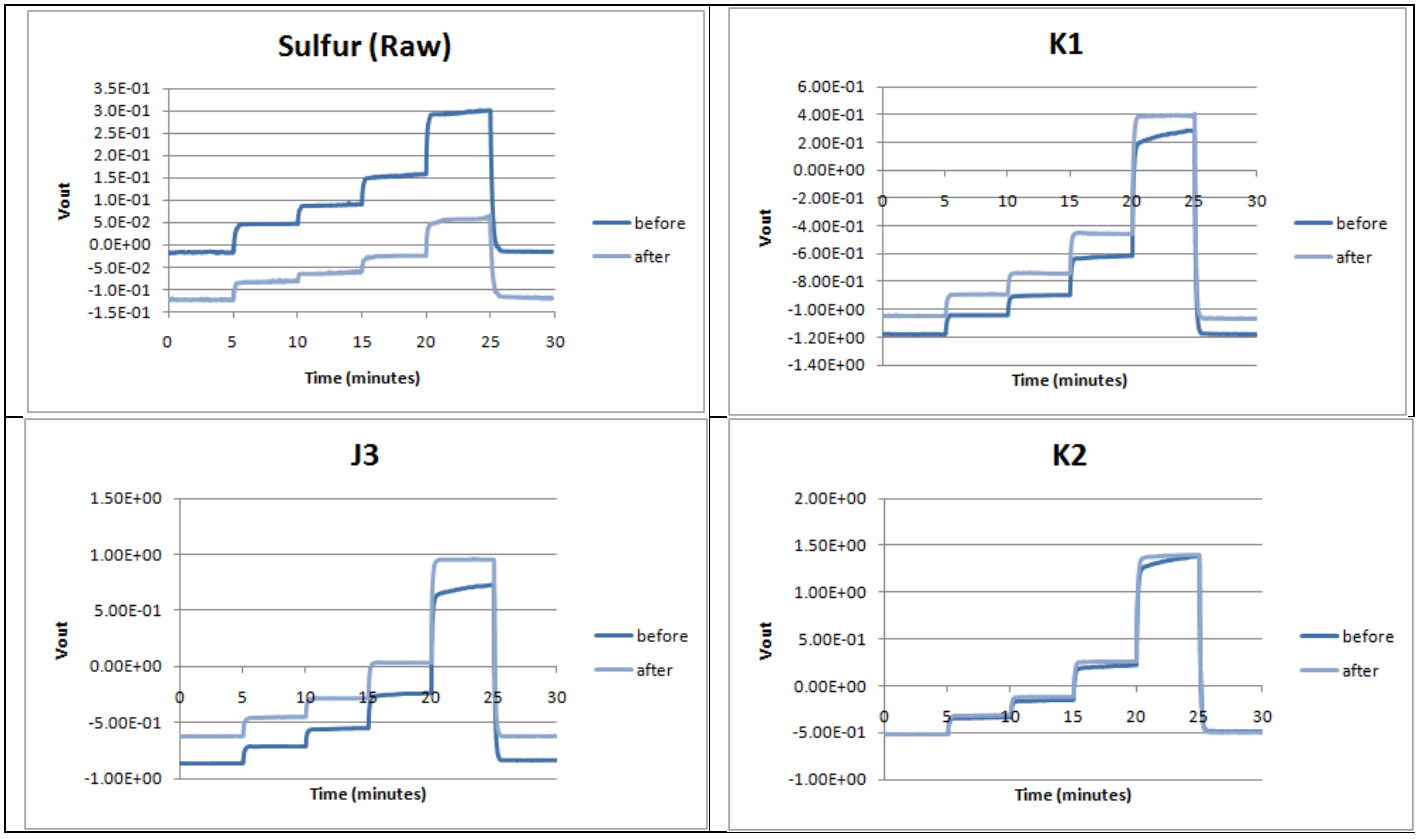

BURN-IN / LONG TERM STABILITY

Sensors powered continuously and routinely (~ weekly) tested by CV and using the bridge circuits. Initially the sensors were held on power at 45 mW per element for the first 16 days and then increased to 70 mW per element. The plots show the change in voltage reading between the gas exposures and clean air.

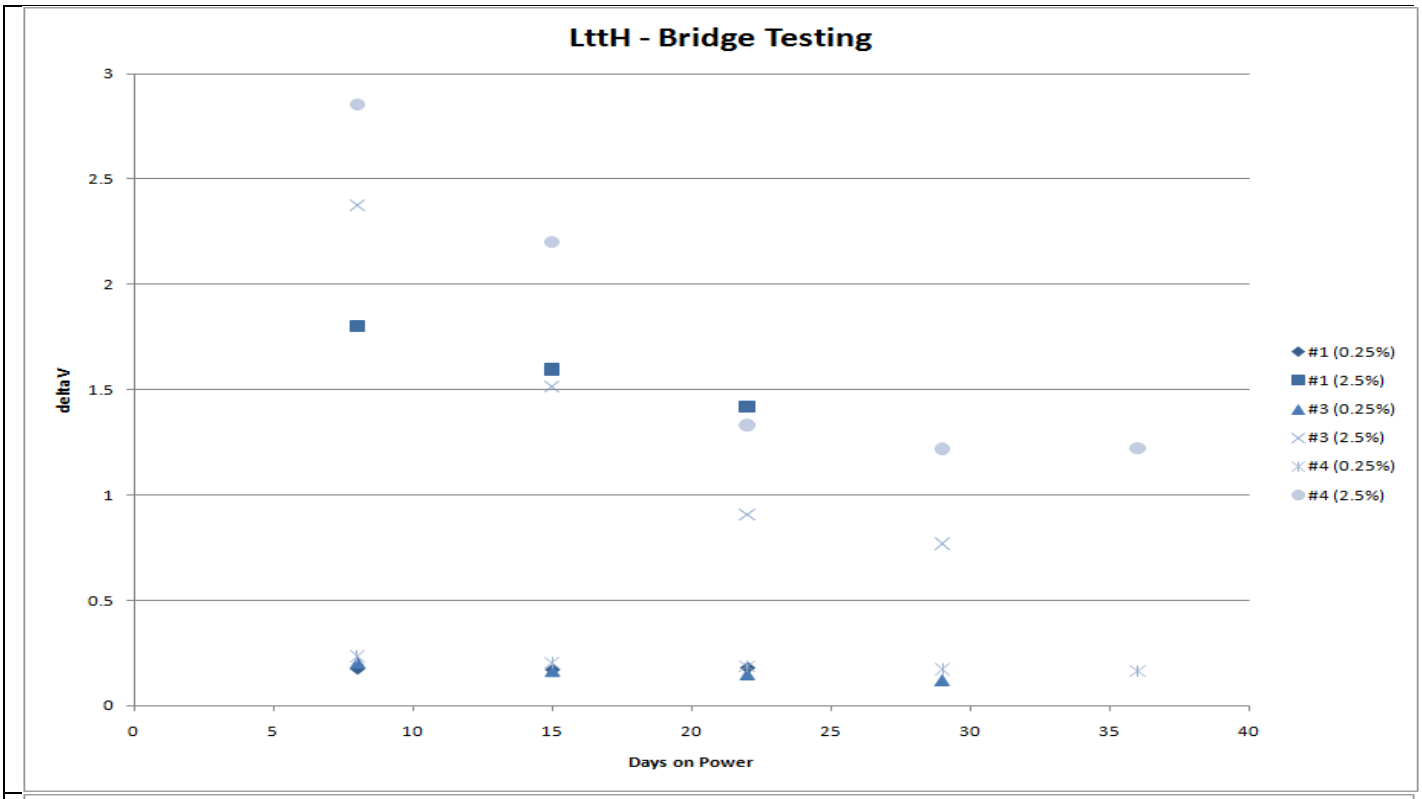
LttH - Bridge Testing
deltaV
Days on Power
#1 (0.25%)
#1 (2.5%)
#3 (0.25%)
#3 (2.5%)
#4 (0.25%)
#4 (2.5%)

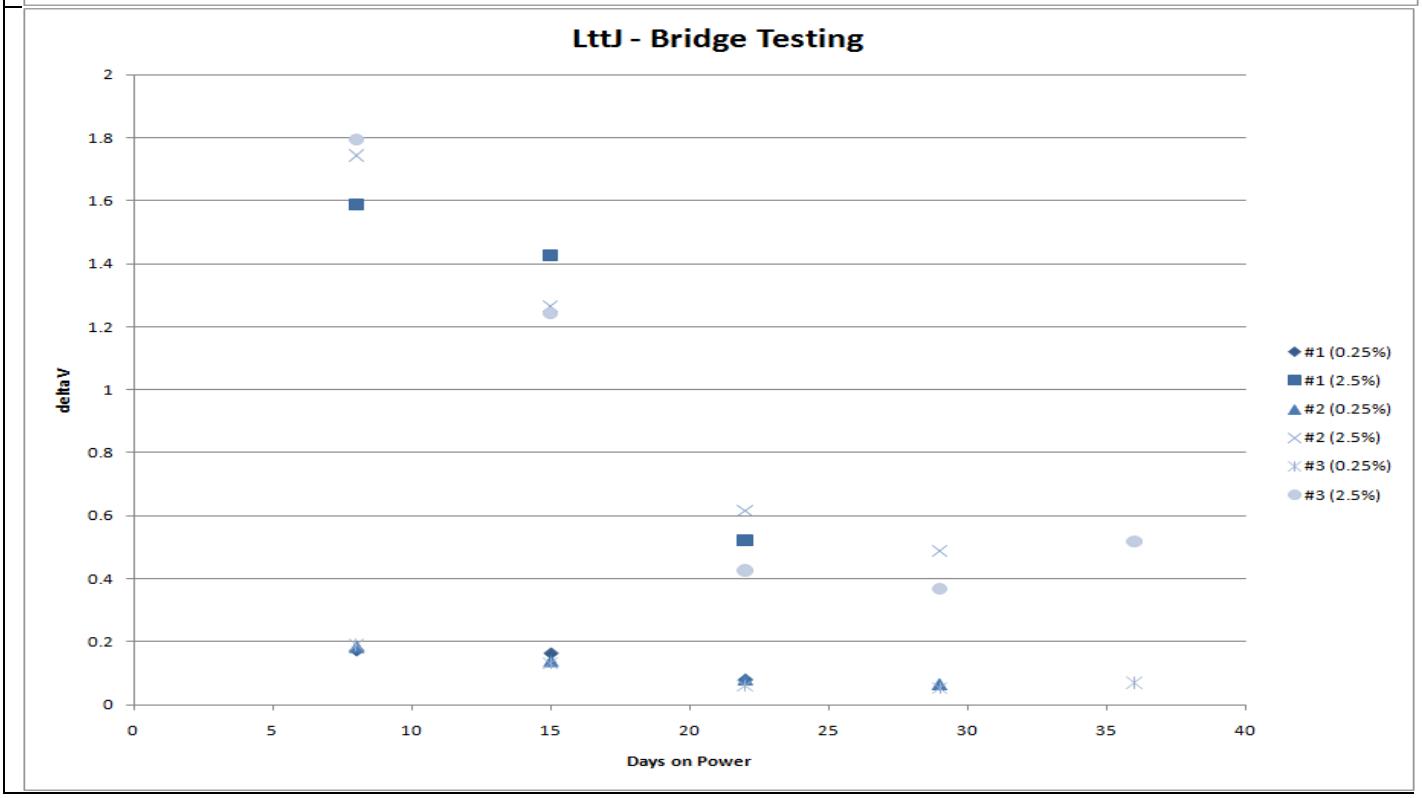
LttJ - Bridge Testing
deltaV
Days on Power
#1 (0.25%)
#1 (2.5%)
#2 (0.25%)
#2 (2.5%)
#3 (0.25%)
#3 (2.5%)

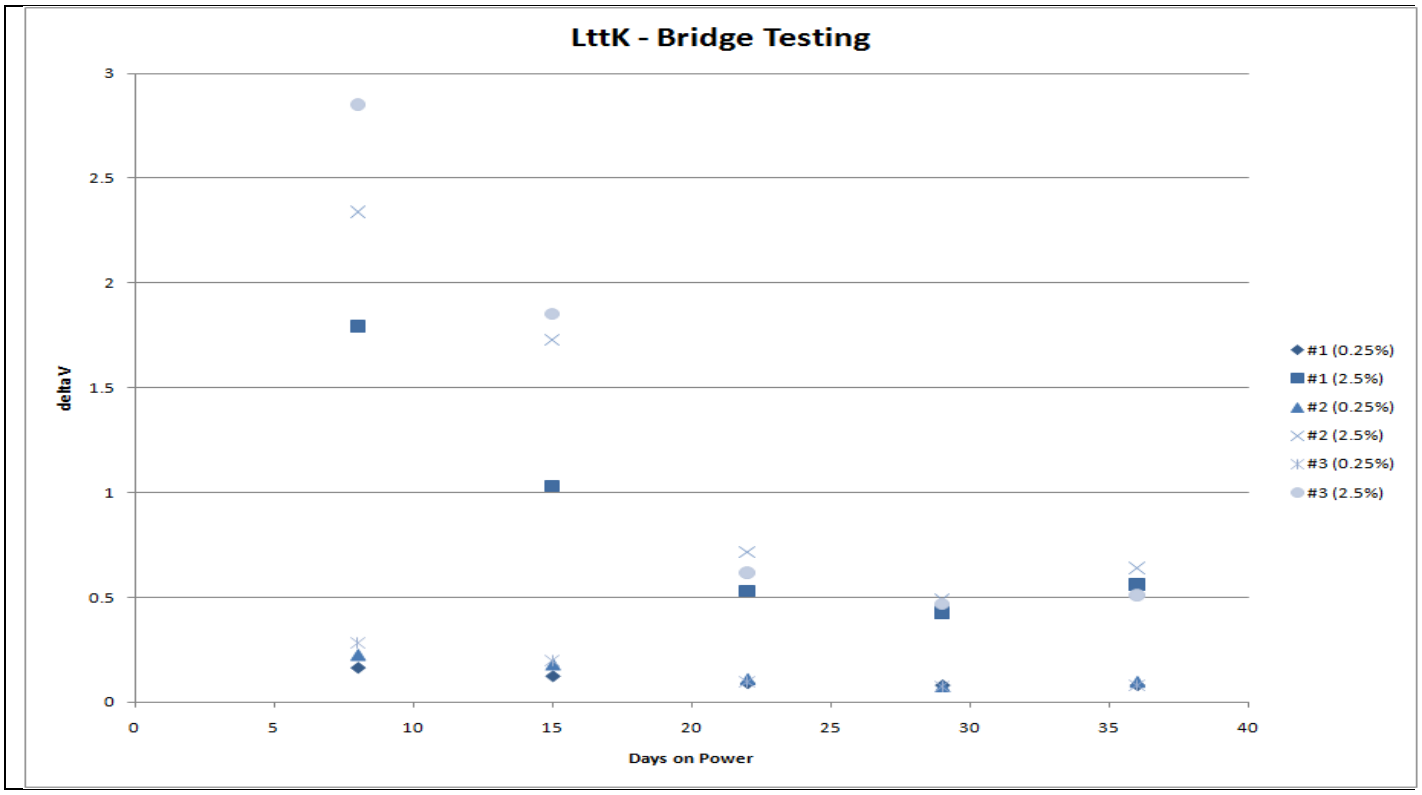

CONCLUSIONS

The LttK sensors (2:1 Pd:Pt) seen to be the best performing sensors, although the sample size was quite small. The two samples of this composition

- showed the best linearity
- performed the best in the calibration experiment based on the linearity data
- had <2% error in repeatability over six exposures to 2.5% methane
- performed as well or better than the other compositions when exposed to higher hydrocarbons (though still had strange curve shap)
- appear to have the best sulfur tolerance
- maintain reasonable sensitivity with time on power (though effect of time on power at 110 mW has not been determined, as this power was selected based on CVs just prior to evaluation.

The negatives of this 2:1 Pd:Pt composition are

- higher power than Pd only (220 mW for a dual element sensor versus 140 mW)
- shows greater effect due to environmental humidity than the other compositions

Appendix F

Evaluation of LttM and LttN

We have run additional testing on a couple of sensor compositions that have been on continuous power and are being exposed to methane on a routine basis. This testing included humidity and hydrocarbon range.

SENSOR INFORMATION

	Ltt M	Ltt N
Composition	**3:1 Pd:Pt, Al_2O_3 bead, heater down (standard)**	**Pd only, Al_2O_3 bead, heater up (bead covers Pt trace)**
Continuous Power	**~75 mW/element**	**~60 mW/element**
Testing Power	**~75 mW/element**	**~60 mW/element**

- **sensors were on power > 8 weeks prior to testing**
- **2.1 design (longer heater), 75 microns**
- **Bridge testing**
- **Evaluation data and this write up are located in \\Hera\ZeusPublic\RD&E\Research Projects\Current Projects\7057 - CGµS - NIH PhII (DR)\1. Results\5. Testing\Analysis**
- **Test data in this file**

LINEARITY

Methane (dry): 0.25, 0.5, 1, 2.5%

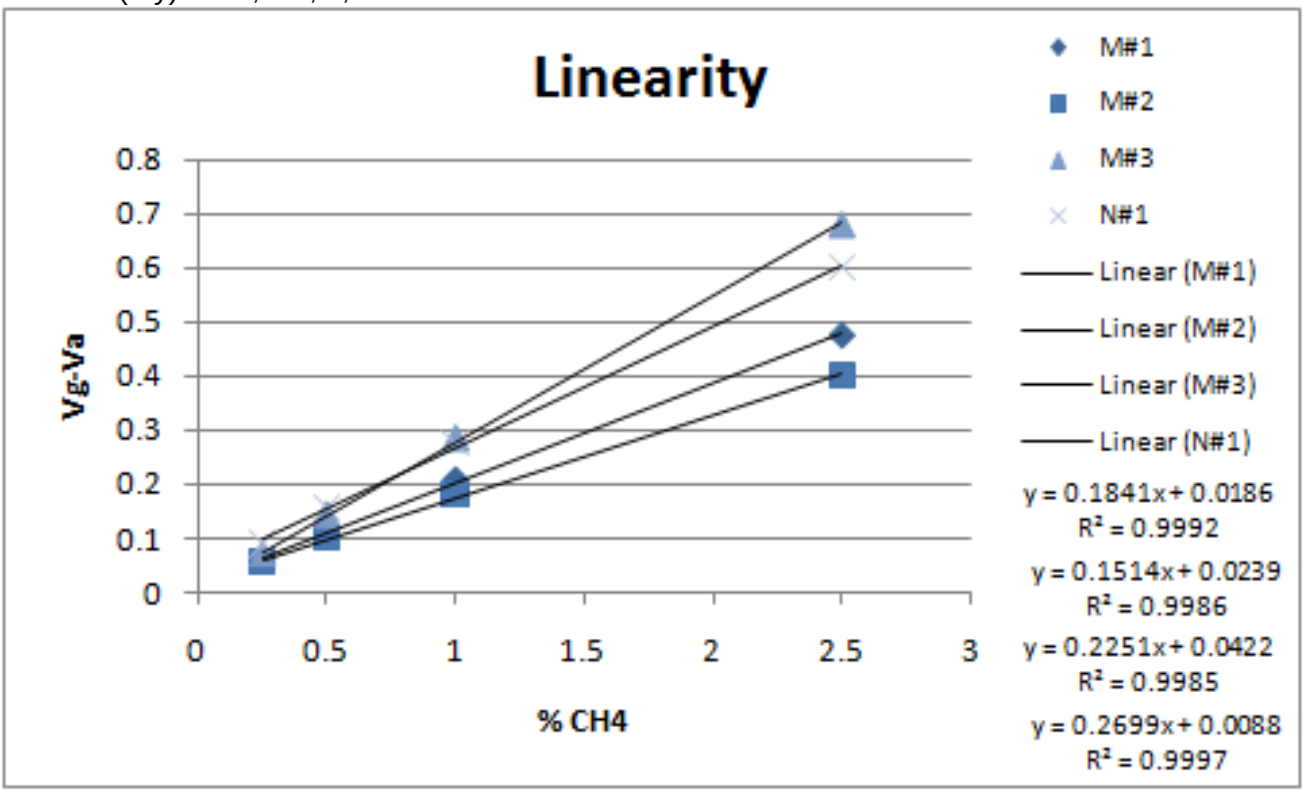

HUMIDITY

Methane linearity dry (0.25, 0.5, 1, 2.5%), 5 minute steps
Methane linearity @ 45%RH (0.25, 0.5, 1%), 5 minute steps
0-15-50-85-0 %RH, 10 minute steps

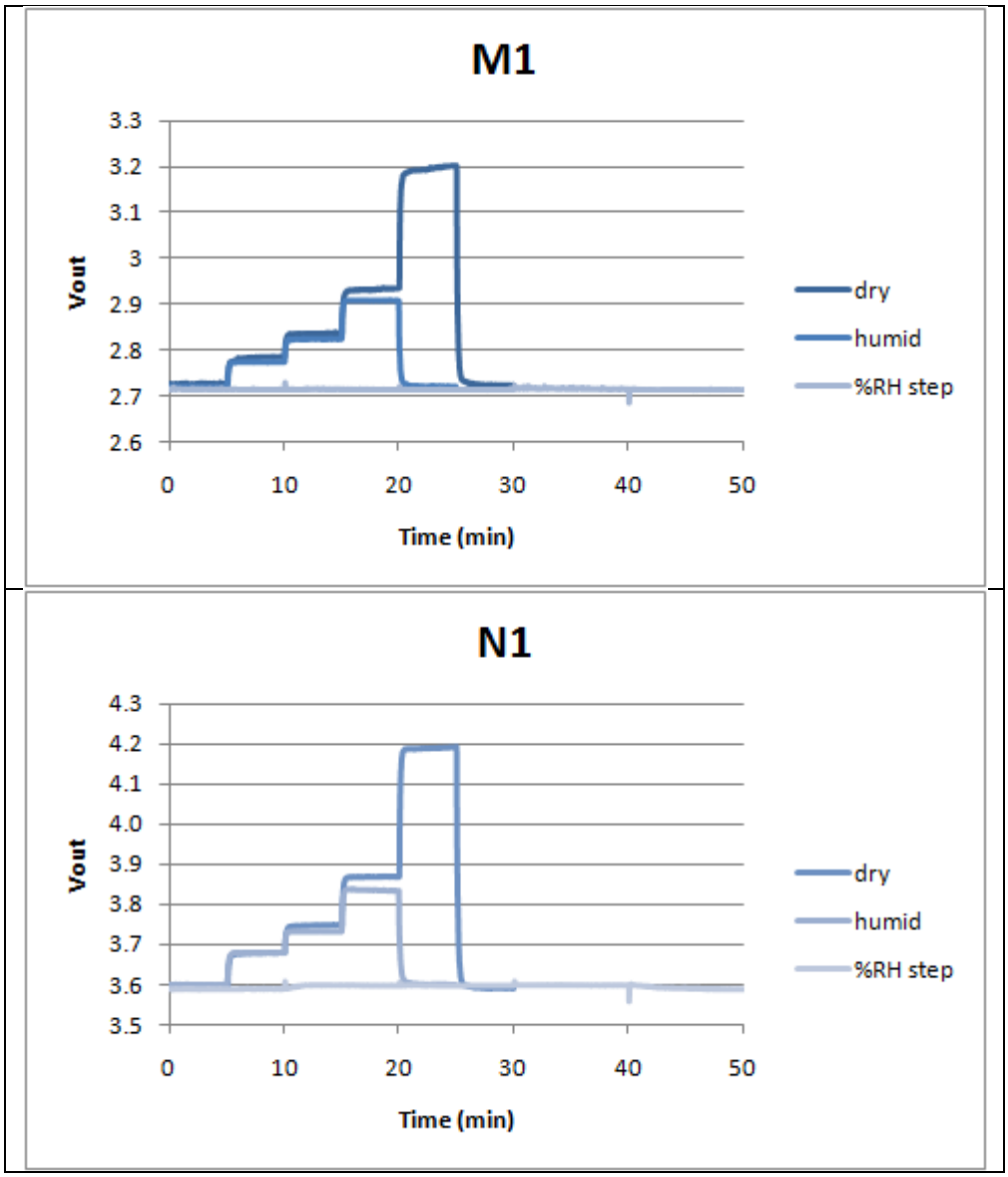

HYDROCARBON RANGE

Methane: 0.25, 0.5, 1.0, 2.5%
Propane: 0.1, 0.25, 0.5, 1%
Pentane: 250, 1000, 5000, 7500 ppm
Hexane: 250, 500, 1000, 5000 ppm

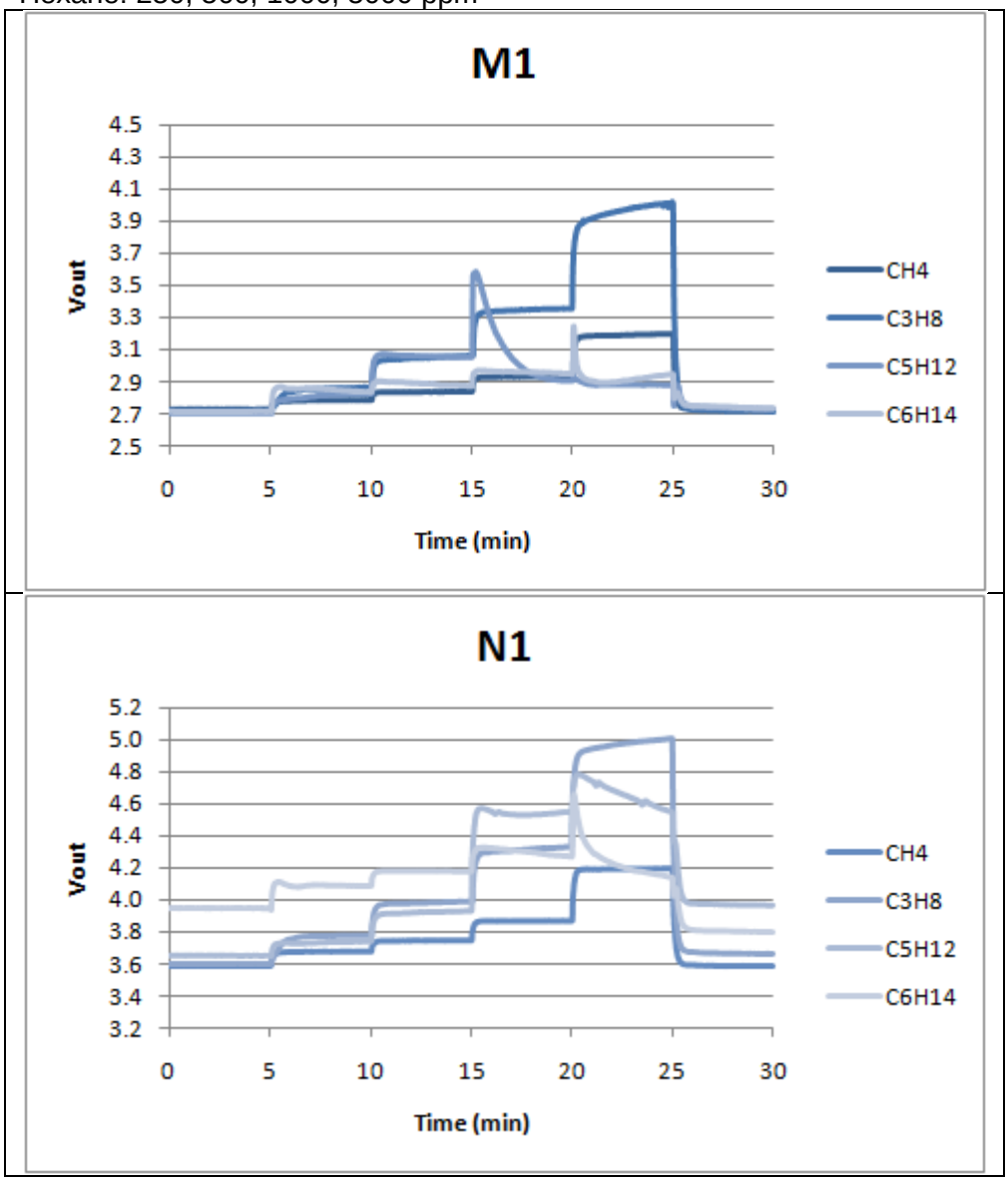

Previously from Jim Miller: The slumping patterns for C5 and C6 are unexpected. Heavier hydrocarbons can cause carbon deposition ("coking") on the catalyst surface, which can cause zero shifts (which you appear to be experiencing here)—but not normally for C5 and C6. This result might be caused by the "alumina-only" support.

Appendix G

Evaluation of LttT and LttU

We have performed an extensive evaluation of the best performing sensors developed through the Phase II work. These are sensors that utilize a ceria/zirconia bead and palladium based catalyst. The sensors had gone through burn-in, were continuously powered and routinely exposed to methane of the course of weeks prior to the full suite of tests being run. Information regarding initial behavior, aging, and performance is discussed below. The testing is outlined in the table of contents above.

SENSOR INFORMATION

	Ltt T	Ltt U
Composition	**Pd only, Ce/Zr bead, heater down**	**2:1 Pd:Pt, Ce/Zr bead, heater down**
Continuous Power	**~70 mW/element**	**~70 mW/element**
Testing Power*	**~85 mW/element**	**~85 mW/element**

***power was increased for evaluation based on CVs run prior to testing.**

- **sensors were on power 8 weeks prior to testing**
- **2.1 design (longer heater), 75 microns thick**
- **Bridge testing (comparison of active/catalyzed element and reference/uncatalyzed element)**
- **3 sensors of each type were tested**
- **A single, representative sensor of each type is presented here for ease of viewing**
- **The Excel file containing the raw data, plots, and calculations is here .**

BURN-IN BEHAVIOR

The plots below present CV curves for the active elements upon initial fabrication and after ~7 weeks of being continuously powered. The reduction in output (Ia-Ig) and the shift of the plateau to a higher power (represented as Volts to heater on the x-axis) are typical behaviors seen during burn-in.

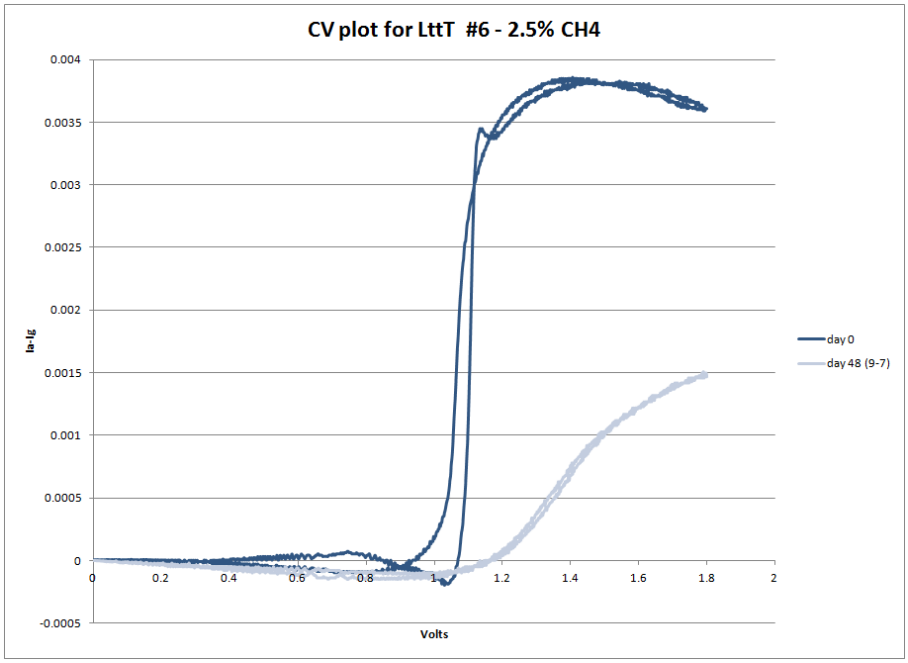

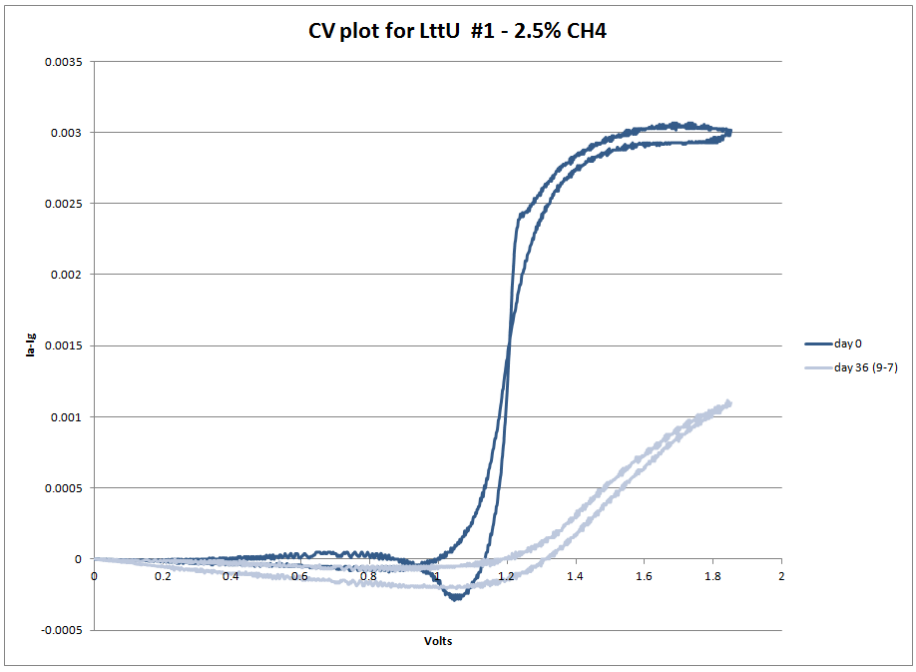

The plots below show the burn-in behavior of the sensors over the course of ~7 weeks when tested using a bridge measurement, a comparison of the response of the active element to the reference element. (Note that all testing reported from here down are bridge measurements.) This data is presented for the entire group of sensors. The output at two concentrations of CH_4 is plotted, 0.25% and 2.5%. The apparent step change in output that is seen coincides with the sensors "falling off the plateau" at the set

operating power. For the analysis below adjustments were made (operating power increased) to account for this. Things considered, the sensors showed reasonable stability over the course of the test.

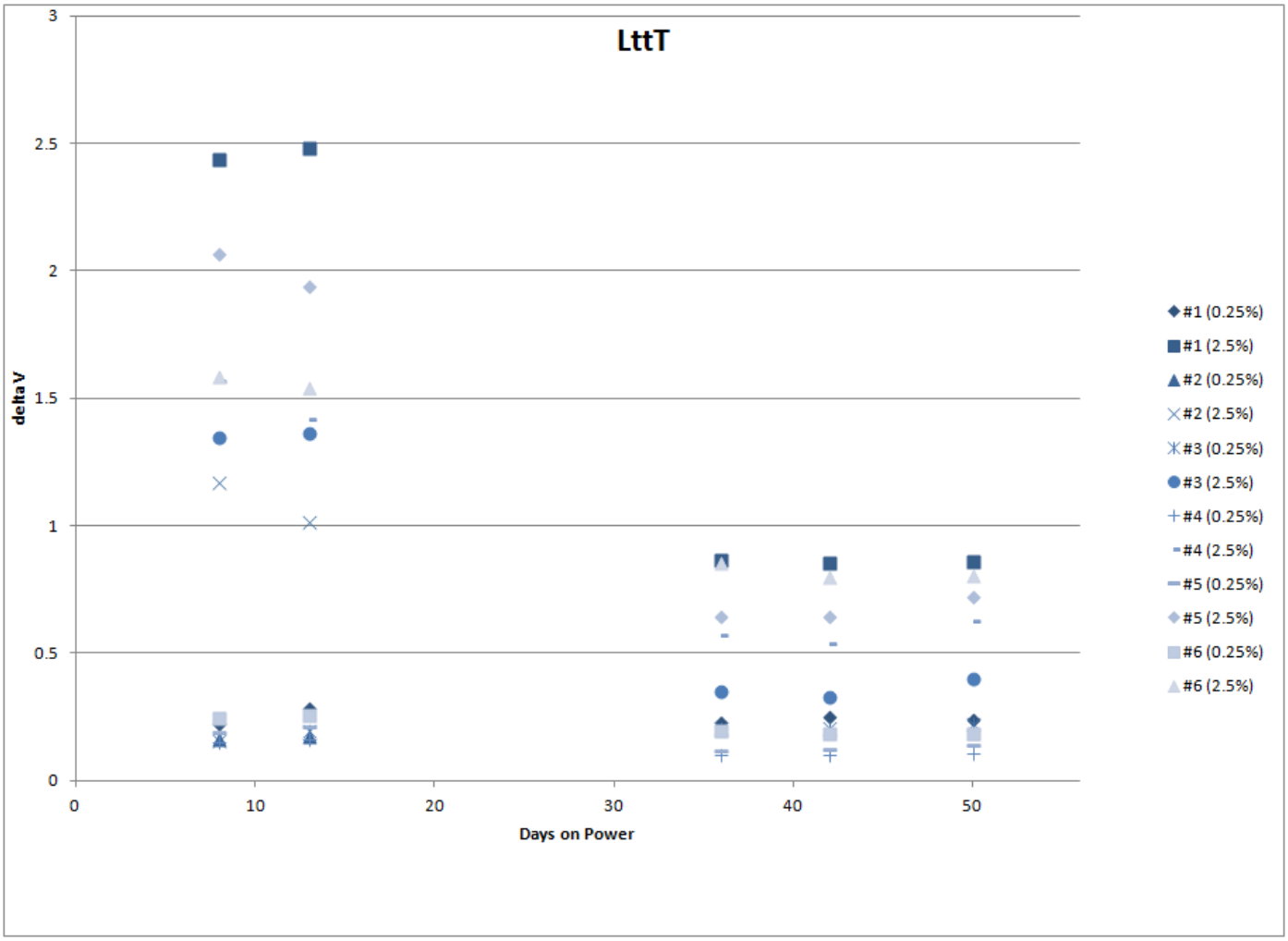

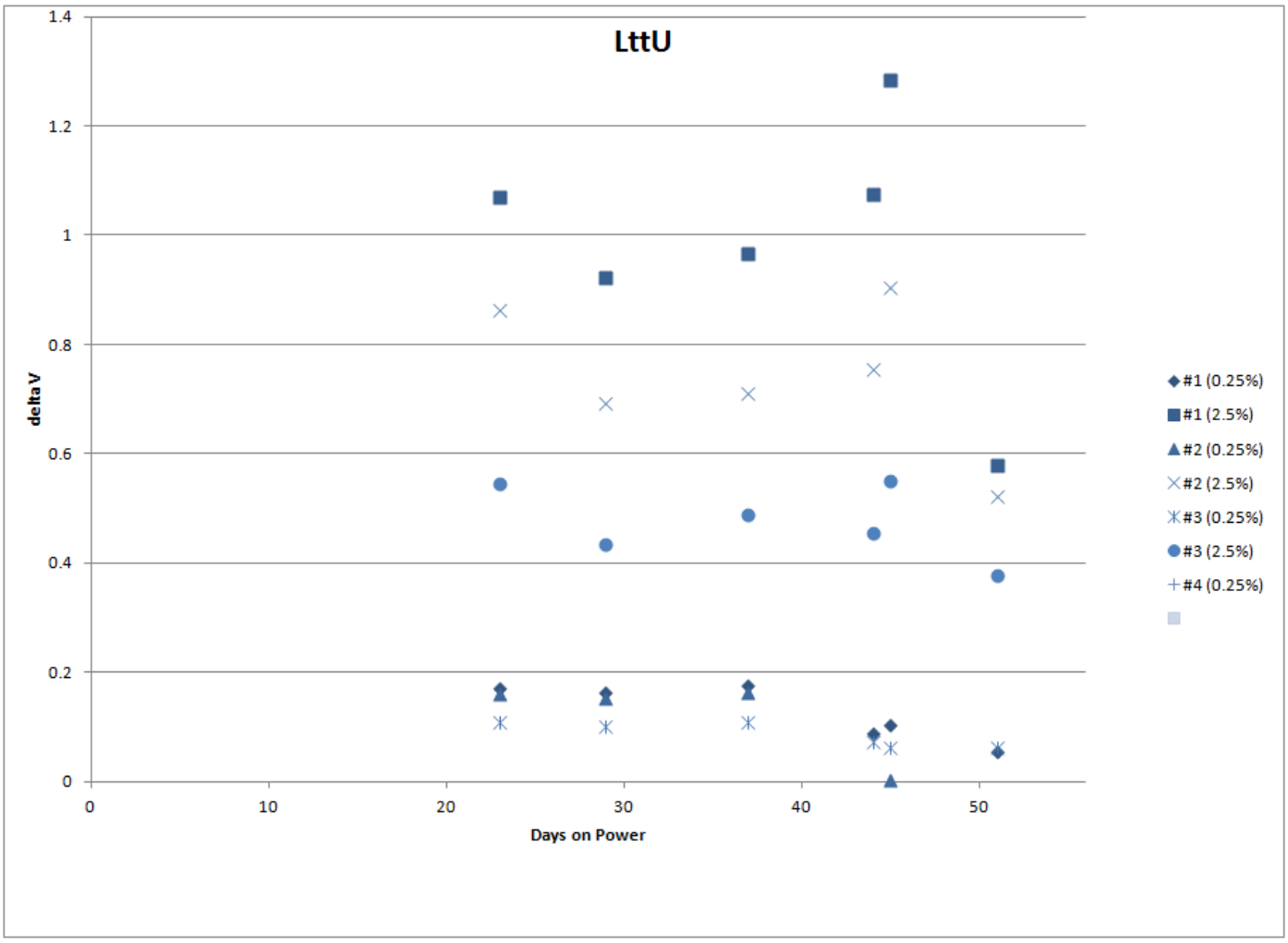
LttU
delta V
Days on Power
1.4
1.2
1
0.8
0.6
0.4
0.2
0
0
10
20
30
40
50
#1 (0.25%)
#1 (2.5%)
#2 (0.25%)
#2 (2.5%)
#3 (0.25%)
#3 (2.5%)
#4 (0.25%)

LINEARITY

- *Methane (dry): 0.25, 0.5, 1, 2.5%*

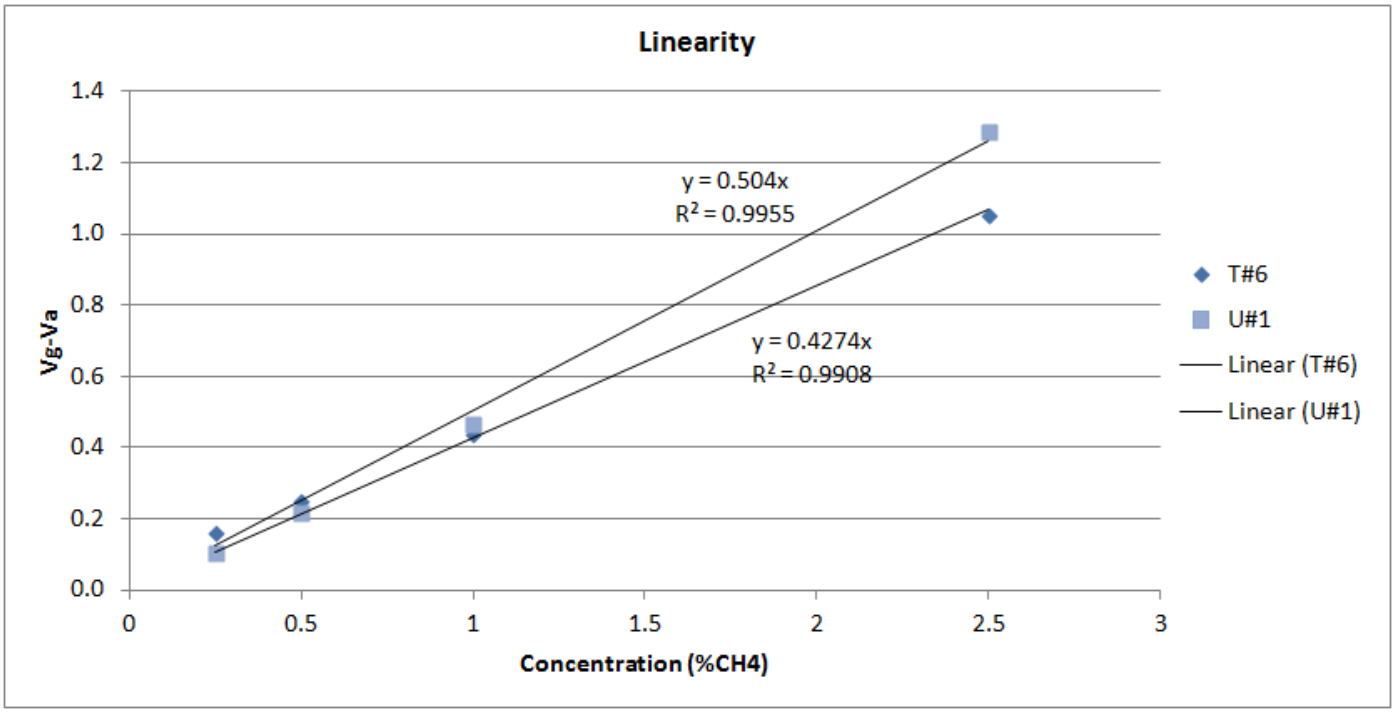

The linearity is reasonable, suggesting that by increasing the power from the 70 mW used for the burn-in period, to 85 mW for the extended evaluation that the sensors were operated on the plateau.

REPEATABILITY

- *Six exposures to 2.5% methane*

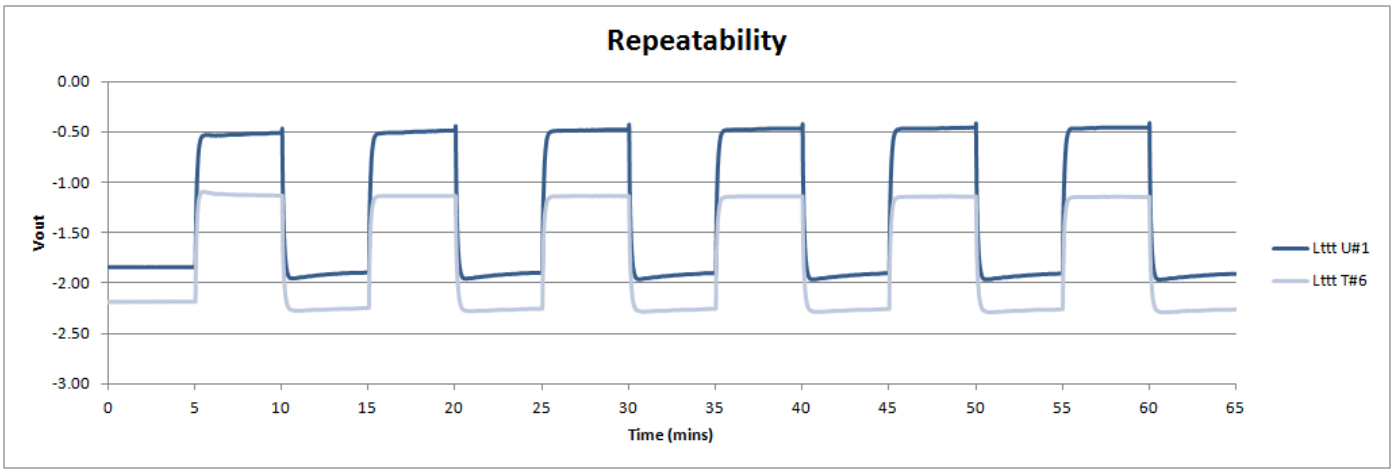

Analysis of this data indicates that both sensors had a relatively significant increase in output between the first and second exposures, 5.4% and 12.5% respectively for T#6 and U#1. Much less additional increase between exposure 2 and 6 was seen, 0.5% and 3.3%, respectively. This increase may be due to "activation" of the catalyst upon initial exposure to methane.

HUMIDITY

- *Methane linearity dry (0.25, 0.5, 1, 2.5%), 5 minute steps*
- *Methane linearity @ 45%RH (0.25, 0.5, 1%), 5 minute steps*
- *0-15-50-85-0 %RH, 10 minute steps*

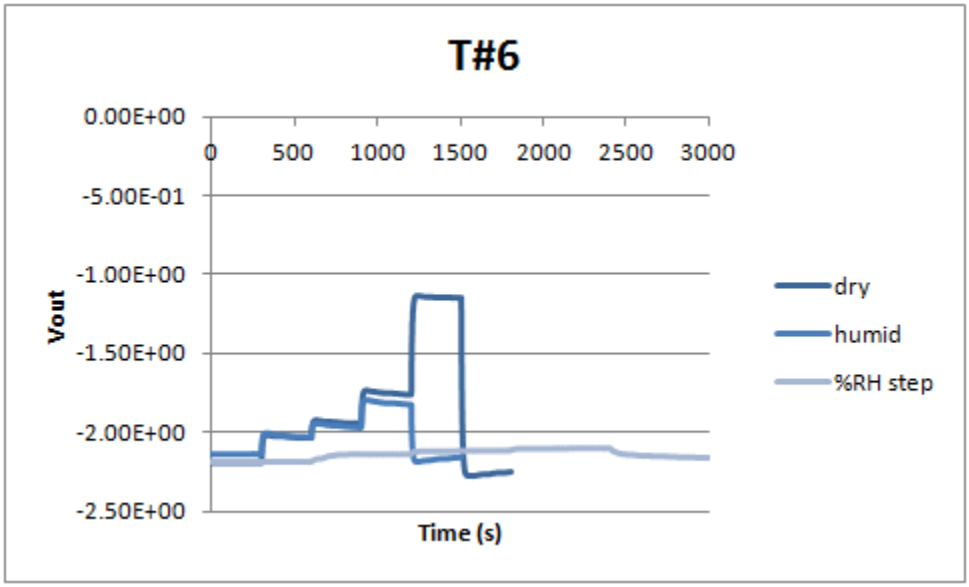

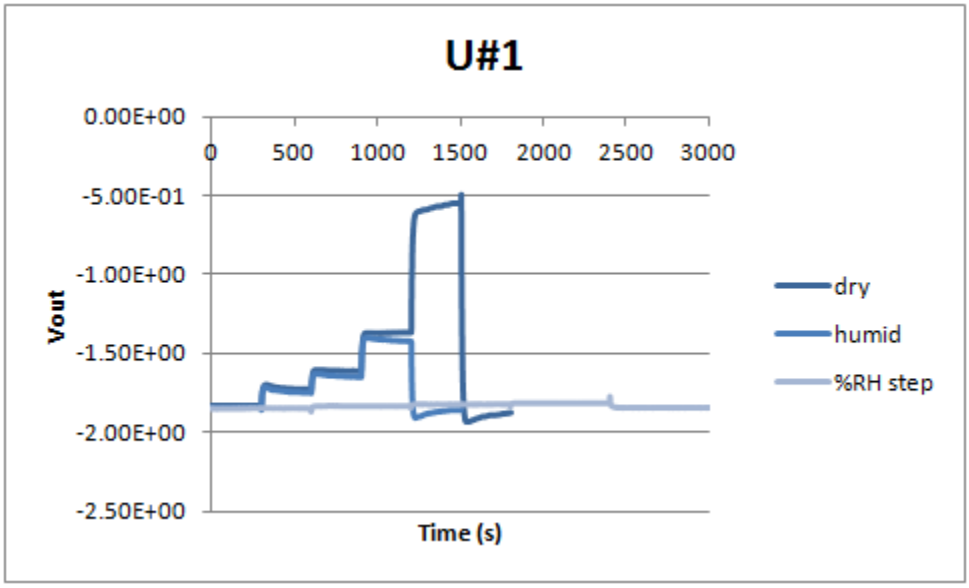

The reference element does a reasonable job to compensate for humidity, however when sensors are exposed to higher concentrations of methane there seems to be some interference seen.

HYDROCARBON RANGE

- *Methane: 0.25, 0.5, 1.0, 2.5%*
- *Propane: 0.1, 0.25, 0.5, 1%*
- *Pentane: 250, 1000, 5000, 7500 ppm*
- *Hexane: 250, 500, 1000, 5000 ppm*

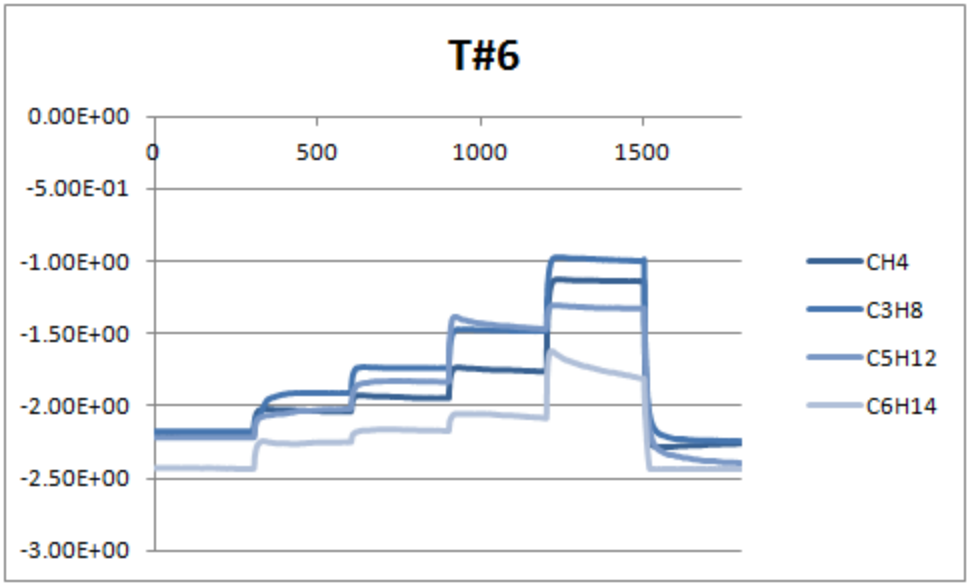

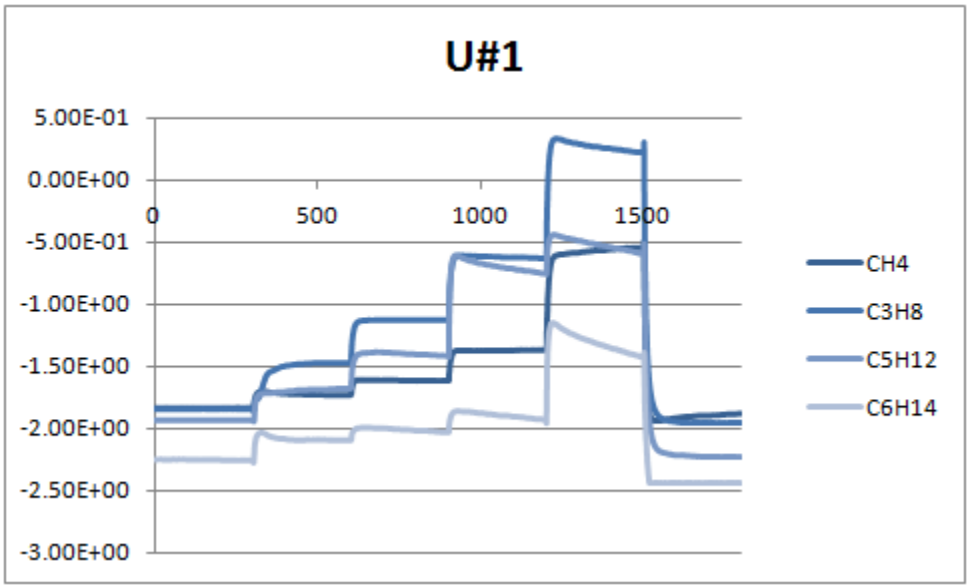

One of the benefits of this final Phase II design, from the use of CeO/ZrO_2 for the bead, is that this material has a great oxygen storage capability than the initial Al_2O_3 beads. This was expected to translate to better performance when sensors are exposed to higher concentrations of the higher hydrocarbons. While there is considerably less "slumping" of the response of these sensors, we are still seeing some of this behavior. This is potentially due to not having sufficient catalytic volume.

TEMPERATURE

- *Methane linearity at:*
  Day 1 – 20°C, 0°C, -20°C, -40°C
  Day 2 – 20°C, 40°C

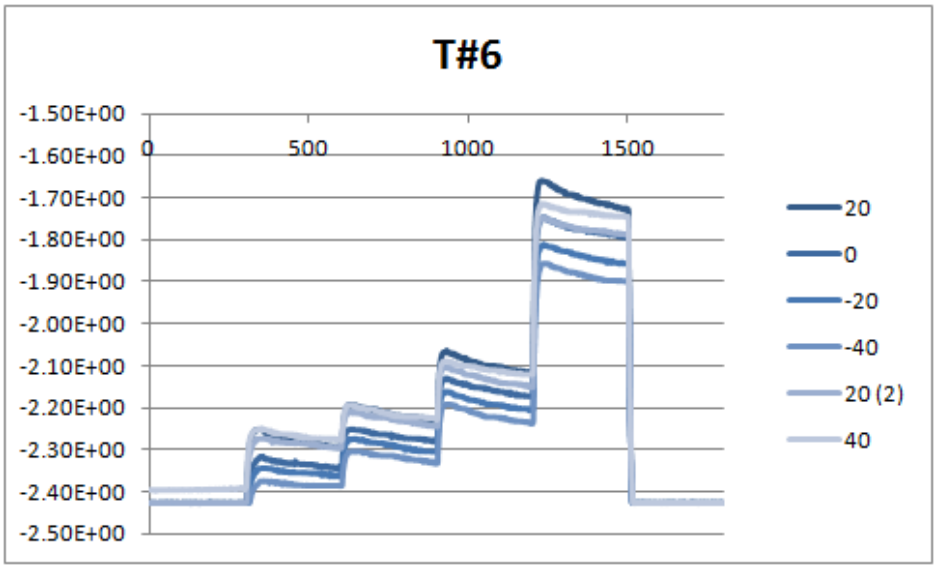

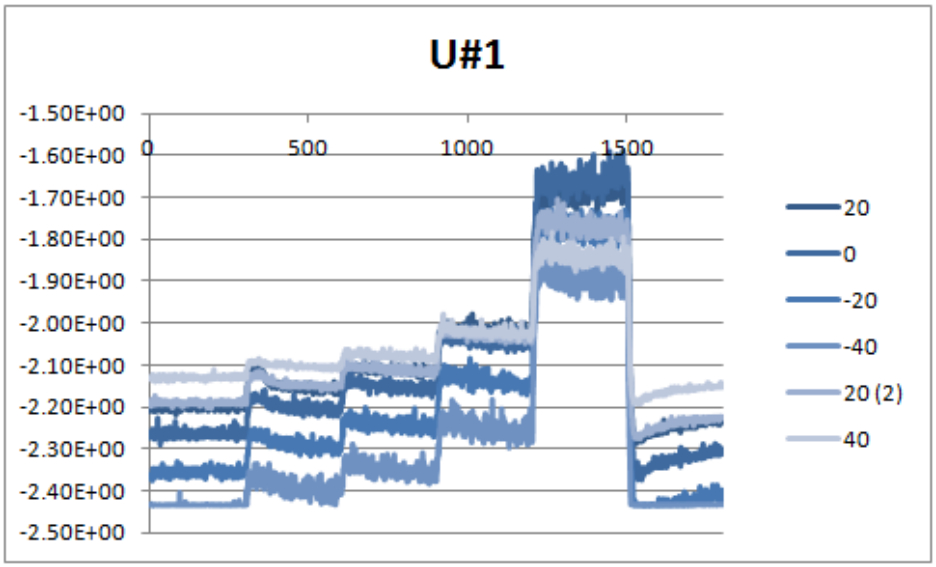

While the magnitude of the response did not seem to change much depending on the temperature, the baseline trended down with decreasing temperature. It is worth noting that there seemed to be a shift in baseline and a decreased magnitude in response between Day 1 and Day 2.

T#1 exhibited an offset of 0.17V when exposed to 2.5% methane at 20°C and -40°C, while U#1 had a 0.27V offset. Based on the initial linearity data these equates to errors of 0.40% and 0.54% methane, respectively.

SULFUR RESISTANCE

- *Methane linearity (0.25, 0.5, 1, 2.5%)*
- *Expose sensor to 10 ppm H_2S for 10 minutes (per proposal)*
- *Methane linearity (0.25, 0.5, 1, 2.5%)*

Note that T#6 was not exposed to sulfur, so T#5 is reported for this experiment.

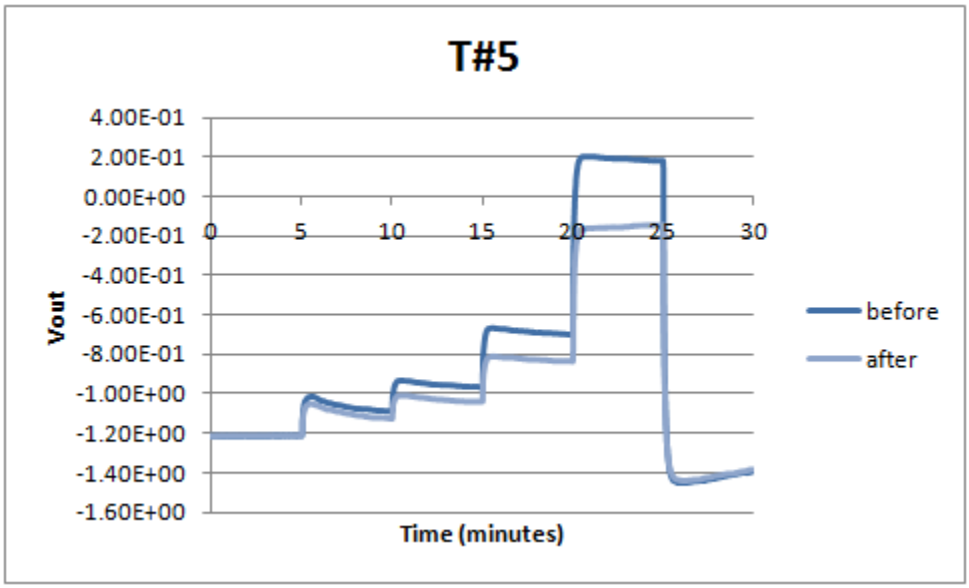

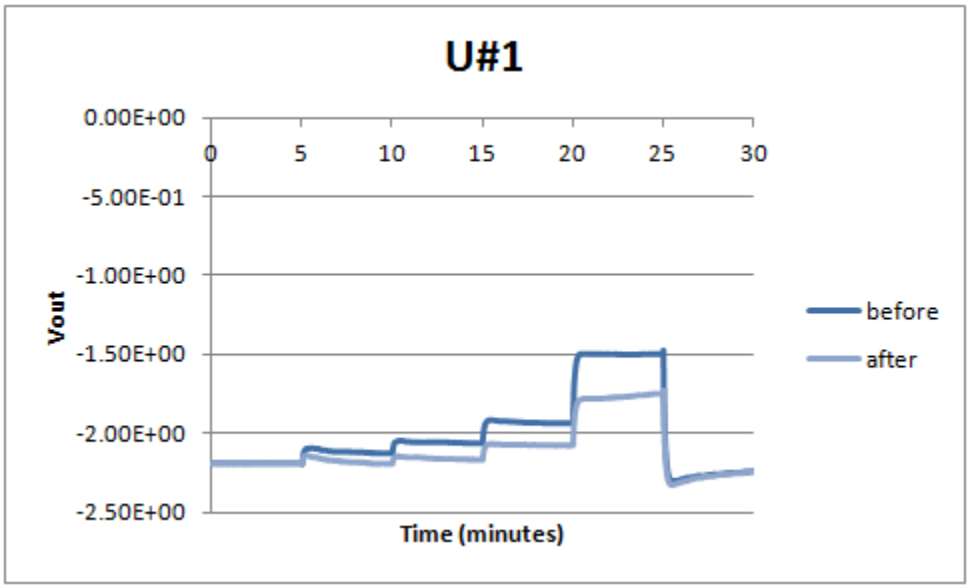

There was a significant effect on sensor output after being exposed to sulfur, although not as much as was seen for sensors with Al_2O_3 beads tested earlier in the project. The CeO/ZrO_2 bead is largely accountable for this improvement, but in the case of the "U" sensors the inclusion of Pt in the catalyst formulation may have contributed as well.

SUMMARY

Over the second year of the Phase II effort, since the decision was made to focus on sensors with beaded elements, considerable progress was made in the development of a commercially viable combustible gas sensors. Improved performance has been achieved, through the use of CeO/ZrO_2 beads and mixed Pd/Pt catalyst formulations. However, there is still work to be done to achieve a commercially viable sensor.

- Good linearity has been achieved.
- Sensor repeatability is decent.
- Humidity effects are minimal.
- Effects of environmental temperature need further consideration. Operating the sensors further out on the plateau may be necessary to mitigate shifts with changing temperature.
- Better performance in regards to higher hydrocarbon has been seen, but more work remains. Approaches to further improve performance may include increasing catalytic volume and operating the sensors further out on the plateau.
- Sulfur resistance has been improved, but more work remains. Increasing the amount of Pt in the catalyst could be considered, as well as other ratios of Ce:Zr in the bead.
- Sensor burn-in appears to be longer than desired (1-2 weeks maximum) and burn-in procedures need to be developed to minimize the burn-in period.
- Long term stability has been improved; however the stability over truly long periods is unknown. This needs to be determined for both the catalyst and sensor heater (as heater stability measurements carried out were done so at lower than the currently used power).
- The targeted power consumption of 50 mW/element has not been achieved. The 170 mW total (active + reference) power used in this evaluation is high enough that it matches the lowest power sensor on the market. If the power was increased as a means of mitigation for performance deficiencies the sensor would operate in the same range as many sensors on the market.

Appendix H

Sensor Module Schematic

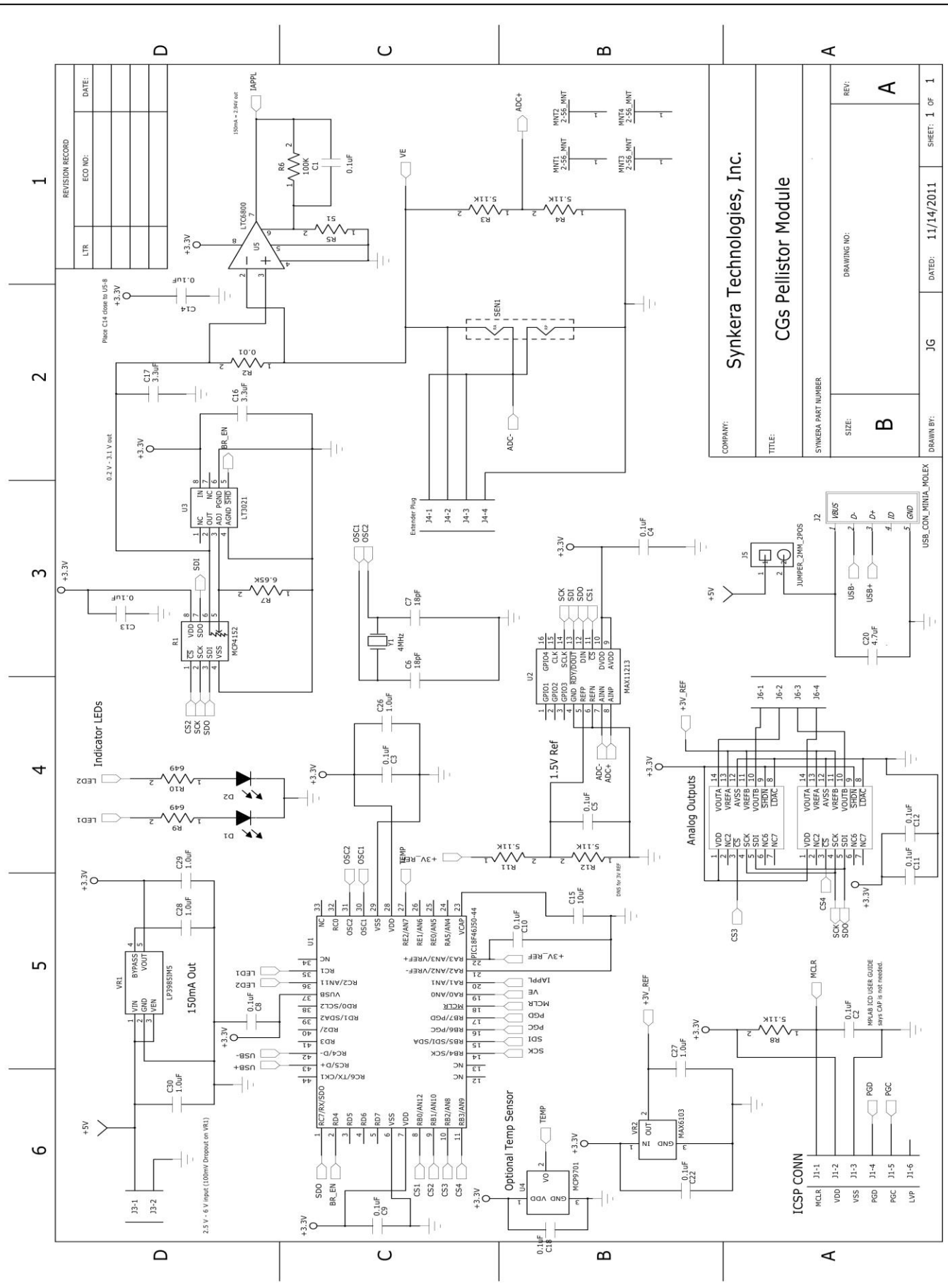
REVISION RECORD
LTR
ECO NO:
DATE:
COMPANY:
Synkera Technologies, Inc.
TITLE:
CGs Pellistor Module
SYNKERA PART NUMBER
SIZE:
B
DRAWING NO:
REV:
A
DRAWN BY:
JG
DATED:
11/14/2011
SHEET: 1 OF 1
Indicator LEDs
150mA Out
Optional Temp Sensor
1.5V Ref
Analog Outputs
ICSP CONN
Extender Plug
USB_CON_MINIA_MOLEX
JUMPER_2MM_2POS
LTC6800
LT3021
MCP4152
MAX11213
PIC18F46J50-44
MCP9701
MAX6103
LP3985IM5
4MHz
Place C14 close to U5-8
2.5 V - 6 V input (100mV Dropout on VR1)
MPLAB ICD USER GUIDE says CAP is not needed.